

# CHAPTER 8

## Electronic Spectra of Transition Metal Complexes:

### ❖ Spectroscopic Ground States

The spectra of transition metal complexes is not as simple as it appears from just the splitting of  $d$ -orbitals with electrons get promoted from the lower energy orbital set to a higher energy orbital set. Actually, energy levels of a transition metal atom or ion with a particular electronic configuration are described not only by the electronic configuration itself but also by different types of electronic interactions such as spin-spin, orbital-orbital or spin-orbital which can be categorized by some special symbols, called as term symbols. The ground state term symbol is predicted by Hund's rule. In other words, the term symbol in quantum mechanics is an abbreviated description of the total angular momentum quantum numbers in a multi-electron atom. However, the quantum mechanical states of a single electron can also be described by a term symbol.

#### ➤ Calculation of Microstates in a Particular Electronic Configuration

The various overall-arrangements of electronic cloud around the nucleus for a particular configuration are not the same as far as the energy and angular momentum are concerned. These different electronic arrangements can be classified on the basis of overall spin, orbital or total angular momentum.

*The term microstates may be defined as the overall electronic arrangements of a particular electronic configuration which can be differentiated in terms of energy or angular momentum.*

The two types of electronic configurations for which the microstate calculation has to be carried out are discussed below.

#### 1. When unpaired electrons are present in the same subshell:

i)  $p^1$ -configuration: Let us consider that we want to study the number of ways in which a single electron can be filled in any  $p$ -subshell.

1	↑		
2	↓		
3		↑	
4		↓	
5			↑
6			↓
	$p_x$	$p_y$	$p_z$

ii)  $p^2$ -configuration: Let us consider that we want to study the number of ways in which two electrons can be filled in any  $p$ -subshell.

1	↑	↑	
2		↑	↑
3	↑		↑
4	↓	↓	
5		↓	↑
6	↓		↓
7	↑	↓	
8		↑	↓
9	↑		↓
10	↓	↑	
11		↓	↑
12	↓		↑
13	↑↓		
14		↑↓	
15			↑↓

$p_x \quad p_y \quad p_z$

Hence, the total number of ways in which one and two electrons can be arranged in the  $p$ -subshell of an atom or ion are six and fifteen, respectively. However, the calculation of the number of microstates for the configurations like  $d^2$  or  $f^2$  using the abovementioned method is quite lengthy and difficult. Moreover, as we are interested only in the number of these electronic arrangements and not in the nature; permutation and combination can be used to find out all these numbers as follows:

$$\text{No. of microstates} = \binom{n}{r} = \frac{n!}{r!(n-r)!}$$

Where  $n$  is twice the number of orbitals present in the subshell under consideration and  $r$  is the number of unpaired electrons in them. The formulation related to the calculation of the number of microstate in particular term symbol will be discussed later in this chapter.

Now, the number of microstates for different electronic configurations can be calculated easily.

i) For  $p^1$ -configuration,  $n = 6$  and  $r = 1$ . Therefore

$$\begin{aligned}\text{No. of microstates} &= \binom{6}{1} = \frac{6!}{1!(6-1)!} \\ \binom{6}{1} &= \frac{6 \times 5 \times 4 \times 3 \times 2 \times 1}{1(5 \times 4 \times 3 \times 2 \times 1)} \\ &= 6 \text{ microstates}\end{aligned}$$

ii) For  $p^2$ -configuration,  $n = 6$  and  $r = 2$ . Therefore

$$\begin{aligned}\text{No. of microstates} &= \binom{6}{2} = \frac{6!}{2!(6-2)!} \\ \binom{6}{2} &= \frac{6 \times 5 \times 4 \times 3 \times 2 \times 1}{2 \times 1(4 \times 3 \times 2 \times 1)} \\ &= 15 \text{ microstates}\end{aligned}$$

iii) For  $d^1$ -configuration,  $n = 10$  and  $r = 1$ . Therefore

$$\begin{aligned}\text{No. of microstates} &= \binom{10}{1} = \frac{10!}{1!(10-1)!} \\ \binom{10}{1} &= \frac{10 \times 9 \times 8 \times 7 \times 6 \times 5 \times 4 \times 3 \times 2 \times 1}{1(9 \times 8 \times 7 \times 6 \times 5 \times 4 \times 3 \times 2 \times 1)} \\ &= 10 \text{ microstates}\end{aligned}$$

iv) For  $d^2$ -configuration,  $n = 10$  and  $r = 2$ . Therefore

$$\begin{aligned}\text{No. of microstates} &= \binom{10}{2} = \frac{10!}{2!(10-2)!} \\ \binom{10}{2} &= \frac{10 \times 9 \times 8 \times 7 \times 6 \times 5 \times 4 \times 3 \times 2 \times 1}{2 \times 1(8 \times 7 \times 6 \times 5 \times 4 \times 3 \times 2 \times 1)} \\ &= 45 \text{ microstates}\end{aligned}$$

The general form of atomic term symbols considers spin-spin (S-S coupling), orbital-orbital (L-L coupling) and spin-orbital (L-S or Russell-Saunders coupling) interactions; therefore, before categorizing all the microstates in these term symbols, it is extremely important to find out all possible microstates for different electronic configurations. The total number of microstates for other different electronic configurations can be calculated using the same method and are listed below.

Table 1. The calculated microstates for different electronic configurations.

Electronic configuration	No. of microstates	Electronic configuration	No. of microstates
$p^1$	6	$d^3$	120
$p^2$	15	$d^4$	210
$p^3$	20	$d^5$	252
$p^4$	15	$d^6$	210
$p^5$	6	$d^7$	120
$p^6$	1	$d^8$	45
$d^1$	10	$d^9$	10
$d^2$	45	$d^{10}$	1

It can be seen that the number of microstates for the same number of unpaired electrons is equal. For example, there are six microstates for  $p^1$  as well as  $p^5$  and forty-five microstates for both  $d^2$  as well as  $d^8$ . It can be explained in terms of electron-hole formalism which will be discussed later in this chapter.

## 2. When unpaired electrons are present in different subshell:

The same approach can also be applied to calculate the microstates in the case when the electrons are present in two different subshells. Therefore, permutation and combination can be used to find out all these numbers as follows:

$$\text{No. of microstates} = \binom{n}{r} \times \binom{m}{s} = \frac{n!}{r!(n-r)!} \times \frac{m!}{s!(m-s)!}$$

Where,  $n$  is twice the number of orbitals and  $r$  is the number of unpaired electrons in one subshell while  $m$  is twice the number of orbitals and  $s$  is the number of unpaired electrons in the other subshell. Now, the number of microstates for different electronic configurations can be calculated easily.

i)  $p^1p^1$ -configuration,  $n = 6$ ,  $r = 1$ ,  $m = 6$  and  $s = 1$ .

$$\begin{aligned} \text{No. of microstates} &= \binom{6}{1} \times \binom{6}{1} = \frac{6!}{1!(6-1)!} \times \frac{6!}{1!(6-1)!} \\ &= \frac{6 \times 5 \times 4 \times 3 \times 2 \times 1}{1(5 \times 4 \times 3 \times 2 \times 1)} \times \frac{6 \times 5 \times 4 \times 3 \times 2 \times 1}{1(5 \times 4 \times 3 \times 2 \times 1)} \\ &= 36 \text{ microstates} \end{aligned}$$

ii)  $d^1d^1$ -configuration,  $n = 10$ ,  $r = 1$ ,  $m = 10$  and  $s = 1$ .

$$\begin{aligned} \text{No. of microstates} &= \binom{10}{1} \times \binom{10}{1} = \frac{10!}{1!(10-1)!} \times \frac{10!}{1!(10-1)!} \\ \binom{10}{1} \times \binom{10}{1} &= \frac{10 \times 9 \times 8 \times 7 \times 6 \times 5 \times 4 \times 3 \times 2 \times 1}{1(9 \times 8 \times 7 \times 6 \times 5 \times 4 \times 3 \times 2 \times 1)} \times \frac{10 \times 9 \times 8 \times 7 \times 6 \times 5 \times 4 \times 3 \times 2 \times 1}{1(9 \times 8 \times 7 \times 6 \times 5 \times 4 \times 3 \times 2 \times 1)} \\ &= 100 \text{ microstates} \end{aligned}$$

iii)  $p^1d^1$ -configuration,  $n = 6$ ,  $r = 1$ ,  $m = 10$  and  $s = 1$ .

$$\begin{aligned} \text{No. of microstates} &= \binom{6}{1} \times \binom{10}{1} = \frac{6!}{1!(6-1)!} \times \frac{10!}{1!(10-1)!} \\ \binom{6}{1} \times \binom{10}{1} &= \frac{6 \times 5 \times 4 \times 3 \times 2 \times 1}{1(5 \times 4 \times 3 \times 2 \times 1)} \times \frac{10 \times 9 \times 8 \times 7 \times 6 \times 5 \times 4 \times 3 \times 2 \times 1}{1(9 \times 8 \times 7 \times 6 \times 5 \times 4 \times 3 \times 2 \times 1)} \\ &= 60 \text{ microstates} \end{aligned}$$

The total number of microstates for different electronic configurations can be calculated using the same method and are listed below.

Table 2. The total number of microstates calculated for the different electronic configurations when unpaired electrons are present in two different subshells.

Electronic configuration	No. of microstates	Electronic configuration	No. of microstates
$p^1p^1$	36	$d^2d^2$	2025
$p^1p^2$	90	$d^2d^3$	5400
$p^2p^2$	225	$p^1d^1$	60
$p^2p^3$	300	$p^1d^2$	270
$d^1d^1$	100	$p^2d^2$	675
$d^1d^2$	450	$p^2d^3$	1800

This table can further be extended for the remaining combination of  $p$ - $p$ ,  $d$ - $d$ ,  $p$ - $d$  or their combinations with  $f$ -subshell. The number of microstates in particular configuration can be distributed to various electronic states, represented by atomic term symbols. The distribution of these microstates in different term symbols will be discussed later in this section.

➤ **Atomic Term Symbols**

Atomic term symbols may be defined as the symbolic representations of various electronic states having different resultant angular momentums resulting from spin-spin, orbital-orbital or spin-orbital interactions and the transitions between two different atomic states may also be represented using their term symbols, to which certain rules apply.

The general form of any atomic term symbol that is used to represent any electronic state resulting from inter-electronic repulsion is:

$$^{2S+1}L_J$$

Where,

$2S+1$  = spin multiplicity

$S$  = resultant spin angular momentum quantum number

$L$  = resultant orbital angular momentum quantum number

$J$  = resultant total angular momentum quantum number

Just like in the case of atomic orbitals, where  $l$  represents the individual orbital angular momentums;  $L$  represents the resultant orbital angular momentum of an electronic state and gives the base designation of any atomic term symbol.

$L$	=	0	1	2	3	4	5	6	7
State	=	S	P	D	F	G	H	I	K

The calculation of resultant spin and orbital angular momentum involves the concepts of space quantization and vector interactions. A somewhat simplified approach for the calculation of resultant orbital angular momentum quantum number ( $L$ ), resultant spin angular momentum quantum number  $S$  and resultant total angular momentum quantum number ( $J$ ) can be given by understanding the spin-spin, orbital-orbital and spin-orbital couplings schemes.

**1. Orbital-orbital coupling ( $l-l$  interaction):** Consider a multielectron system, then the resultant orbital angular momentum quantum number can be deduced as:

$$L = (l_1 + l_2), (l_1 + l_2 - 1) \dots \dots \dots |l_1 - l_2|$$

Where  $l_1$  and  $l_2$  are the individual orbital angular momentum quantum numbers for electrons and modulus sign shows that the value of resultant orbital angular momentum quantum number is always positive. Given the eigenstates of  $l_1$  and  $l_2$ , the construction of eigenstates of  $L$  (which still is conserved) is the coupling of the angular momenta of electrons 1 and 2.

i) For  $p^1p^1$ -configuration,  $l_1 = 1$  and  $l_2 = 1$ , therefore

$$L = (1 + 1), (1 + 1 - 1), (1 - 1)$$

$$L = 2, 1, 0$$

$$\text{States} = D, P, S$$

Similarly,

ii) For  $d^1d^1$ -configuration,  $l_1 = 2$  and  $l_2 = 2$ , therefore

$$L = (2 + 2), (2 + 2 - 1) \dots\dots (2 - 2)$$

$$L = 4, 3, 2, 1, 0$$

$$\text{States} = G, F, D, P, S$$

Although the above-mentioned procedure provides the resultant orbital angular momentum quantum number (L) quite easily, the exact concept of orbital-orbital coupling can be understood only after knowing the concepts of space quantization. One thing that is totally clear is that these symbols are nothing but the mathematical shorthand of the electronic arrangements around the nucleus. The quantization of individual orbital angular momentums can be used to calculate the resultant value as follows:

i) For  $p^1p^1$ -configuration,  $l_1 = 1$  and  $l_2 = 1$ , therefore orbital angular momentum for each of the electron is  $\sqrt{2}$  and it is a well-known fact from the quantum mechanics that  $\sqrt{2}$  angular momentum can be oriented in space with three different ways (+1, 0 and -1). The different combinations of orbital angular momentum can be calculated as

$l_1(z)$	=	+1	+1	+1	0	0	0	-1	-1	-1
$l_2(z)$	=	+1	0	-1	+1	0	-1	+1	0	-1
$L_z$	=	+2	+1	0	+1	0	-1	0	-1	-2

Hence, the orbital angular momentums of two  $p$ -electrons can interact in nine ways, creating nine combinations; out of which, three quantum-mechanically allowed series can be fashioned.

$$L_z = (+2, +1, 0, -1, -2), (+1, 0, -1), (0)$$

or

$$L = 2, 1, 0$$

Hence

$$\text{States} = D, P, S$$

Therefore, we can say that there are nine ways in which the orbital motion can interact.

Similarly,

ii) For  $d^1 d^1$ -configuration,  $l_1 = 2$  and  $l_2 = 2$ , therefore orbital angular momentum for each of the electron is  $\sqrt{6}$  and it is a well-known fact from the quantum mechanics that  $\sqrt{6}$  angular momentum can be oriented in space with five different ways (+2, +1, 0, -1 and -2). The different combinations of orbital angular momentum can be calculated as:

$$\begin{array}{rcl} l_1(z) & = & +2 \quad +2 \quad +2 \quad +2 \quad +2 \quad +1 \quad +1 \quad +1 \quad +1 \quad +1 \\ l_2(z) & = & +2 \quad +1 \quad 0 \quad -1 \quad -2 \quad +2 \quad +1 \quad 0 \quad -1 \quad -2 \\ L_z & = & +4 \quad +3 \quad +2 \quad +1 \quad 0 \quad +3 \quad +2 \quad +1 \quad 0 \quad -1 \end{array}$$

and

$$\begin{array}{rcl} l_1(z) & = & 0 \quad 0 \quad 0 \quad 0 \quad 0 \quad -1 \quad -1 \quad -1 \quad -1 \quad -1 \\ l_2(z) & = & +2 \quad +1 \quad 0 \quad -1 \quad -2 \quad +2 \quad +1 \quad 0 \quad -1 \quad -2 \\ L_z & = & +2 \quad +1 \quad 0 \quad -1 \quad -2 \quad +1 \quad 0 \quad -1 \quad -2 \quad -3 \end{array}$$

and

$$\begin{array}{rcl} l_1(z) & = & -2 \quad -2 \quad -2 \quad -2 \quad -2 \\ l_2(z) & = & +2 \quad +1 \quad 0 \quad -1 \quad -2 \\ L_z & = & 0 \quad -1 \quad -2 \quad -3 \quad -4 \end{array}$$

Hence, the orbital angular momentums of two  $d$ -electrons can interact in twenty-five ways, creating twenty-five combinations; out of which, five quantum-mechanically allowed series can be fashioned.

$$L_z = (+4, +3, +2, +1, 0, -1, -2, -3, -4), (+3, +2, +1, 0, -1, -2, -3), (+2, +1, 0, -1, -2), (+1, 0, -1), (0)$$

or

$$L = 4, 3, 2, 1, 0$$

Which means

$$\text{States} = G, F, D, P, S$$

**2. Spin-spin coupling (s-s interaction):** Consider a multielectron system, then the resultant spin angular momentum quantum number can be deduced as:

$$S = (s_1 + s_2), (s_1 + s_2 - 1) \dots \dots \dots |s_1 - s_2|$$

Where  $s_1$  and  $s_2$  are the individual spin angular momentum quantum numbers for electrons and modulus sign shows that the value of resultant spin angular momentum quantum number is always positive.

i) For  $p^1p^1$  or  $d^1d^1$ -configuration,  $s_1 = 1/2$  and  $s_2 = 1/2$ , therefore

$$S = (1/2 + 1/2), (1/2 - 1/2)$$

or

$$S = 1, 0$$

Which means

$$\text{Multiplicity} = (2S + 1) = 3 \text{ and } 1$$

The aforementioned procedure offers the resultant spin angular momentum quantum number ( $S$ ) quite easily but the exact concept of spin-spin interaction can be understood only after knowing the concepts of space quantization. The quantization of individual spin angular momentums can be used to calculate the resultant value as follows:

i) For  $p^1p^1$  or  $d^1d^1$ -configuration,  $s_1 = 1/2$  and  $s_2 = 1/2$ , therefore spin angular momentum for each of the electrons is  $\sqrt{0.75}$  and it is a well-known fact from the quantum mechanics that  $\sqrt{0.75}$  angular momentum can be oriented in space with two different ways ( $+1/2$  and  $-1/2$ ). The different combinations of spin angular momentum can be calculated as:

$s_1(z)$	=	$+1/2$	$+1/2$	$-1/2$	$-1/2$
$s_2(z)$	=	$+1/2$	$+1/2$	$-1/2$	$-1/2$
$S_z$	=	$+1$	$0$	$0$	$-1$

Hence, the spin angular momentums of two  $p$  or  $d$ -electrons can interact in four ways, creating four combinations; out of which, two quantum-mechanically allowed series can be fashioned.

$$S_z = (+1, 0, -1), (0)$$

or

$$S = 1, 0$$

$$\text{Multiplicity} = (2S + 1) = 3 \text{ and } 1$$

The multiplicity actually represents the number of orientations possible for the total spin relative to the total orbital angular momentum  $L$ , and thus to the number of near-degenerate levels that differ only in their spin-orbit coupling energy. For example, the ground state of the carbon atom is a  $^3P$  state. The superscript of three specifies that the multiplicity  $2S+1 = 3$  i.e. triplet, so that the total spin  $S = 1$ . This spin is due to two unpaired electrons, as a result of Hund's rule which favors the single filling of degenerate orbitals. The spin multiplicity is a primary factor in governing the overall energy of an electronic state and maybe summarised for different electron combination.

Table 3. Spin multiplicities for the different number of unpaired electron in an electronic configuration.

Unpaired Electrons	S	2S+1	State
0	0	1	Singlet
1	1/2	2	Doublet
2	1	3	Triplet
3	3/2	4	Quartet
4	2	5	Quintet

**3. Spin-orbital coupling (L-S interaction):** In a multi-electron system, the resultant orbital angular momentum (L) and resultant spin angular momentum (S) interact with each other to give total angular momentum which is defined by the quantum number J.

$$J = (L + S), (L + S - 1) \dots \dots \dots |L - S|$$

Where L and S are the quantum numbers for resultant orbital angular momentum and resultant spin angular momentum, respectively. The modulus sign shows that the value of the resultant total angular momentum quantum number is always positive. The value of J is assigned as the subscript of the overall term symbol.

i) For  $p^1p^1$ -configuration, 9 combinations given by orbital-orbital coupling (L = 2, 1, 0) and 4 combinations given by spin-spin coupling (S = 1, 0) combine to create a total of 36 microstates. therefore

$$L = 0, 1, 2 \text{ and } S = 1, 0$$

$$\text{States} = {}^3S, {}^3P, {}^3D, {}^1S, {}^1P, {}^1D$$

The summarization of spin-orbital coupling for  $p^1p^1$ -configurations is given below.

Table 4. Splitting of the term symbols for  $p^1p^1$ -configuration due to L-S coupling.

State	Value L and S	Value of J	States after L-S coupling
${}^3S$	L = 0 and S = 1	$J = (0 + 1) = 1$	${}^3S_1$
${}^3P$	L = 1 and S = 1	$J = (1 + 1) \dots (1 - 1) = 2, 1, 0$	${}^3P_2, {}^3P_1, {}^3P_0$
${}^3D$	L = 2 and S = 1	$J = (2 + 1) \dots (2 - 1) = 3, 2, 1$	${}^3D_3, {}^3D_2, {}^3D_1$

Table 4. Continued on the next page...

$^1S$	$L = 0$ and $S = 0$	$J = (0 + 0) = 0$	$^1S_0$
$^1P$ state:	$L = 1$ and $S = 0$	$J = (1 + 0) = 1$	$^1P_1$
$^1D$ state:	$L = 2$ and $S = 0$	$J = (2 + 0) = 2$	$^1D_2$

ii) For  $d^1d^1$ -configuration, 25 combinations given by orbital-orbital coupling ( $L = 4, 3, 2, 1, 0$ ) and 4 combinations given by spin-spin coupling ( $S = 1, 0$ ) couple to create a total of 100 microstates. therefore

$$L = 4, 3, 2, 1, 0$$

$$S = 1, 0$$

$$\text{States} = ^3S, ^3P, ^3D, ^3F, ^3G, ^1S, ^1P, ^1D, ^1F, ^1G$$

The summarization of spin-orbital coupling for  $d^1d^1$ -configurations is given below.

Table 5. Splitting of the term symbols for  $d^1d^1$ -configuration due to L-S coupling.

State	Value L and S	Value of J	States after L-S coupling
$^3S$	$L = 0$ and $S = 1$	$J = (0 + 1) = 1$	$^3S_1$
$^3P$	$L = 1$ and $S = 1$	$J = (1 + 1), (1 + 0), (1 - 1) = 2, 1, 0$	$^3P_2, ^3P_1, ^3P_0$
$^3D$	$L = 2$ and $S = 1$	$J = (2 + 1) \dots (2 - 1) = 3, 2, 1$	$^3D_3, ^3D_2, ^3D_1$
$^3F$	$L = 3$ and $S = 1$	$J = (3 + 1) \dots (3 - 1) = 4, 3, 2$	$^3F_4, ^3F_3, ^3F_2$
$^3G$	$L = 4$ and $S = 1$	$J = (4 + 1) \dots (4 - 1) = 5, 4, 3$	$^3G_5, ^3G_4, ^3G_3$
$^1S$	$L = 0$ and $S = 0$	$J = (0 + 0) = 0$	$^1S_0$
$^1P$	$L = 1$ and $S = 0$	$J = (1 + 0) = 1$	$^1P_1$
$^1D$	$L = 2$ and $S = 0$	$J = (2 + 0) = 2$	$^1D_2$
$^1F$	$L = 3$ and $S = 0$	$J = (3 + 0) = 3$	$^1F_3$
$^1G$	$L = 4$ and $S = 0$	$J = (4 + 0) = 4$	$^1G_4$

The quantization of individual orbital angular momentums can be used to calculate the resultant value as follows: For  $^3P$  state of  $p^1p^1$ -configuration,  $L = 1$  and  $S = 1$ . Therefore, the different combinations of resultant orbital angular momentum and resultant spin angular momentum can be calculated:

$L_z$	=	+1	+1	+1	0	0	0	-1	-1	-1
$S_z$	=	+1	0	-1	+1	0	-1	+1	0	-1
$J_z$	=	+2	+1	0	+1	0	-1	0	-1	-2

Hence, the resultant orbital angular momentums and resultant spin angular momentums of  $^3P$  can interact in nine ways, creating nine microstates; out of which, three quantum-mechanically allowed series can be fashioned.

$$J_z = (+2, +1, 0, -1, -2), (+1, 0, -1), (0)$$

or

$$J = 2, 1, 0$$

Which means

$$\text{States} = ^3P_2, ^3P_1 \text{ and } ^3P_0$$

➤ **Derivation of the Term Symbols for Unpaired Electrons in the Same Subshell**

In the previous section, we have distributed all the 36 microstates for  $p^1p^1$ -configuration in six electronic states labeled by  $^3S$ ,  $^3P$ ,  $^3D$ ,  $^1S$ ,  $^1P$  and  $^1D$  term symbols. However, for  $p^2$ -configuration (both of the unpaired electrons in same subshell), many microstates that were possible in  $p^1p^1$ -configuration cannot exist if they violate the Pauli exclusion principle. Therefore, there are only 15 microstates (complying with Pauli principle) for  $p^2$ -configuration which can be distributed in three electronic states labeled by  $^1S$ ,  $^3P$  and  $^1D$  term symbols.

Similarly, all the 100 microstates for  $d^1d^1$ -configuration ( $^3S$ ,  $^3P$ ,  $^3D$ ,  $^3F$ ,  $^3G$ ,  $^1S$ ,  $^1P$ ,  $^1D$ ,  $^1F$  and  $^1G$ ) cannot exist if they both the electrons are present in the same  $d$ -subshell. Therefore, there are only 45 microstates (complying with Pauli principle) for  $d^2$ -configuration which can be distributed in five electronic states labeled by  $^1S$ ,  $^3P$ ,  $^1D$ ,  $^3F$  and  $^1G$  term symbols.

Term symbols for electronic configurations with unpaired electrons in the same subshell can be derived using “pigeon hole” diagrams. The principal steps for such operations are:

1. Create vertical columns for all allowed orientation or effect of individual orbital angular momentum in the reference direction. For example, +1, 0 and -1 are the allowed orientations of the orbital angular momentum corresponding to  $l = 1$  value.
2. Fill up the electrons in these columns by exhausting all the possibilities of parallel, paired and opposite orientations.

- Sum-up all the  $l_z$  values of every column to find out the resultant  $L_z$  values.
- Quantum mechanically allowed series set-up should be carried out for different parallel, paired and opposite orientation, which in turn can be used to provide the resultant orbital angular momentum quantum number  $L$  for particular resultant spin quantum number  $S$ .
- Combine the values of  $L$  and  $S$  to find out the term symbols for allowed electronic states.

### 1. $s^1$ -configuration:

$l_z$	
0	↑
$L_z$	0

As  $L_z = 0$ , the value of resultant orbital angular momentum quantum number  $L = 0$ . There is only one unpaired electron, therefore  $S = 1/2$ .

From  $L = 0$ , the state is S; and from  $S = 1/2$ , the multiplicity is 2. Thus, the overall term symbol is  $^2S$ .

### 2. $s^2$ -configuration:

$l_z$	
0	↑↓
$L_z$	0

As  $L_z = 0$ , the value of resultant orbital angular momentum quantum number  $L = 0$ . There are no unpaired electrons, therefore  $S = 0$ .

From  $L = 0$ , the state is S; and from  $S = 0$ , the multiplicity is 1. Thus, the overall term symbol is  $^1S$ .

### 3. $p^1$ and $p^5$ -configuration:

$l_z$			
-1			↑
0		↑	
+1	↑		
$L_z$	+1	0	-1

As  $L_z = +1, 0, -1$ ; the value of resultant orbital angular momentum quantum number  $L = 1$ . There is one unpaired electron, therefore  $S = 1/2$ .

From  $L = 1$ , the state is P; and from  $S = 1/2$ , the multiplicity is 2. Thus, the overall term symbol is  $^2P$ . Hence, all the 6 microstates for  $p^1$  and  $p^5$ -configurations are distributed in  $^2P$  term symbol.

**4.  $p^2$  and  $p^4$ -configuration:**

For parallel arrangements,

$l_z$			
-1		↑	↑
0	↑		↑
+1	↑	↑	
$L_z$	+1	0	-1

As  $L_z = +1, 0, -1$ ; the value of resultant orbital angular momentum quantum number  $L = 1$ .

There are two unpaired electrons, therefore  $S = 1$ .

From  $L = 1$ , the state is P.

From  $S = 1$ , the multiplicity is 3.

Thus, the overall term symbol is  $^3P$ .

Similarly,

For paired and opposite arrangements,

$l_z$						
-1		↑↓	↓	↓	↓	
0	↑↓		↓		↑	
+1	↑↓		↑	↑		
$L_z$	+2	0	-2	+1	0	-1

Out of six values of  $L_z$  (resultant orbital angular momentum in reference direction), two quantum-mechanically allowed series can be setup. One with  $L_z = +2, +1, 0, -1, -2$ ; giving resultant orbital angular momentum quantum number  $L = 2$ . The second series with  $L_z = 0$ ; giving resultant orbital angular momentum quantum number  $L = 0$ .

There are zero unpaired electrons, therefore  $S = 0$ .

From  $L = 2$  and  $0$ ; the states are D and S, respectively.

From  $S = 0$ , the multiplicity is 1.

Thus, the overall term symbols are  $^1D$  and  $^1S$ .

Hence, all the 15 microstates for  $p^2$  and  $p^4$  electronic configurations which can be distributed in  $^1S$ ,  $^3P$  and  $^1D$  term symbols.

**5.  $p^3$ -configuration:**

$l_z$										
-1	↑		↑	↑		↑↓	↑↓	↓	↓	
0	↑	↑		↑↓	↑↓		↑	↑	↓	
+1	↑							↑	↑	
$L_z$	0		+2	+1	-1	+1	-1	-2	0	0
	Parallel		Paired and opposite							

For parallel arrangements,

As  $L_z = 0$ ; the value of resultant orbital angular momentum quantum number  $L = 0$ . There are three unpaired electrons, therefore  $S = 3/2$ .

From  $L = 0$ , the state is S; and from  $S = 3/2$ , the multiplicity is 4. Thus, the overall term symbol is  $^4S$ .

For paired and opposite arrangements,

Out of eight values of  $L_z$ , two quantum-mechanically allowed series can be setup. One with  $L_z = +2, +1, 0, -1, -2$ ; giving resultant orbital angular momentum quantum number  $L = 2$ . The second series with  $L_z = +1, 0, -1$ ; giving resultant orbital angular momentum quantum number  $L = 1$ . There is one unpaired electron, therefore  $S = 1/2$ .

From  $L = 2$  and 1 the states are D and P, respectively.

From  $S = 1/2$ , the multiplicity is 2.

Thus, the overall term symbols are  $^2D$  and  $^2P$ .

Hence, all the 20 microstates for  $p^3$ -configurations are distributed in  $^4S$ ,  $^2P$  and  $^2D$  term symbols.

**6.  $p^6$ -configuration:**

$l_z$	
-1	↑↓
0	↑↓
+1	↑↓
$L_z$	0

As  $L_z = 0$ , the value of resultant orbital angular momentum quantum number  $L = 0$ ; and zero unpaired electrons, therefore  $S = 0$ . Thus, the overall term symbol is  $^1S$  which contains the one and only microstate of  $p^6$ -electronic configuration.

7.  $d^1$  and  $d^9$ -configuration:

$l_z$					
-2					↑
-1				↑	
0			↑		
+1		↑			
+2	↑				
$L_z$	+2	+1	0	-1	-2

As  $L_z = +2, +1, 0, -1, -2$ ; the value of resultant orbital angular momentum quantum number  $L = 2$ .

There is only one unpaired electron, therefore  $S = 1/2$ .

From  $L = 2$ , the state is D; and from  $S = 1/2$ , the multiplicity is also 2.

Thus, the overall term symbol is  ${}^2D$ .

Hence, all the 10 microstates for  $d^1$  and  $d^9$ -configurations are distributed in  ${}^2D$  term symbols.

8.  $d^2$  and  $d^8$ -configuration:

For parallel arrangements,

$l_z$										
-2				↑			↑		↑	
-1			↑			↑		↑		
0		↑			↑		↑	↑		
+1	↑				↑	↑	↑			
+2	↑	↑	↑	↑						
$L_z$	+3	+2	+1	0	+1	0	-1	-1	-2	-3

Out of ten values of  $L_z$ , two quantum-mechanically allowed series can be setup. One with  $L_z = +3, +2, +1, 0, -1, -2, -3$ ; giving resultant orbital angular momentum quantum number  $L = 3$ . The second series with  $L_z = +1, 0, -1$ ; giving resultant orbital angular momentum quantum number  $L = 1$ . There are two unpaired electrons, therefore  $S = 1$ .

From  $L = 3$  and 1, the states are F and P, respectively. From  $S = 1$ , the multiplicity is 3. Thus, the overall term symbols are  ${}^3F$  and  ${}^3P$ .

For paired and opposite arrangements,

$l_z$															
-2					↑↓				↓			↓		↓	
-1				↑↓				↓			↓		↓	↑	
0			↑↓				↓			↓		↑	↑		
+1		↑↓				↓				↑	↑	↑			
+2	↑↓					↑	↑	↑	↑						
$L_z$	+4	+2	0	-2	-4	+3	+2	+1	0	+1	0	-1	-1	-2	-3

Out of fifteen values of  $L_z$ , three quantum-mechanically allowed series can be setup. First with  $L_z = +4, +3, +2, +1, 0, -1, -2, -3, -4$ ; giving resultant orbital angular momentum quantum number  $L = 4$ . Second series with  $L_z = +2, +1, 0, -1, -2$ ; giving resultant orbital angular momentum quantum number  $L = 2$ . The third series with  $L_z = 0$ ; giving resultant orbital angular momentum quantum number  $L = 0$ . There are zero unpaired electrons, therefore  $S = 0$ .

From  $L = 4, 2$  and  $0$  the states are G, D and S, respectively. From  $S = 0$ , the multiplicity is 1. Thus, the overall term symbols are  $^1G$ ,  $^1D$  and  $^1S$ .

Hence, all the 45 microstates for  $d^2$  and  $d^8$ -configurations are distributed in  $^1S$ ,  $^3P$ ,  $^1D$ ,  $^3F$  and  $^1G$  term symbols.

### 9. $d^3$ and $d^7$ -configuration:

For parallel arrangements,

$l_z$									
-2			↑		↑	↑		↑	↑
-1		↑		↑		↑	↑	↑	
0	↑			↑	↑	↑	↑		↑
+1	↑	↑	↑	↑	↑			↑	
+2	↑	↑	↑				↑	↑	↑
$L_z$	+3	+2	+1	0	-1	-3	+1	-1	-2

Out of ten values of  $L_z$ , two quantum-mechanically allowed series can be setup.

One with  $L_z = +3, +2, +1, 0, -1, -2, -3$ ; giving resultant orbital angular momentum quantum number  $L = 3$ .

The second series with  $L_z = +1, 0, -1$ ; giving resultant orbital angular momentum quantum number  $L = 1$ .

There are three unpaired electrons, therefore  $S = 3/2$ .

From  $L = 3$  and 1; the states are F and P, respectively. From  $S = 3/2$ , the multiplicity is 4. Thus, the overall term symbols are  ${}^4F$  and  ${}^4P$ .

For paired and opposite arrangements,

$l_z$				↑			↑			↑			↑		
-2				↑			↑			↑			↑		
-1			↑			↑			↑			↑↓	↑↓	↑↓	
0		↑			↑				↑↓	↑↓	↑↓	↑↓		↑	
+1	↑				↑↓	↑↓	↑↓	↑↓			↑				↑
+2	↑↓	↑↓	↑↓	↑↓					↑				↑		
$L_z$	+5	+4	+3	+2	+2	+1	0	+4	-1	-2	+1	+2	-4	-2	-1

and

$l_z$															
-2		↑↓	↑↓	↑↓	↑↓								↓	↓	↓
-1	↑↓	↑											↑	↑	
0			↑										↑		↑
+1				↑										↑	
+2	↑				↑								↑	↑	
$L_z$	0	-5	-4	-3	-2	+3	+2	+1	0	-1	-3	+1	-1	-2	0

Out of thirty values of  $L_z$ , six quantum-mechanically allowed series can be setup. First with  $L_z = +5, +4, +3, +2, +1, 0, -1, -2, -3, -4, -5$ ; giving resultant orbital angular momentum quantum number  $L = 5$ . Second series with  $L_z = +4, +3, +2, +1, 0, -1, -2, -3, -4$ ; giving resultant orbital angular momentum quantum number  $L = 4$ . The third series with  $L_z = +3, +2, +1, 0, -1, -2, -3$ ; giving resultant orbital angular momentum quantum number  $L = 3$ . Fourth and fifth series with  $L_z = +2, +1, 0, -1, -2$ ; giving resultant orbital angular momentum quantum number  $L = 2$  and 2, respectively. The sixth series is consisted of  $L_z = +1, 0, -1$ ; giving resultant orbital angular momentum quantum number  $L = 1$ .

There is one unpaired electron, therefore  $S = 1/2$ .

From  $L = 5, 4, 3, 2, 2$  and 1; the states are H, G, F, D, D and P, respectively.

From  $S = 1/2$ , the multiplicity is 2.

Thus, the overall term symbols are  ${}^2\text{H}$ ,  ${}^2\text{G}$ ,  ${}^2\text{F}$ ,  ${}^2\text{D}$ ,  ${}^2\text{D}$  and  ${}^2\text{P}$ .

Hence, all the 120 microstates for  $d^3$  and  $d^7$ -configurations are distributed in  ${}^4\text{F}$ ,  ${}^4\text{P}$ ,  ${}^2\text{H}$ ,  ${}^2\text{G}$ ,  ${}^2\text{F}$ ,  ${}^2\text{D}$ ,  ${}^2\text{D}$  and  ${}^2\text{P}$  term symbols.

### 10. $d^4$ and $d^6$ -configuration:

For parallel arrangements,

$l_z$					
-2		↑	↑	↑	↑
-1	↑		↑	↑	↑
0	↑	↑		↑	↑
+1	↑	↑	↑		↑
+2	↑	↑	↑	↑	
$L_z$	+2	+1	0	-1	-2

Out of five values of  $L_z$ , only one quantum-mechanically allowed series can be set up with  $L_z = +2, +1, 0, -1, -2$ ; giving resultant orbital angular momentum quantum number  $L = 2$ .

There are four unpaired electrons, therefore  $S = 2$ .

From  $L = 2$ , the state is D.

From  $S = 2$ , the multiplicity is 5.

Thus, the overall term symbol is  ${}^5\text{D}$ .

For two electrons paired or opposite arrangement,

$l_z$															
-2			↑		↑	↑		↑	↑		↑	↑			
-1		↑	↑	↑		↑	↑		↑		↑		↑		↑
0	↑			↑	↑		↑	↑		↑			↑↓	↑↓	↑↓
+1	↑	↑	↑				↑↓	↑↓	↑↓	↑↓	↑↓	↑↓		↑	
+2	↑↓	↑↓	↑↓	↑↓	↑↓	↑↓				↑	↑	↑		↑	↑
$L_z$	+5	+4	+2	+3	+2	+1	+1	0	-1	+4	+3	+2	-3	+3	+1

and

$l_z$															
-2	↑		↑			↑		↑	↑	↑↓	↑↓	↑↓	↑↓	↑↓	
-1		↑		↑↓	↑↓	↑↓	↑↓	↑↓	↑↓			↑		↑	
0	↑↓	↑↓	↑↓		↑		↑		↑		↑		↑	↑	
+1		↑	↑	↑			↑	↑		↑			↑	↑	
+2	↑			↑	↑	↑				↑	↑	↑			
$L_z$	0	0	-1	+1	0	-2	-1	-3	-4	-1	-2	-3	-3	-4	-5

and

$l_z$															
-2		↓	↓	↓	↓	↑	↑	↑	↑		↑	↑	↑	↑	
-1	↓		↑	↑	↑	↑	↑	↓		↑		↑	↑	↑	
0	↑	↑		↑	↓	↓	↓	↑	↑	↑			↓	↓	
+1	↑	↑	↑	↑	↑	↑	↑	↓	↓	↓	↓	↓		↑	
+2	↑	↑	↑	↑	↑	↑	↑	↑	↑	↑	↑	↑	↑		
$L_z$	+2	+1	0	-1	-2	+2	+1	0	-1	-2	+2	+1	0	-1	-2

Out of forty-five values of  $L_z$ , seven quantum-mechanically allowed series can be setup as. First with  $L_z = +5, +4, +3, +2, +1, 0, -1, -2, -3, -4, -5$ ; giving resultant orbital angular momentum quantum number  $L = 5$ . Second series with  $L_z = +4, +3, +2, +1, 0, -1, -2, -3, -4$ ; giving resultant orbital angular momentum quantum number  $L = 4$ . The third and fourth series with  $L_z = +3, +2, +1, 0, -1, -2, -3$ ; giving resultant orbital angular momentum quantum number  $L = 3$  and 3. fifth series with  $L_z = +2, +1, 0, -1, -2$ ; giving resultant orbital angular momentum quantum number  $L = 2$ . The sixth and seventh series is consisted of  $L_z = +1, 0, -1$ ; giving resultant orbital angular momentum quantum number  $L = 1$  and 1, respectively.

There are two unpaired electrons, therefore  $S = 1$ .

From  $L = 5, 4, 3, 3, 2, 1$  and 1; the states are H, G, F, F, D, P and P, respectively.

From  $S = 1$ , the multiplicity is 3.

Thus, the overall term symbols are  ${}^3H, {}^3G, {}^3F, {}^3F, {}^3D, {}^3P$  and  ${}^3P$ .

Similarly,

For all electrons paired or opposite arrangement,

$l_z$ 

-2				↑↓			↑↓		↑↓	↑↓			↓		↓	
-1			↑↓			↑↓		↑↓		↑↓			↓		↓	
0		↑↓			↑↓			↑↓	↑↓			↓			↑	↑
+1	↑↓				↑↓	↑↓	↑↓					↑	↑	↑		
+2	↑↓	↑↓	↑↓	↑↓								↑↓	↑↓	↑↓	↑↓	↑↓
$L_z$	+6	+4	+2	0	+1	0	-2	-2	-4	-6	+5	+4	+2	+3	+2	

and

 $l_z$ 

-2	↓		↓	↓			↓	↓			↓		↓		
-1	↑	↓		↑			↓	↑			↓		↑↓		↑↓
0		↑	↑	↓			↑↓	↑↓	↑↓	↑↓	↑↓	↑↓	↑↓		↓
+1		↑↓	↑↓	↑↓	↑↓	↑↓	↑↓	↑↓	↑↓	↑↓	↑	↑	↑	↓	
+2	↑↓				↑	↑	↑	↑	↑	↑	↑	↑		↑	↑
$L_z$	+1	+1	0	-1	+4	+3	+2	-3	+3	+1	0	0	-1	+1	0

and

 $l_z$ 

-2	↓		↓	↓	↑↓	↑↓	↑↓	↑↓	↑↓	↑↓		↓	↓	↓	↓
-1	↑↓	↑↓	↑↓	↑↓			↓		↓	↓	↓	↓	↓	↓	↓
0		↓		↑		↓		↓		↑	↓	↓		↑	↑
+1		↑	↑		↓			↑	↑		↑	↑	↑		↑
+2	↑				↑	↑	↑				↑	↑	↑	↑	
$L_z$	-2	-1	-3	-4	-1	-2	-3	-3	-4	-5	+2	+1	0	-1	-2

and

$l_z$					
-2		↓	↓	↓	↓
-1	↓		↑	↑	↑
0	↑	↑		↓	↓
+1	↓	↓	↓		↑
+2	↑	↑	↑	↑	
$L_z$	+2	+1	0	-1	-2

Out of fifty values of  $L_z$ , eight quantum-mechanically allowed series can be setup as. First with  $L_z = +6, +5, +4, +3, +2, +1, 0, -1, -2, -3, -4, -5, -6$ ; giving resultant orbital angular momentum quantum number  $L = 6$ . Second and third series with  $L_z = +4, +3, +2, +1, 0, -1, -2, -3, -4$ ; giving resultant orbital angular momentum quantum number  $L = 4$  and  $4$ , respectively. The fourth series with  $L_z = +3, +2, +1, 0, -1, -2, -3$ ; giving resultant orbital angular momentum quantum number  $L = 3$ . Fifth and sixth series with  $L_z = +2, +1, 0, -1, -2$ ; giving resultant orbital angular momentum quantum number  $L = 2$  and  $2$ , respectively. The seventh and eighth series is consisted of  $L_z = 0$ ; giving resultant orbital angular momentum quantum number  $L = 0$  and  $0$ , respectively. There are zero unpaired electrons, therefore  $S = 0$ .

From  $L = 6, 4, 4, 3, 2, 2, 0$  and  $0$ ; the states are  $^1G, ^1G, ^1F, ^1D, ^1D, ^1S$  and  $^1S$ , respectively. From  $S = 0$ , the multiplicity is 1. Thus, the overall term symbols are  $^1G, ^1G, ^1F, ^1D, ^1D, ^1S$  and  $^1S$ .

Hence, all the 210 microstates for  $d^4$  and  $d^6$ -configurations are distributed in  $^5D, ^3H, ^3G, ^3F, ^3F, ^3D, ^3P, ^3P, ^1I, ^1G, ^1G, ^1F, ^1D, ^1D, ^1S$  and  $^1S$  term symbols.

### 11. $d^5$ -configuration:

For parallel arrangements,

$l_z$	
-2	↑
-1	↑
0	↑
+1	↑
+2	↑
$L_z$	0

As  $L_z = 0$ ; the value of resultant orbital angular momentum quantum number  $L = 0$ . There are five unpaired electrons, therefore  $S = 5/2$ .

From  $L = 0$ , the state is S. From  $S = 5/2$ , the multiplicity is 6. Thus, the overall term symbol is  ${}^6S$ .

For two electrons paired or opposite arrangement,

$l_z$

-2		↑	↑	↑		↑	↑	↑		↑	↑	↑		↑	↑
-1	↑		↑	↑	↑		↑	↑	↑		↑	↑	↑↓	↑↓	↑↓
0	↑	↑		↑	↑	↑		↑	↑↓	↑↓	↑↓	↑↓	↑		↑
+1	↑	↑	↑		↑↓	↑↓	↑↓	↑↓	↑	↑		↑	↑	↑	
+2	↑↓	↑↓	↑↓	↑↓	↑	↑	↑	↑	↑	↑	↑		↑	↑	↑
$L_z$	+4	+3	+2	+1	+3	+2	+1	-1	+2	+1	-1	-2	+1	-1	-2

and

$l_z$

-2	↑	↑↓	↑↓	↑↓	↑↓	↑↓	↑	↑	↑
-1	↑↓		↑	↑	↑	↑	↑	↑	↑
0	↑	↑		↑	↑	↑	↑	↑	↑
+1	↑	↑	↑		↑	↑	↑	↑	↑
+2		↑	↑	↑		↑	↑	↑	↑
$L_z$	-3	-1	-2	-3	-4	0	0	0	0

Out of twenty-four values of  $L_z$ , four quantum-mechanically allowed series can be setup as. First with  $L_z = +4, +3, +2, +1, 0, -1, -2, -3, -4$ ; giving resultant orbital angular momentum quantum number  $L = 4$ . Second series with  $L_z = +3, +2, +1, 0, -1, -2, -3$ ; giving resultant orbital angular momentum quantum number  $L = 3$ . The third series with  $L_z = +2, +1, 0, -1, -2$ ; giving resultant orbital angular momentum quantum number  $L = 3$ . The fourth series is consisted of  $L_z = +1, 0, -1$ ; giving resultant orbital angular momentum quantum number  $L = 1$ .

There are three unpaired electrons, therefore  $S = 3/2$ .

From  $L = 4, 3, 2$  and  $1$ ; the states are G, F, D and P, respectively.

From  $S = 3/2$ , the multiplicity is 4.

Thus, the overall term symbols are  ${}^4G, {}^4F, {}^4D$  and  ${}^4P$ .

For four electrons paired or opposite arrangement,

$l_z$

-2			↑			↑			↑	↑↓	↑↓	↑↓			↑
-1		↑			↑		↑↓	↑↓	↑↓			↑		↑	
0	↑			↑↓	↑↓	↑↓		↑			↑		↑↓	↑↓	↑↓
+1	↑↓	↑↓	↑↓	↑			↑			↑			↑↓	↑↓	↑↓
+2	↑↓	↑↓	↑↓	↑↓	↑↓	↑↓	↑↓	↑↓	↑↓	↑↓	↑↓	↑↓	↑		
$L_z$	+6	+5	+4	+5	+3	+2	+3	+2	0	+1	0	-1	+4	+1	0

and

$l_z$

-2			↑	↑↓	↑↓	↑↓	↑↓	↑	↑↓	↑↓	↑↓	↑↓	↑↓	↑↓	↑↓
-1	↑↓	↑↓	↑↓		↑	↑↓	↑↓	↑↓	↑↓		↑	↑↓	↑↓	↑↓	↑↓
0		↑		↑	↑↓	↑↓	↑↓	↑↓	↑↓	↑↓	↑↓				↑
+1	↑↓	↑↓	↑↓	↑↓	↑↓	↑↓	↑			↑			↑		
+2	↑			↑			↑			↑			↑		
$L_z$	+2	0	-2	0	-2	-3	0	-1	-4	-2	-3	-5	-4	-5	-6

and

$l_z$

-2		↓	↓	↓		↓	↓	↓		↓	↓	↓		↓	↓
-1	↓		↑	↑	↓		↑	↑	↓		↑	↑	↑↓	↑↓	↑↓
0	↑	↑		↑	↑	↑		↑	↑↓	↑↓	↑↓	↑↓	↓		↑
+1	↑	↑	↑		↑↓	↑↓	↑↓	↑↓	↑	↑		↑	↑	↑	
+2	↑↓	↑↓	↑↓	↑↓	↑	↑	↑		↑	↑	↑		↑	↑	↑
$L_z$	+4	+3	+2	+1	+3	+2	+1	-1	+2	+1	-1	-2	+1	-1	-2

and

$l_z$ 

-2	↓	↑↓	↑↓	↑↓	↑↓		↑	↑	↑		↑	↑	↑		↑
-1	↑↓		↓	↓	↓	↑		↓	↓	↑		↓	↓	↑	
0	↑	↓		↑	↑	↓	↓		↑	↓	↓		↑	↑↓	↑↓
+1	↑	↑	↑		↑	↑	↑			↑↓	↑↓	↑↓	↑↓	↓	↓
+2		↑	↑	↑		↑↓	↑↓	↑↓	↑↓	↑	↑	↑		↑	↑
$L_z$	-3	-1	-2	-3	-4	+4	+3	+2	+1	+3	+2	+1	-1	+2	+1

and

 $l_z$ 

-2	↑	↑		↑	↑	↑	↑↓	↑↓	↑↓	↑↓	↓	↑	↑	↑	↑
-1	↓	↓	↑↓	↑↓	↑↓	↑↓	↑	↑	↑	↑	↓	↓	↑	↑	↓
0	↑↓	↑↓	↑	↓	↓	↓	↑	↑	↑	↑	↑	↓	↓	↑	↑
+1		↑	↓	↓	↑	↑	↓	↓	↑	↑	↑	↑	↓	↓	↓
+2	↑		↑	↑	↑	↑	↑	↑	↑	↑	↑	↑	↑	↓	↑
$L_z$	-1	-2	+1	-1	-2	-3	-1	-2	-3	-4	0	0	0	0	0

Out of seventy-five values of  $L_z$ , eleven quantum-mechanically allowed series can be setup. First with  $L_z = +6, +5, +4, +3, +2, +1, 0, -1, -2, -3, -4, -5, -6$ ; giving resultant orbital angular momentum quantum number  $L = 6$ . Second series with  $L_z = +5, +4, +3, +2, +1, 0, -1, -2, -3, -4, -5$ ; giving resultant orbital angular momentum quantum number  $L = 5$ . The third and fourth series with  $L_z = +4, +3, +2, +1, 0, -1, -2, -3, -4$ ; giving resultant orbital angular momentum quantum number  $L = 4$ . Fifth and sixth series with  $L_z = +3, +2, +1, 0, -1, -2, -3$ ; giving resultant orbital angular momentum quantum number  $L = 3$  and 3, respectively. The seventh, eighth and ninth series are consisted of  $L_z = +2, +1, 0, -1, -2$ ; giving resultant orbital angular momentum quantum number  $L = 2, 2$  and 2, respectively. The tenth and eleventh series are consisted of  $L_z = +1, 0, -1$  and  $L_z = 0$ ; giving resultant orbital angular momentum quantum number  $L = 1$  and 0, respectively.

There is one unpaired electron which  $S = 1/2$ .

From  $L = 6, 5, 4, 4, 3, 3, 2, 2, 2, 1$  and 0; the states are I, H, G, G, F, F, D, D, D, P and S, respectively. From  $S = 1/2$ , the multiplicity is 2. Thus, the overall term symbols are  $^2I, ^2H, ^2G, ^2G, ^2F, ^2F, ^2D, ^2D, ^2D, ^2P$  and  $^2S$ .

Hence, all the 252 microstates for  $d^5$ -configurations are distributed in  $^2I, ^2H, ^2G, ^2G, ^2F, ^2F, ^2D, ^2D, ^2D, ^2P, ^2S, ^4G, ^4F, ^4D, ^4P$  and  $^6S$  term symbols.

12.  $d^{10}$ -configuration:

$l_z$	
-2	↑↓
-1	↑↓
0	↑↓
+1	↑↓
+2	↑↓
$L_z$	0

As  $L_z = 0$ ; the value of resultant orbital angular momentum quantum number  $L = 0$ . There are no unpaired electrons, therefore  $S = 0$ .

From  $L = 0$ , the state is S. From  $S = 0$ , the multiplicity is 1. Thus, the overall term symbol is  $^1S$  which contains the only microstate of  $d^{10}$ -configuration.

It can clearly be seen that the number of microstates, as well as the term symbols for  $dn$  and  $d^{10-n}$  configurations, are the same. This is due to the fact that the number of unpaired electrons is the same for both of the configurations. In other words, the possible arrangements for unpaired electrons in less than half-filled or for holes in more than half-filled configurations are the same. The same analogy is true for  $s$ ,  $p$  or  $f$ -subshell.

Moreover, the number of microstates distributed in any term symbol can be calculated using the following relations:

1. Term symbols without J-value:  $(2L+1) \times (2S+1)$
2. Term symbols without J-value:  $(2J+1)$

Let us tally the number of microstates for  $p^2$  electronic configuration with term symbols distribution.

	$(2L+1) \times (2S+1)$	$(2J+1)$
Distribution of 15 microstates of $p^2$ -configuration in $^1S$ , $^3P$ , $^1D$ term symbols	$^1S = (2 \times 0 + 1) \times (2 \times 0 + 1) = 1$ $^3P = (2 \times 1 + 1) \times (2 \times 1 + 1) = 9$ $^1D = (2 \times 2 + 1) \times (2 \times 0 + 1) = 5$	$^1S_0 = 2 \times 0 + 1 = 1$ $^3P_2 = 2 \times 2 + 1 = 5$ $^3P_1 = 2 \times 1 + 1 = 3$ $^3P_0 = 2 \times 0 + 1 = 1$ $^1D_2 = 2 \times 2 + 1 = 5$

➤ **Determination of Spectroscopic Ground State Term**

In a particular configuration, the classification of various microstates in different term symbols also distinguishes them energetically. It can be explained in terms of the effect of spin-spin, orbital-orbital and spin-orbital coupling. There are two different approaches, both are based upon some conclusive results from quantum mechanics, to find out the term symbol for ground electronic state.

**1. From correlation diagram:** This approach is based on the correlation of all the free ion term of a particular atom or ion and then the ground state term is calculated with the help of certain rules.

i) The energy of different terms (electronic states) depends primarily on the Hund's rule, which states that the most stable state should have the highest multiplicity. Hence, triplet states are more stable than the singlet one. In other words, the higher the value of  $2S+1$ , the greater will be the stability.

ii) If the value of spin multiplicities for two different states is the same, the value of resultant angular momentum will be the deciding factor in the determination of the lower energy term. A higher value of  $L$  gives the lower energy state and the vice-versa is also true.

iii) The energy dependence of different terms upon total angular momentum is configuration-specific in nature. The perturbed Hamiltonian of spin-orbital interaction can have both types of effect, stabilization or destabilization, over the energy states and depends upon the magnitude of  $J$ -value. It has been proved that the interaction of spin-orbital motion destabilizes the less than half filled configuration and stabilizes the more than half-filled. Hence, a lower  $J$ -value for less than half-filled and a higher  $J$ -value of more than half will give the lower energy.

Let us apply this procedure to find out the ground state term symbol for  $p^2$ -configuration:

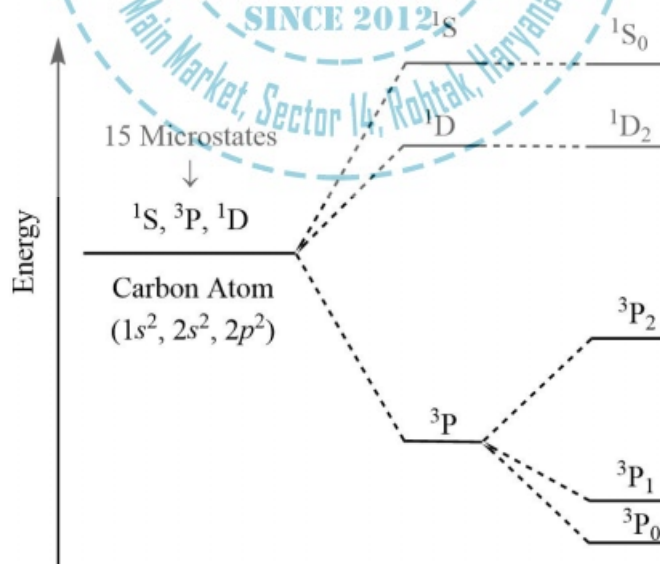


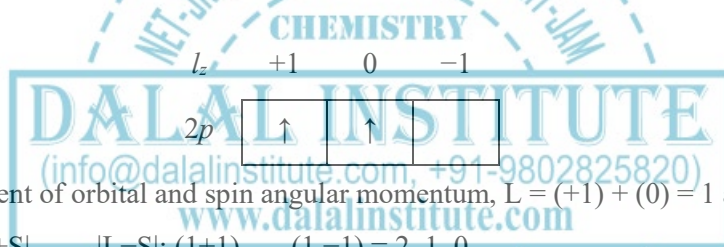
Figure 1. Splitting of free ion terms in the carbon atom.

The effect of spin-spin interaction makes the triplet ( $^3P$ ) state more stable in comparison to the singlet  $^1D$  or  $^1S$ . Furthermore, the stabilization of  $^1D$  state after the consideration of orbital-orbital interaction can be attributed to the higher value of orbital angular momentum. Finally, as the  $p^2$ -configuration is less than half-filled; the splitting of  $^3P$  state goes with  $^3P_0$  as the ground state term symbol.

**2. Using L-S coupling scheme:** This procedure is applicable only to find out the ground state term symbol. We do not need to calculate all the microstates but only present in the ground electronic state. Various steps involved in this procedure are:

1. The electron filling in the valence subshell should be carried out in such a way that a maximum spin multiplicity ( $2S+1$ ) is produced.
2. Maximize the value of resultant orbital angular momentum component by filing electrons first in the orbitals with the positive component of individual orbital angular momentum.
3. Select maximum J-value for more than half-filled and minimum J-value for less than half-filled configuration.

Let us determine the ground state term symbol for carbon atom. The electronic configuration for carbon is  $1s^2, 2s^2, 2p^2$ .

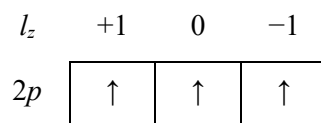


From the total component of orbital and spin angular momentum,  $L = (+1) + (0) = 1$  and  $S = 1/2 + 1/2 = 1$ .

From L-S coupling,  $|L+S| \dots \dots |L-S|$ ;  $(1+1) \dots (1-1) = 2, 1, 0$ .

Now, as the configuration is less than half-filled, the lower J-value is selected for lower energy. Thus, this gives rise to a  $^3P_0$  state.

For nitrogen atom, the determination of the ground state term symbol can be calculated through the same route. The electronic configuration for nitrogen is  $1s^2, 2s^2, 2p^3$ .



From the total component of orbital and spin angular momentum,  $L = (+1) + (0) + (-1) = 0$  and  $S = 1/2 + 1/2 + 1/2 = 3/2$ .

From L-S coupling,  $|L+S| \dots \dots |L-S|$ ;  $(0 + 3/2) = 3/2$ .

Now, as the configuration is half-filled, the only J-value is bound to be selected for lower energy. Thus, this gives rise to a  $^4S_{3/2}$  state.

For trivalent vanadium ion ( $V^{3+}$ ), the electronic configuration can be given as  $1s^2, 2s^2, 2p^6, 3s^2, 3p^6, 4s^0, 3d^2$ .

$l_z$	+2	+1	0	-1	-2
$3d$	↑	↑			

From the total component of orbital and spin angular momentum,  $L = (+2) + (+1) = 3$  and  $S = 1/2 + 1/2 = 1$ .

From L-S coupling,  $|L+S| \dots |L-S|$ ;  $(3 + 1) \dots (3 - 1) = 4, 3, 2$ . Now, as the configuration is less than half-filled, the lower J-value is selected for lower energy. Thus, this gives rise to a  ${}^3F_2$  state. However, the ground state term symbol for  $d^8$ -configuration will be  ${}^3F_4$ .

All the free ions terms (including ground states) for different electronic configurations are summarized in the following table. However, it must be kept in mind that the ground state term symbol after L-S coupling will be different for more than half-filled and less than half-filled counterparts.

Table 6. The free ion terms and the corresponding ground electronic states for different types of electronic configuration.

Electronic configuration	Free ion terms	Ground State
$s^1$	${}^2S$	${}^2S$
$s^2$	${}^1S$	${}^1S$
$p^1, p^5$	${}^2P$	${}^2P$
$p^2, p^4$	${}^1S, {}^3P, {}^1D$	${}^3P$
$p^3$	${}^4S, {}^2P, {}^2D$	${}^4S$
$p^6$	${}^1S$	${}^1S$
$d^1, d^9$	${}^2D$	${}^2D$
$d^2, d^8$	${}^1S, {}^3P, {}^1D, {}^3F, {}^1G$	${}^3F$
$d^3, d^7$	${}^4F, {}^4P, {}^2H, {}^2G, {}^2F, {}^2D, {}^2D, {}^2P$	${}^4F$
$d^4, d^6$	${}^5D, {}^3H, {}^3G, {}^3F, {}^3F, {}^3D, {}^3P, {}^3P, {}^1I, {}^1G, {}^1G, {}^1F, {}^1D, {}^1D, {}^1S, {}^1S$	${}^5D$
$d^5$	${}^2I, {}^2H, {}^2G, {}^2G, {}^2F, {}^2F, {}^2D, {}^2D, {}^2D, {}^2P, {}^2S, {}^4G, {}^4F, {}^4D, {}^4P, {}^6S$	${}^6S$
$d^{10}$	${}^1S$	${}^1S$

It is also worthy to note that the ground state term symbol for all fully-filled subshells like  $s^2$ ,  $p^6$ , or  $d^{10}$  is  ${}^1S$  always which also includes the one and only microstate available.

### ❖ Correlation and Spin-Orbit Coupling in Free Ions for 1st Series of Transition Metals

The energy of different free ion terms primarily depends on the spin-spin interaction, yielding the most stable state with the highest multiplicity. Furthermore, if the values of spin multiplicity for two different states are equivalent, the value of resultant angular momentum will be the deciding factor in the determination of the lower energy term. A higher value of  $L$  gives the lower energy state and the vice-versa is also true. The energy dependence of different terms upon total angular momentum is configuration-specific in nature. The perturbed Hamiltonian of spin-orbital interaction can have both types of effect, stabilization or destabilization, over the energy states and depends upon the magnitude of  $J$ -value. It has been proved that the interaction of spin-orbital motion destabilizes the less than half filled configuration and stabilizes the more than half-filled.

Hence, a lower  $J$ -value for less than half-filled and a higher  $J$ -value for more than half will give the lower energy. However, the actual value of the energies for different terms, and hence their relative ordering, must be determined from the analysis of spectroscopic data. The correlation diagram of different free ion terms and thereafter the effect of  $L$ - $S$  interaction for different ions can be given as:

#### 1. $\text{Sc}^{2+}$ and $\text{Cu}^{2+}$ ( $d^1$ , $d^9$ ):

The number of unpaired electrons and hence microstates in  $\text{Sc}^{2+}$  ( $d^1$ ) and  $\text{Cu}^{2+}$  ( $d^9$ ) are the same. The one and only term symbol containing all the 10 microstates is  ${}^2D$ , which also represents the ground electronic state. However, the splitting pattern of  ${}^2D$  term due to  $L$ - $S$  coupling for  $\text{Cu}^{2+}$  ( $d^9$ ) is just the reverse of what is for  $\text{Sc}^{2+}$  ( $d^1$ ).

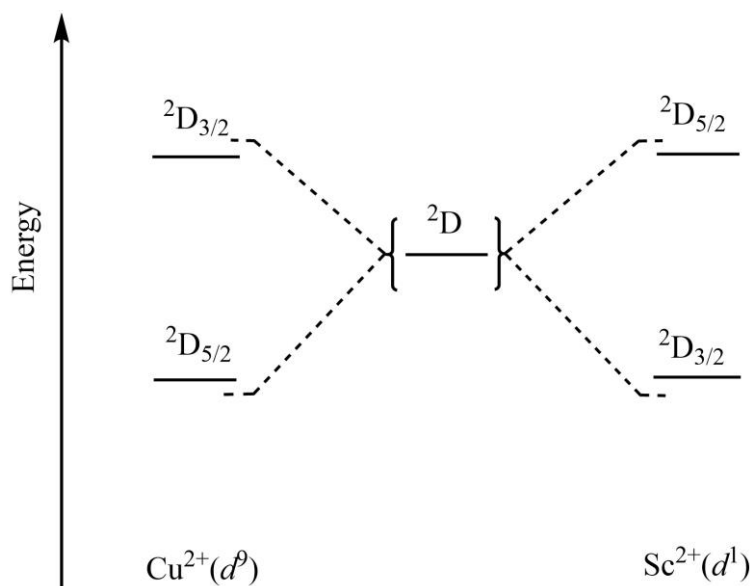


Figure 2. Correlation and spin-orbital coupling of free ion terms of  $\text{Sc}^{2+}$  and  $\text{Cu}^{2+}$ .

## 2. $V^{3+}$ and $Ni^{2+}$ ( $d^2$ , $d^8$ ):

The number of unpaired electrons and hence microstates in  $V^{3+}$  ( $d^2$ ) and  $Ni^{2+}$  ( $d^8$ ) are the same. All the 45 microstates for  $d^2$  and  $d^8$ -configurations are distributed in  $^1S$ ,  $^3P$ ,  $^1D$ ,  $^3F$  and  $^1G$  term symbols with  $^3F$  as the ground electronic state. However, the splitting pattern of  $^3F$  term due to L-S coupling for  $Ni^{2+}$  ( $d^8$ ) is just the reverse of what is for  $V^{3+}$  ( $d^2$ ).

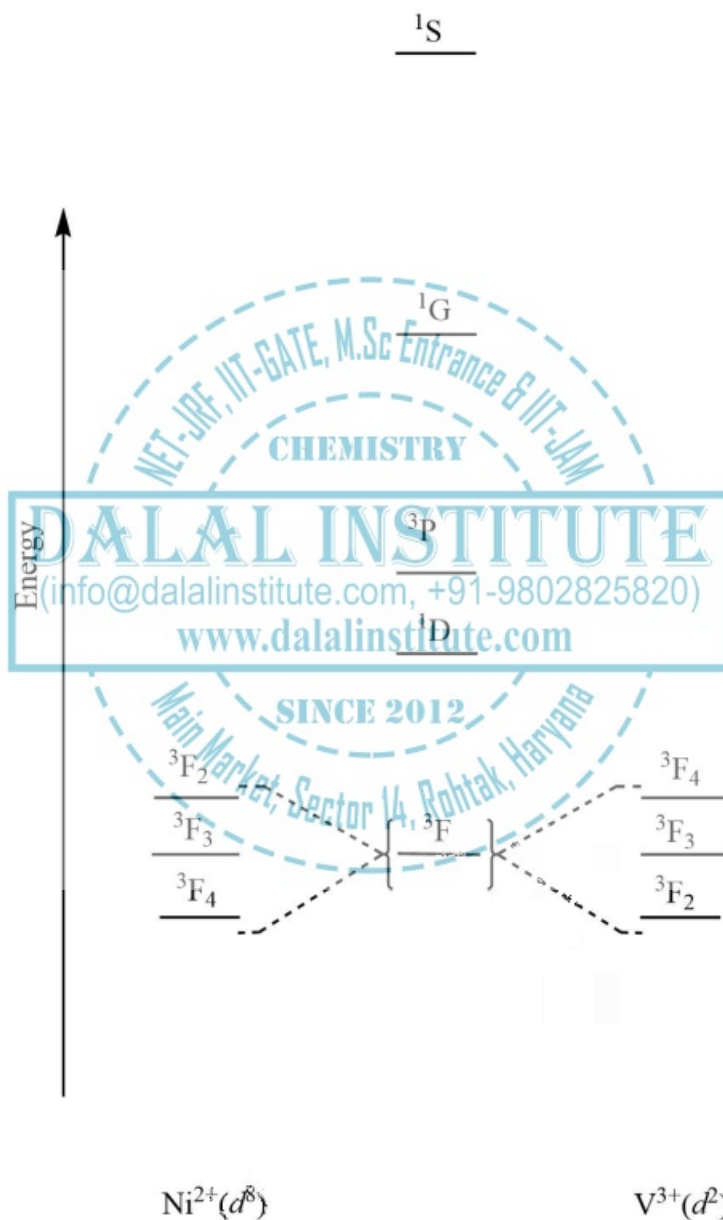


Figure 3. Correlation and spin-orbital coupling of free ion terms of  $V^{3+}$  and  $Ni^{2+}$ .

### 3. $\text{Cr}^{3+}$ and $\text{Co}^{2+}$ ( $d^3$ , $d^7$ ):

The number of unpaired electrons and hence microstates in  $\text{Cr}^{3+}$  ( $d^3$ ) and  $\text{Co}^{2+}$  ( $d^7$ ) are the same. All the 120 microstates for  $d^3$  and  $d^7$ -configurations are distributed in  $^4\text{F}$ ,  $^4\text{P}$ ,  $^2\text{H}$ ,  $^2\text{G}$ ,  $^2\text{F}$ ,  $^2\text{D}$ ,  $^2\text{D}$  and  $^2\text{P}$  term symbols with  $^4\text{F}$  as the ground electronic state. However, the splitting pattern of  $^4\text{F}$  term due to L-S coupling for  $\text{Co}^{2+}$  ( $d^7$ ) is just the reverse of what is for  $\text{Cr}^{3+}$  ( $d^3$ ).

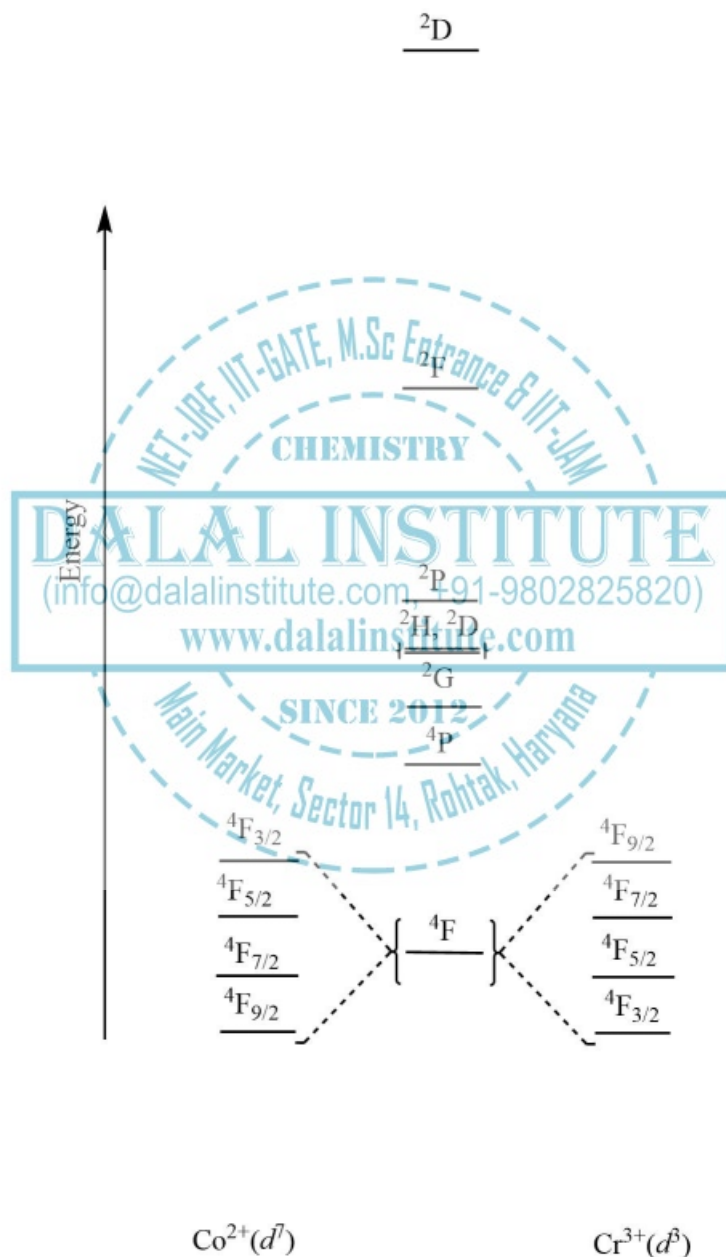


Figure 4. Correlation and spin-orbital coupling of free ion terms of  $\text{Cr}^{3+}$  and  $\text{Co}^{2+}$ .

#### 4. $\text{Mn}^{3+}$ and $\text{Fe}^{2+}$ ( $d^4$ , $d^6$ ):

The number of unpaired electrons and hence microstates in  $\text{Mn}^{3+}$  ( $d^4$ ) and  $\text{Fe}^{2+}$  ( $d^6$ ) are the same. All the 210 microstates for  $d^4$  and  $d^6$ -configurations are distributed in  ${}^5\text{D}$ ,  ${}^3\text{H}$ ,  ${}^3\text{G}$ ,  ${}^3\text{F}$ ,  ${}^3\text{F}$ ,  ${}^3\text{D}$ ,  ${}^3\text{P}$ ,  ${}^3\text{P}$ ,  ${}^1\text{I}$ ,  ${}^1\text{G}$ ,  ${}^1\text{G}$ ,  ${}^1\text{F}$ ,  ${}^1\text{D}$ ,  ${}^1\text{D}$ ,  ${}^1\text{S}$  and  ${}^1\text{S}$  term symbols with  ${}^5\text{D}$  as the ground electronic state. However, the splitting pattern of  ${}^5\text{D}$  term due to L-S coupling for  $\text{Fe}^{2+}$  ( $d^6$ ) is just the reverse of what is for  $\text{Mn}^{3+}$  ( $d^4$ ).

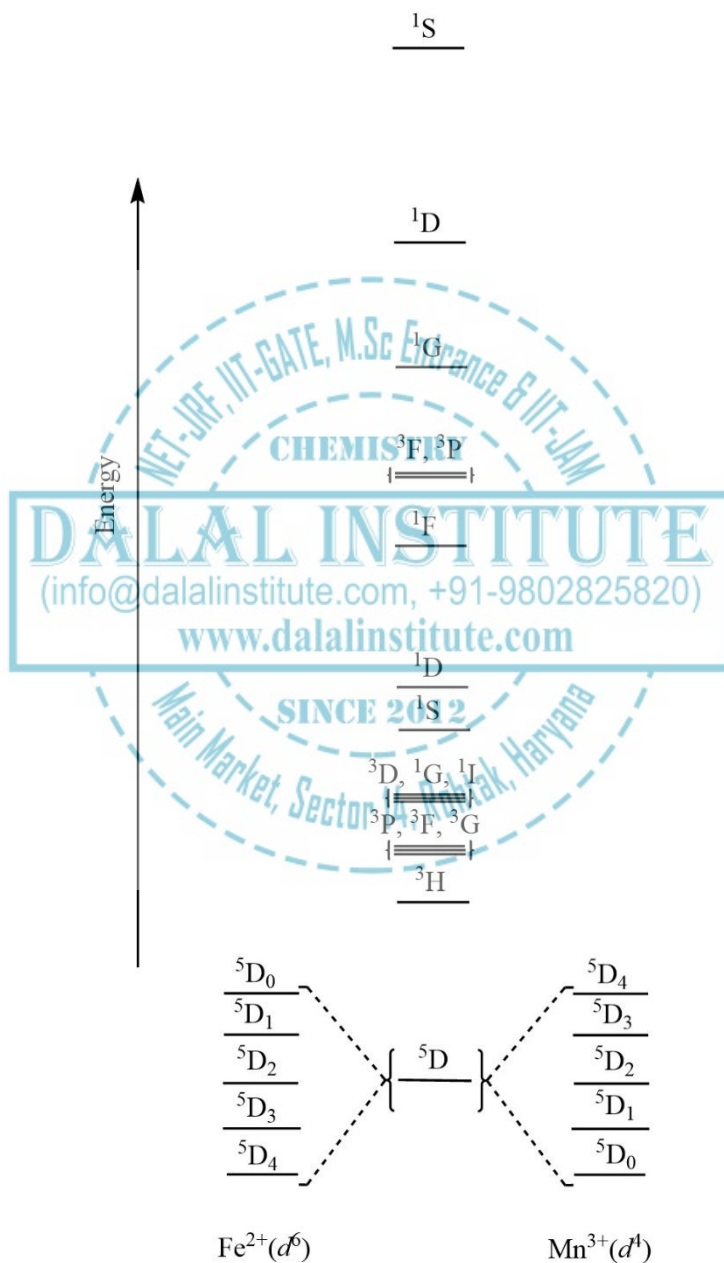


Figure 5. Correlation and spin-orbital coupling of free ion terms of  $\text{Mn}^{3+}$  and  $\text{Fe}^{2+}$ .

**5. Fe<sup>3+</sup> and Mn<sup>2+</sup> (d<sup>5</sup>):**

The number of unpaired electrons and hence microstates in Fe<sup>3+</sup> (d<sup>5</sup>) and Mn<sup>2+</sup> (d<sup>5</sup>) are the same. All the 252 microstates for d<sup>5</sup>-configurations are distributed in <sup>2</sup>I, <sup>2</sup>H, <sup>2</sup>G, <sup>2</sup>G, <sup>2</sup>F, <sup>2</sup>F, <sup>2</sup>D, <sup>2</sup>D, <sup>2</sup>D, <sup>2</sup>D, <sup>2</sup>P, <sup>2</sup>S, <sup>4</sup>G, <sup>4</sup>F, <sup>4</sup>D, <sup>4</sup>P and <sup>6</sup>S term symbols with <sup>6</sup>S as the ground electronic state. Moreover, the splitting of <sup>6</sup>S term due to L-S coupling is not possible because of the absence of resultant orbital motion. However, higher-energy free ion terms with 4 or two multiplicities will get split.

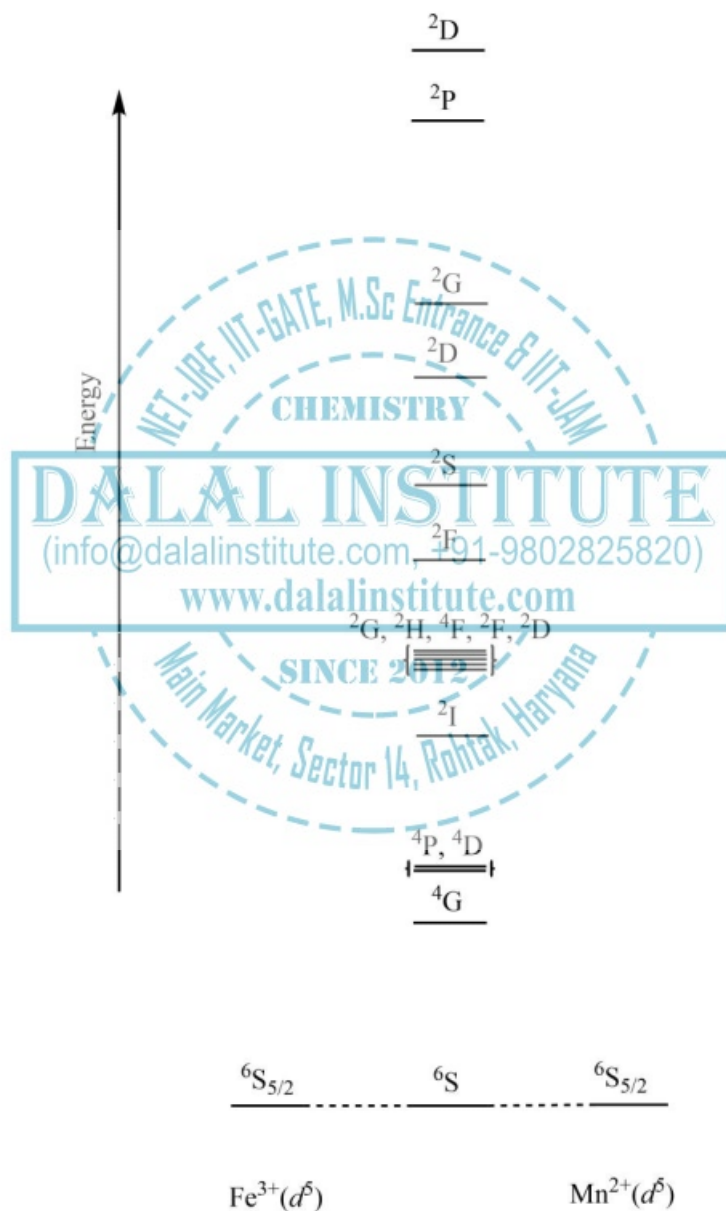


Figure 6. Correlation and spin-orbital coupling of free ion terms of Fe<sup>3+</sup> and Mn<sup>2+</sup>.

## ❖ Orgel and Tanabe-Sugano Diagrams for Transition Metal Complexes ( $d^1 - d^9$ States)

It is a well-known fact that electronic transitions are always accompanied by vibrational as well as rotational changes which results in a considerable broadening of the bands in the UV-visible spectra of transition metal complexes too. The nature of these transitions is quite complex to understand and requires some basic knowledge of quantum mechanics and chemical applications of group theory.

### The selection rules:

The selection rules governing the electronic spectra of transition metal complexes are given below.

1. There should be no change in the number of unpaired electrons. In other words, for all the multiplicity allowed transitions,  $\Delta S = 0$ . Hence, a triplet-triplet or singlet-singlet transitions will be multiplicity allowed while a singlet-triplet or triplet-singlet will be multiplicity forbidden.
2. If the complex possesses the center of symmetry, all the transitions which do not involve a change of  $\pm 1$  in angular momentum quantum number are Laporte forbidden. In other words, in molecular geometries with the centre of symmetry, electronic transitions with  $\Delta l = \pm 1$  are Laporte allowed. Hence, are the  $d-d$  transitions in free ions as well as in perfectly octahedral environment are Laporte forbidden.

Relaxation of the abovementioned rules can occur through two mechanisms. The first one is the spin-orbit coupling which gives rise to weak spin forbidden bands. The second one is the absence of perfect octahedral geometry due to the presence of a different ligand or vibronic coupling in which a perfect octahedral complex may have some allowance of  $d-d$  transitions. vibrations where the molecule is asymmetric and the absorption of light at that moment is then possible. Both of these effects (vibronic coupling or six dissimilar ligands) generally mixes the  $d$  and  $p$ -orbitals of the transition metal so that the transitions are no longer purely  $d-d$  in nature. For example, the tetrahedral  $[\text{MnCl}_4]^{2-}$  is colored because it does not possess the centre of symmetry and  $[\text{Co}(\text{NH}_3)_5\text{Cl}]^{2+}$  also lacking the center of symmetry due to the presence of one  $\text{Cl}^-$  ligand, and therefore is colored. However, the perfect octahedral geometries like  $[\text{Mn}(\text{H}_2\text{O})_6]^{2+}$  with a  $d^5$ -electronic configuration is expected to be colorless (spin forbidden and Laporte forbidden) but does show a pale-pink color which can be explained in term of slight vibronic allowance.

### The splitting of free ion terms:

It is pretty interesting to note that the degeneracy of free-ion terms like  $^2D$  or  $^3F$  can be removed not only by L-S coupling alone but can also be removed by the perturbation produced by the ligands. Moreover, the wavefunctions for S, P, D, F or G states have the same symmetry as that  $s$ ,  $p$ ,  $d$ ,  $f$  or  $g$  orbitals sets; which means that the splitting pattern of D and F states will same as  $d$  and  $f$ -subshell, respectively.

The  $s$ -orbital is spherically symmetric in nature and is not affected by any crystal field. Hence, S state also does not get split in any type of ligand field. The  $p$ -orbitals are directional in nature and are affected by different types of crystal field differently. Hence, P state may or may not get split in the presence of ligand field. For example, P state does not get split in octahedral or tetrahedral field but does get split in square planar

crystal field. The  $d$ -orbitals are also directional in nature and are affected by different types of crystal field differently. Hence, D state does get split in the presence of the ligand field. For example, D state does get split in the octahedral or tetrahedral field with triply and doubly degenerate sets but the splitting pattern and degeneracy are totally different in pentagonal bipyramidal crystal field. The splitting profile of different electronic states in octahedral and tetrahedral crystal fields in the following tables, which will be used very frequently in the further text of this chapter.

Table 7. Splitting of free ion terms in the tetrahedral crystal field.

Electronic state	Symmetry designation in the tetrahedral field (Mulliken symbols)
S	$A_1$
P	$T_1$
D	$E + T_2$
F	$A_2 + T_1 + T_2$
G	$A_1 + E + T_1 + T_2$
H	$E + T_1 + T_1 + T_2$
I	$A_1 + A_2 + E + T_1 + T_2 + T_2$

Table 8. Splitting of free ion terms in the octahedral crystal field.

Electronic state	Symmetry designation in the octahedral field (Mulliken symbols)
S	$A_{1g}$
P	$T_{1g}$
D	$E_g + T_{2g}$
F	$A_{2g} + T_{1g} + T_{2g}$
G	$A_{1g} + E_g + T_{1g} + T_{2g}$
H	$E_g + T_{1g} + T_{1g} + T_{2g}$
I	$A_{1g} + A_{2g} + E_g + T_{1g} + T_{2g} + T_{2g}$

The A, E and T represent singly, doubly and triply degenerate states, respectively. The presence of “g” in symmetry designations of the octahedral field is for the gerade or centrosymmetric environment.

### Terms correlation in the tetrahedral and octahedral field:

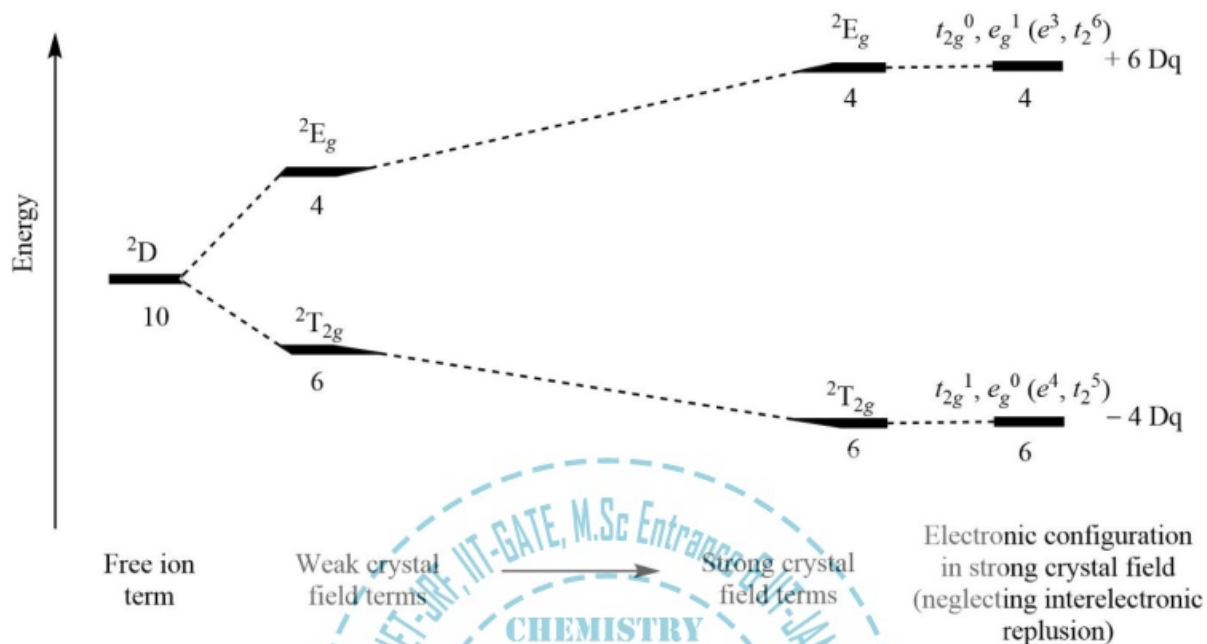
The qualitative description of different energy term for  $d^n$  and  $d^{10-n}$  configuration, from free ion to strong crystal field configurations ignoring inter-electronic repulsions, can be given as:

1. The total number of energy levels remain the same under the influence of weak and strong crystal fields.
2. The one to one correspondence of different energy levels in a strong crystal field may get stabilized or destabilized in comparison to the weak field case.
3. Energy levels of the same symmetry never cross each other and each level has a contribution in its energy from all other energy states of the same symmetry.
4. Term correlation for  $d^1, d^9, d^2, d^8$  configuration are shown completely while for  $d^3, d^4, d^5, d^6, d^7$  are shown partially by taking only lower energy levels.
5. According to hole formalism, the number of microstates and hence all free ion terms for  $d^n$  and  $d^{10-n}$  configuration are same. Now, as the magnitude of the crystal field experienced positive electrons is the same as what experienced by the negative electrons, but is of opposite sign. Therefore, the splitting pattern for  $d^n$  and  $d^{10-n}$  configurations are opposite of each other.
6. Owing to the hole formalism in quantum mechanics, strong field configuration of  $t_{2g}^4, t_{2g}^5, e_g^3$  give rise to the same terms as given by the strong field configuration of  $t_{2g}^2, t_{2g}^1, e_g^1$ . However, weaker inter-electronic repulsion is considered as the perturbation over stronger  $V_o$ .
7. The splitting pattern of  $d^n$  tetrahedral is just the opposite of what is for  $d^n$  octahedral. However, no  $g$  or  $u$  are used in the tetrahedral case because there is no center of symmetry in a tetrahedral geometry.

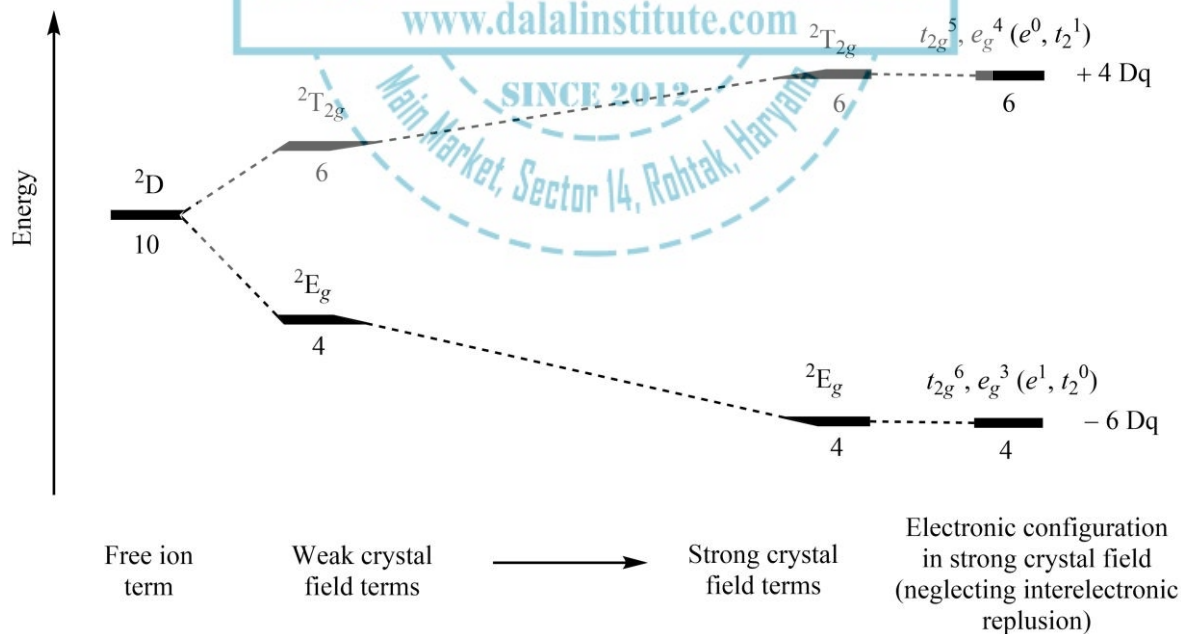
It has already been discussed that the total number of microstates for electronic configuration without inter-electronic repulsion or with inter-electronic repulsion (free ion terms) remains the same. Furthermore, the number of microstates also remains same even in the presence of weak or strong crystal field; and when the inter-electronic repulsion is completely neglected in comparison to the ligand field strength, the calculation of microstates is carried out individually for  $t_{2g}$  and  $e_g$  set and multiplied afterward to give the total.

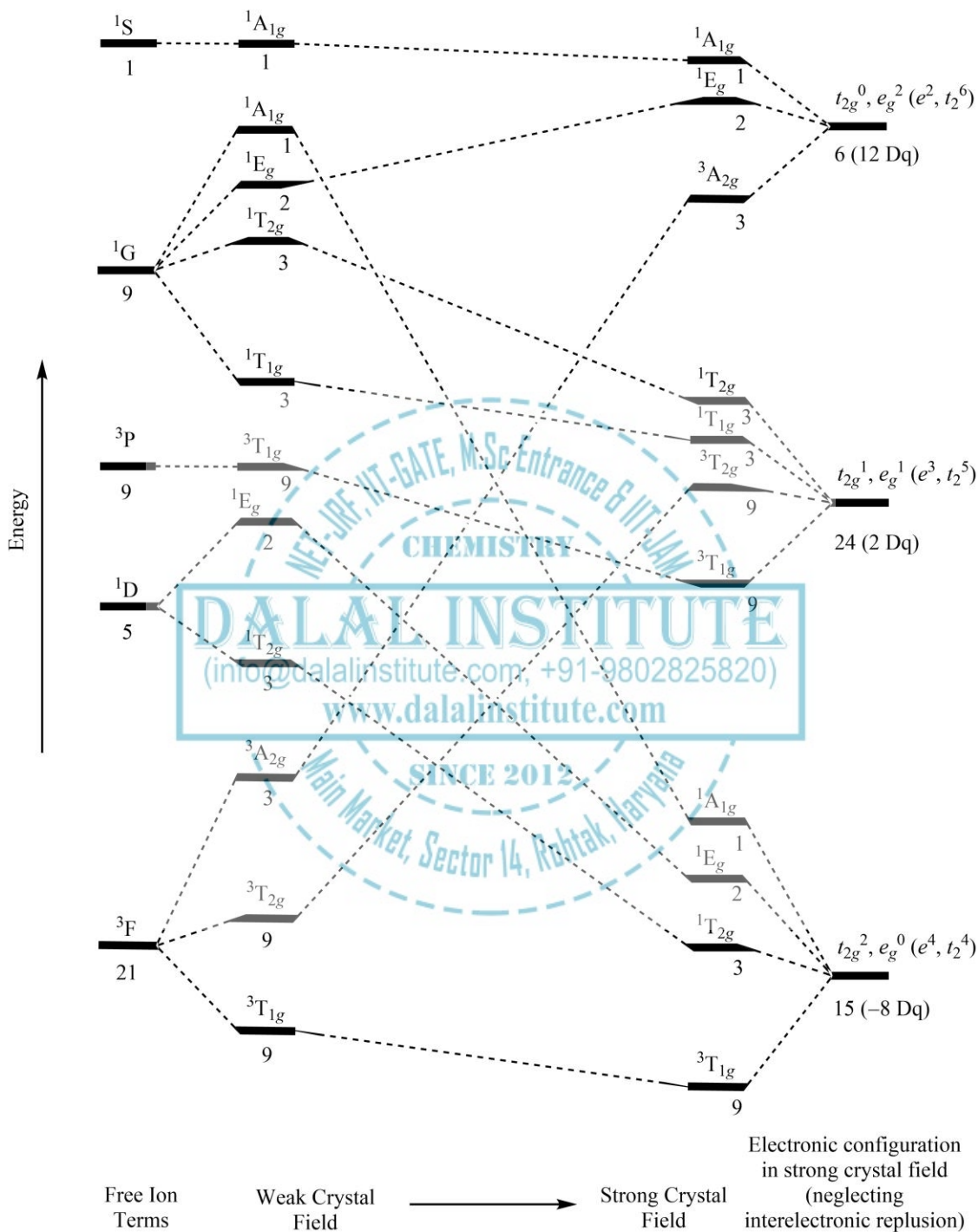
Furthermore, the strength of the crystal field does not alter the ground state Mulliken symbol in the case of  $d^1, d^9$ -octahedral or tetrahedral complexes. However, in the case of  $d^2-d^8$  electronic configurations, the splitting pattern of free ion term at weak and strong crystal fields is quite different. Generally, the energy of some irreducible component of low multiplicity free ion term decreases so rapidly with the increase in the strength of the crystal field that it becomes the ground state symbol. In other words, the ground state term symbol of metal complexes with  $d^2-d^8$  electronic configurations is different in weak and strong crystal fields. For example, the ground state term symbol for  $d^5$ -configuration with small ligand field is  ${}^6A_{1g}$  (from  ${}^6S$ ) but as the magnitude of crystal field increases, the  ${}^2T_{2g}$  Mulliken state (from  ${}^2I$ ) becomes highly stable and also make up the ground electronic state.

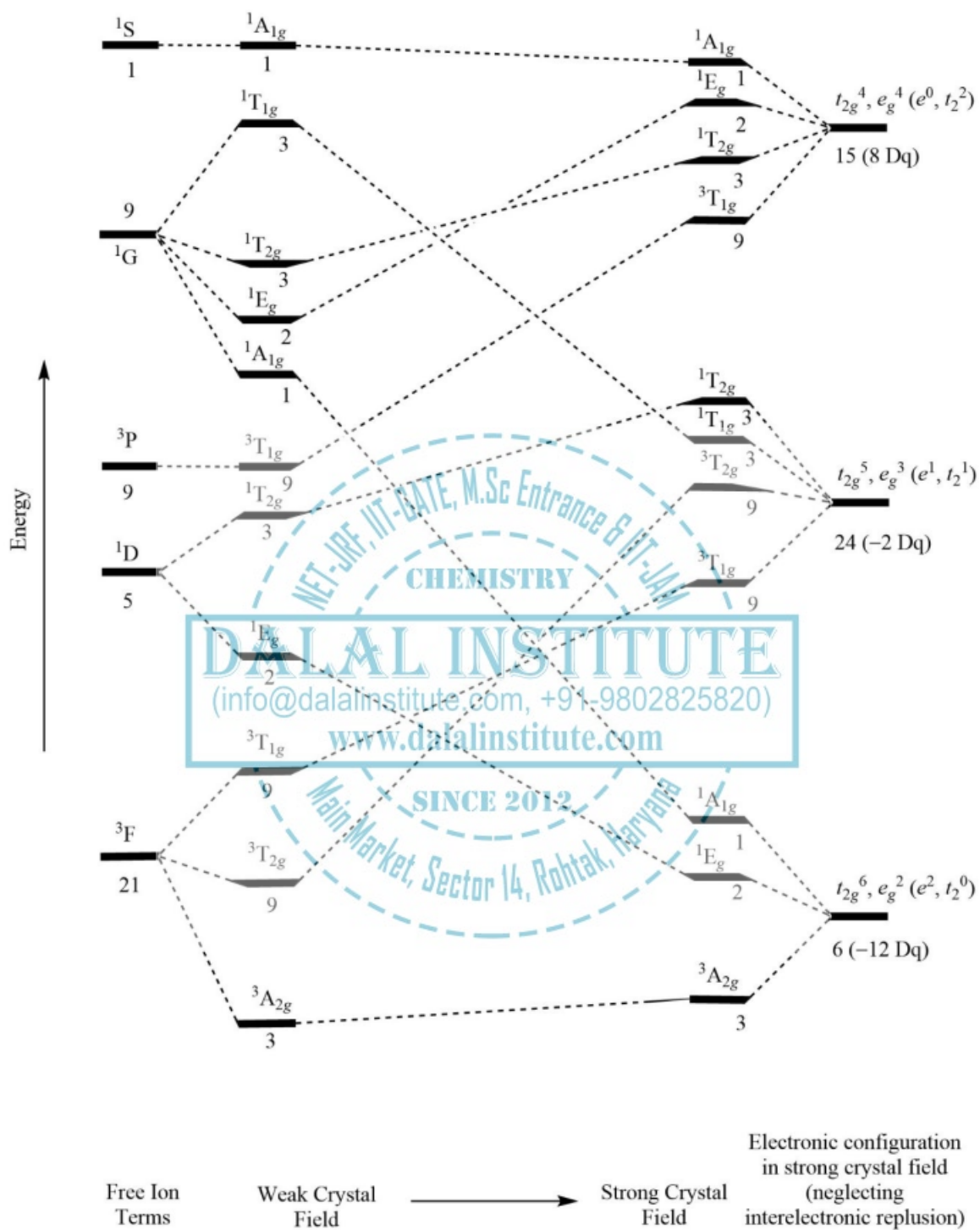
The correlation diagrams (with the corresponding microstates shown below each level) for different electronic configurations in transition metal complexes with four-coordinated tetrahedral and six-coordinated octahedral symmetry are given below.

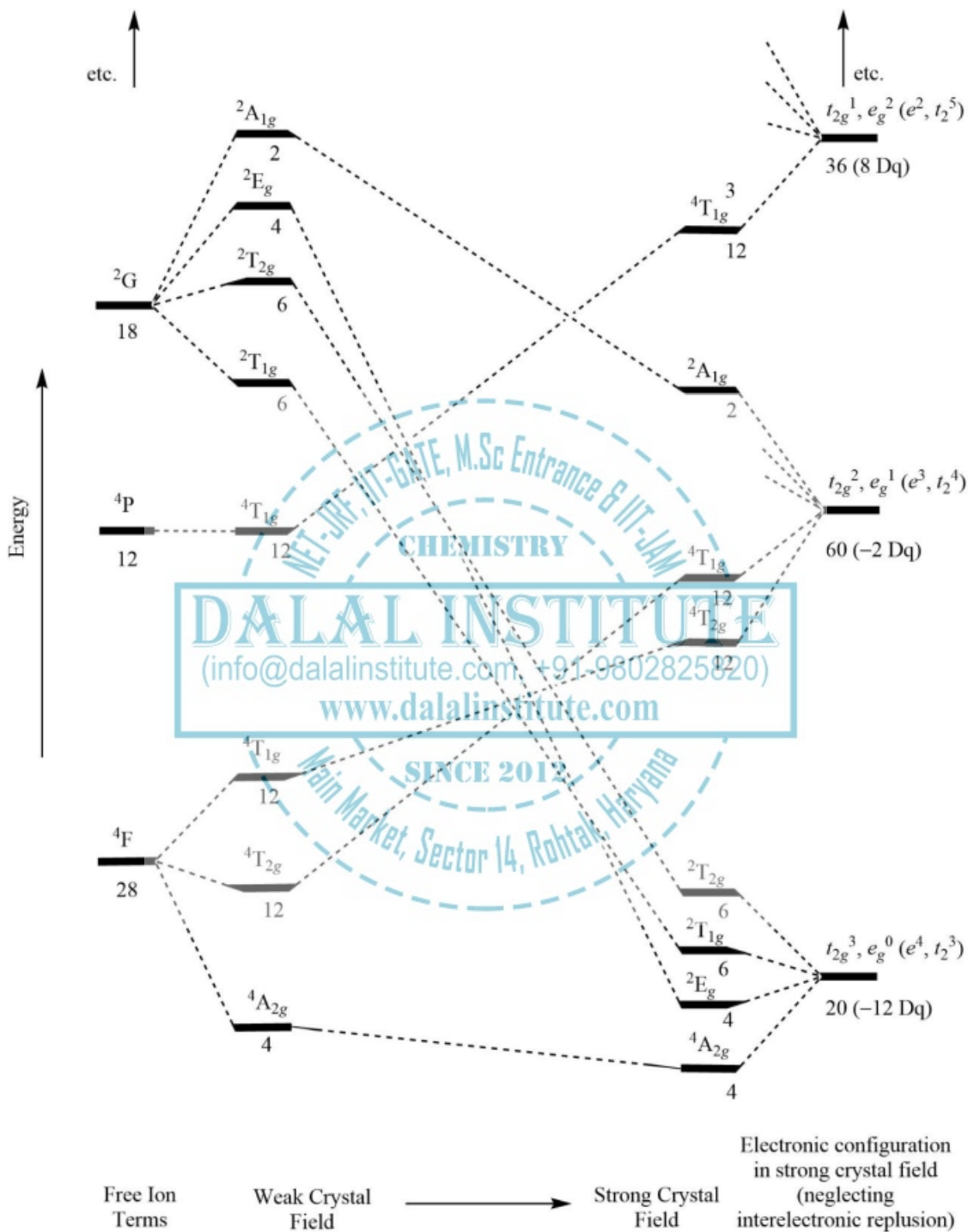
1.  $d^1, d^9$  systems:

 Figure 7. Qualitative correlation diagram for  $d^1$  octahedral and  $d^9$  tetrahedral complexes.

and


 Figure 8. Qualitative correlation diagram for  $d^9$  octahedral and  $d^1$  tetrahedral complexes.

2.  $d^2, d^8$  systems:Figure 9. Qualitative correlation diagram for  $d^2$  octahedral and  $d^8$  tetrahedral complexes.


 Figure 10. Qualitative correlation diagram for  $d^8$  octahedral and  $d^2$  tetrahedral complexes.

3.  $d^3, d^7$  systems:Figure 11. Qualitative correlation diagram for  $d^3$  octahedral and  $d^7$  tetrahedral complexes.

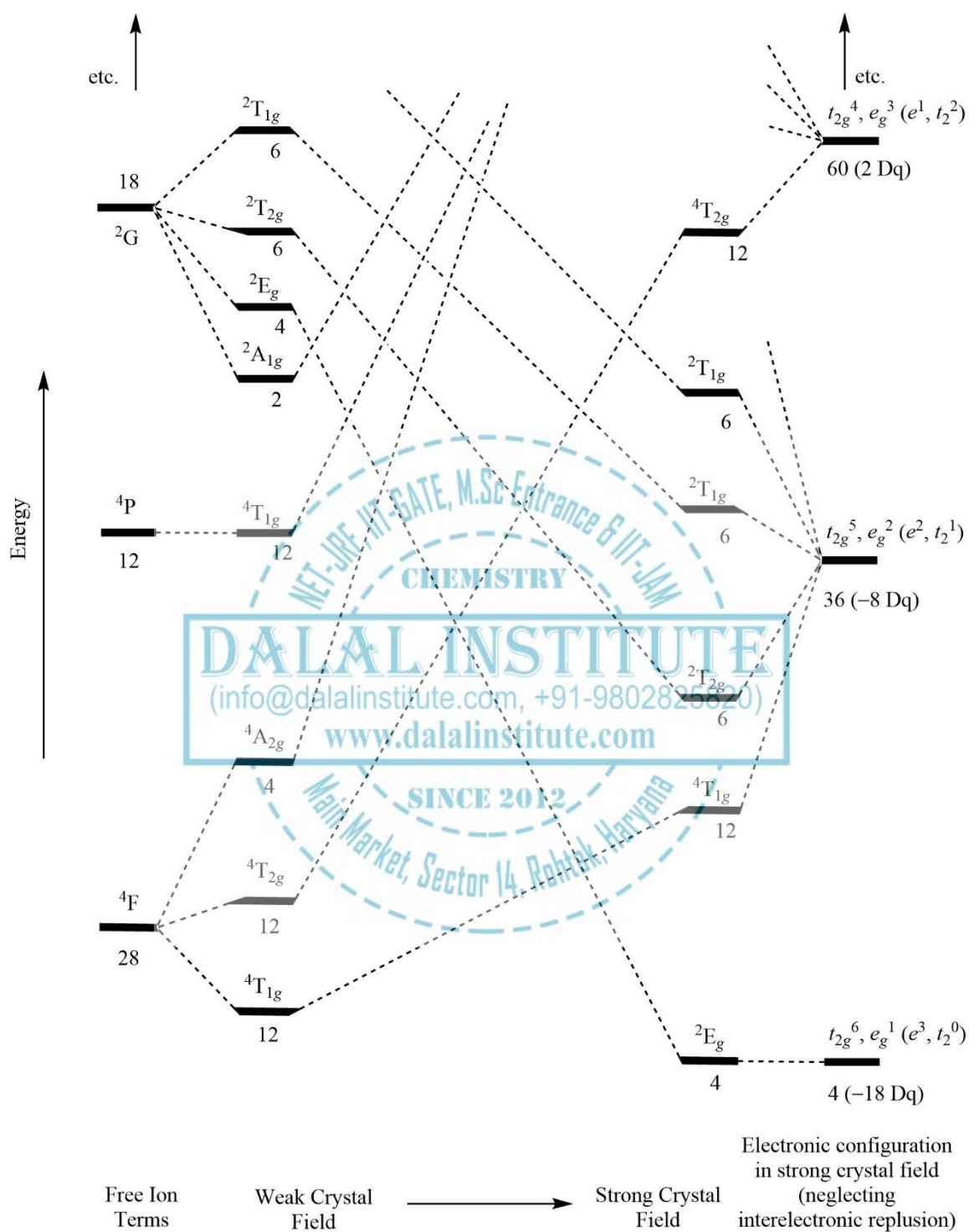
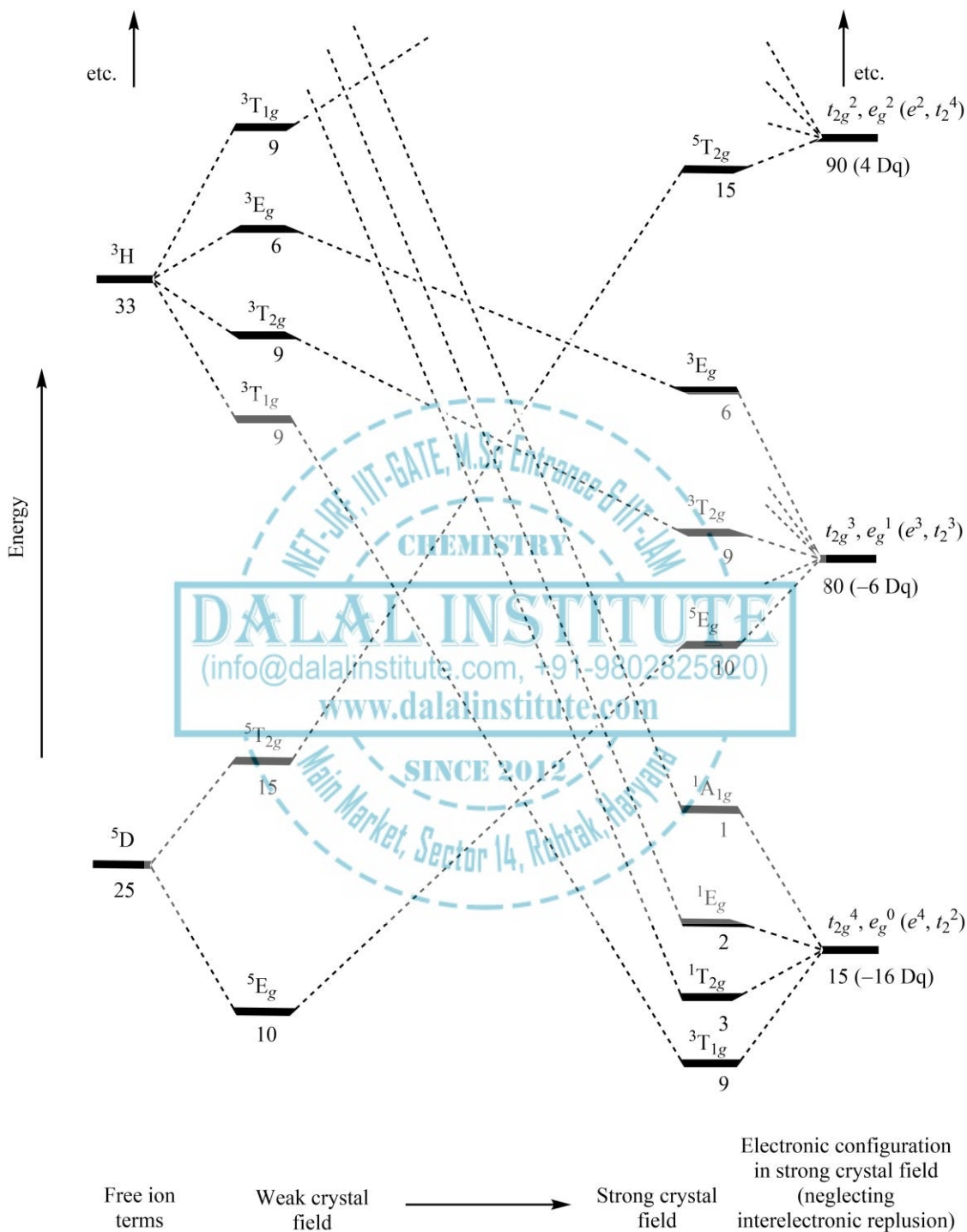
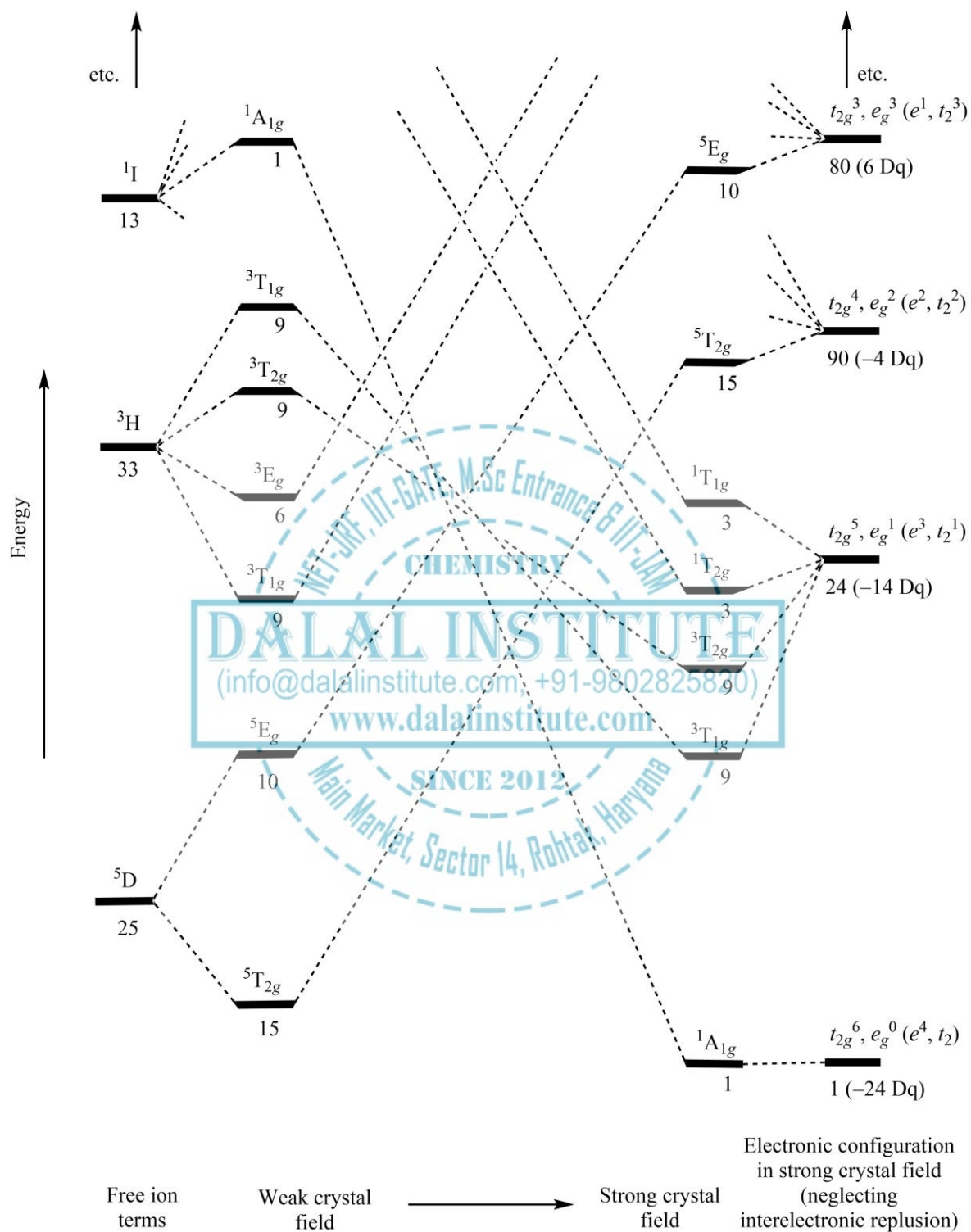
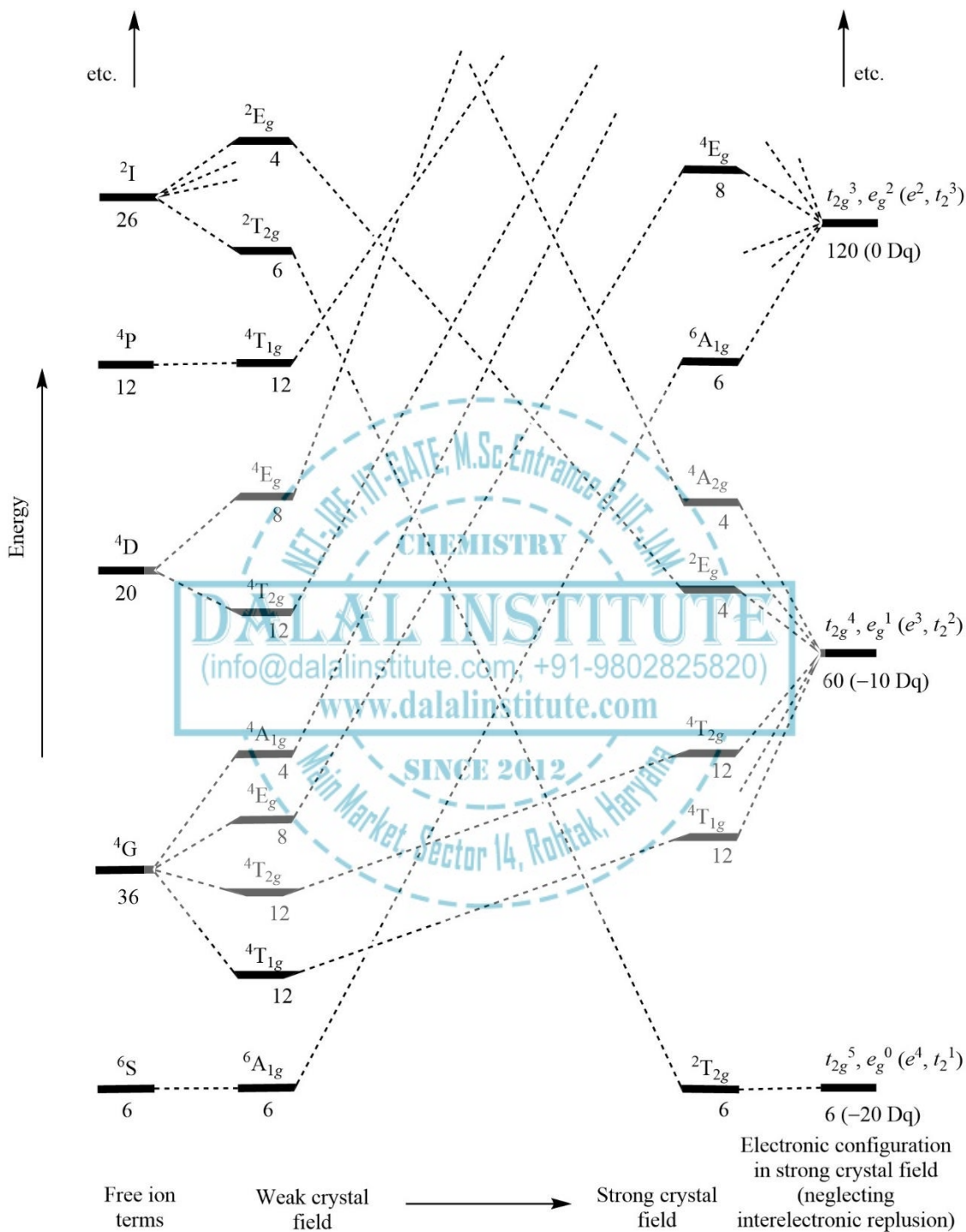


Figure 12. Qualitative correlation diagram for  $d^7$  octahedral and  $d^3$  tetrahedral complexes.

4.  $d^4$ ,  $d^6$  systems:Figure 13. Qualitative correlation diagram for  $d^4$  octahedral and  $d^6$  tetrahedral complexes.


 Figure 14. Qualitative correlation diagram for  $d^6$  octahedral and  $d^4$  tetrahedral complexes.

5.  $d^5$  systems:Figure 15. Qualitative correlation diagram for  $d^5$  octahedral and tetrahedral complexes.

### ➤ Orgel Diagrams

Orgel diagrams are the oversimplified version of correlation diagrams that show the relative energies of electronic terms in transition metal complexes. They are named after their inventor, Leslie Orgel. These diagrams are restricted only to show weak field cases and offer no information about strong field cases. Because Orgel diagrams are qualitative, no energy calculations can be performed from these diagrams. Moreover, Orgel diagrams only show the symmetry states of the highest spin multiplicity instead of all possible terms, unlike a general correlation diagram. Thus, Orgel diagrams include only those transitions which are spin-allowed in nature, along with corresponding symmetry designations.

In an Orgel diagram, the parent term (P, D, or F) in the presence of no ligand field is located in the center of the diagram; and the Mulliken terms arising from different electronic configurations in a ligand field are represented at each side. There are two Orgel diagrams, one for  $d^1$ ,  $d^4$ ,  $d^6$ , and  $d^9$  configurations and the other with  $d^2$ ,  $d^3$ ,  $d^7$ , and  $d^8$  configurations. An Orgel diagram for  $d^5$  has also been very popular which includes spin-forbidden transitions too. In the Orgel diagram, lines with the same Russell-Saunders terms will diverge due to the non-crossing rule, but all other lines will be linear.

#### 1. $d^1$ , $d^9$ , $d^4$ , $d^6$ systems:

For the “D” Orgel diagram, the left side contains  $d^1$  and  $d^6$  octahedral, and  $d^4$  and  $d^9$  tetrahedral complexes. The right side contains  $d^4$  and  $d^9$  octahedral, and  $d^1$  and  $d^6$  tetrahedral complexes. The lowest energy absorption band on the left side of the spectrum is  $T_{2g} \rightarrow E_g$  while on the right side of the spectrum it is  $E_g \rightarrow T_{2g}$  transition.

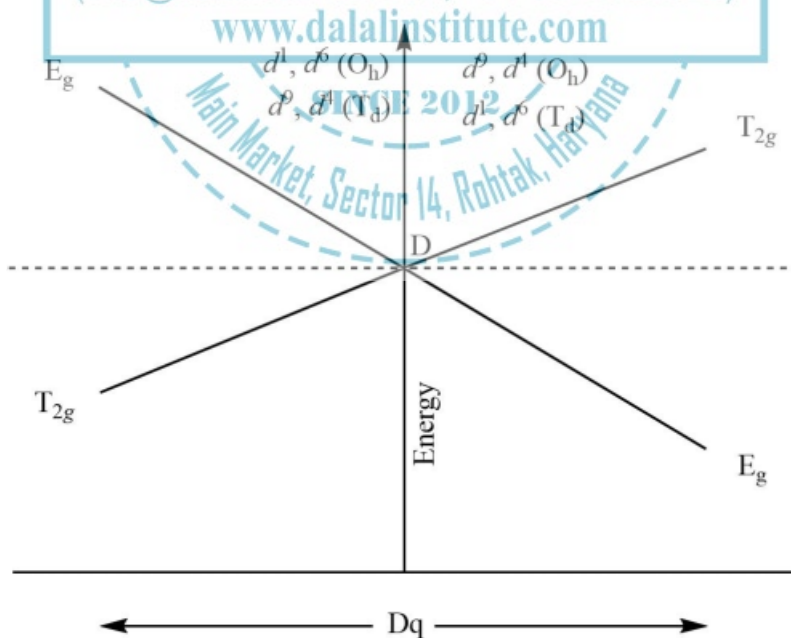


Figure 16. Orgel diagram for  $d^1$ ,  $d^9$ ,  $d^4$ ,  $d^6$  complexes in octahedral ( $O_h$ ) and tetrahedral ( $T_d$ ) crystal fields.

i) Spectra of  $d^1$  and  $d^9$  octahedral complexes:

The ground state term symbol for  $d^1$  and  $d^9$  complexes is  ${}^2D$ ; but the splitting pattern of their  ${}^2D$  states is just the opposite of each other, which can be attributed to the electron-hole inverse relationship or simply the hole-formalism. In other words, a  $d^9$  metal has an electron vacancy or “hole” in its  $d$ -subshell and thus can be considered as the inverse of the  $d^1$  arrangement. Therefore, despite having identical ground state term symbol  ${}^2D$  (split into  ${}^2T_{2g}$  and  ${}^2E_g$  in the octahedral field), the energy order of Mulliken states in  $d^9$ -configuration complexes will be just the inverse of what is in  $d^1$  system.

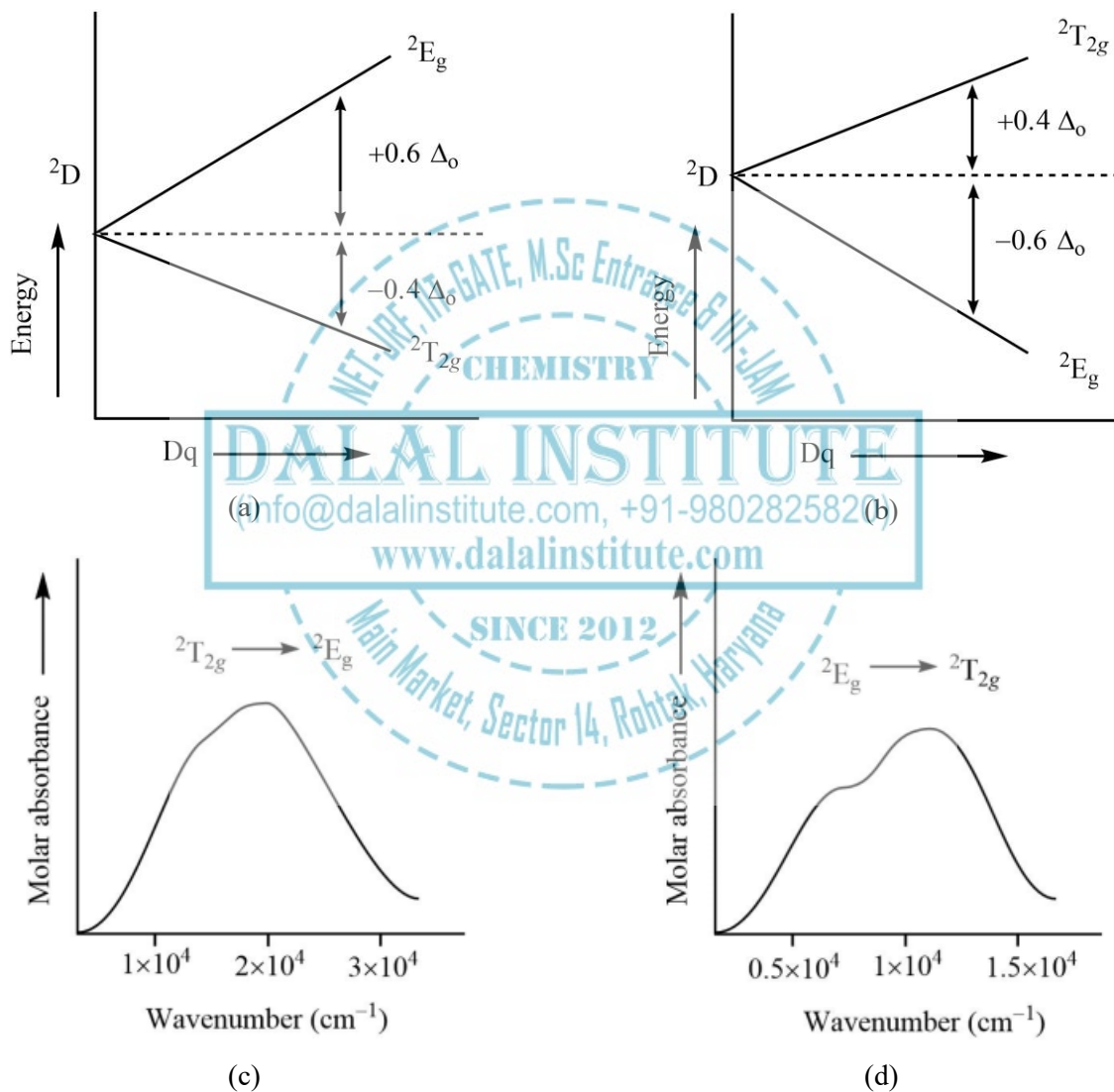


Figure 17. The splitting pattern of  ${}^2D$  state in octahedral complexes with (a)  $d^1$ -configuration and (b)  $d^9$ -configuration; and the corresponding electronic spectra of (c)  $[\text{Ti}(\text{H}_2\text{O})_6]^{3+}$  and (d)  $[\text{Cu}(\text{H}_2\text{O})_6]^{2+}$ .

ii) Spectra of  $d^1$  and  $d^9$  tetrahedral complexes:

In addition to the electron-hole inverse relationship for  $d^1$  and  $d^9$  octahedral complexes, an inverse relationship for octahedral-tetrahedral crystal field symmetries also exists. This is simply because the crystal fields of these two symmetries produce the inverse splitting patterns of the  $d$ -subshell. Therefore, despite having identical ground state term symbol  ${}^2D$  (split into  ${}^2T_2$  and  ${}^2E$  in the tetrahedral field), the energy order of Mulliken states in the tetrahedral field will be just the inverse of what is in octahedral systems. However, it is worthy to note that the subscript “g” or “u” cannot be used due to the lack of the center of symmetry.

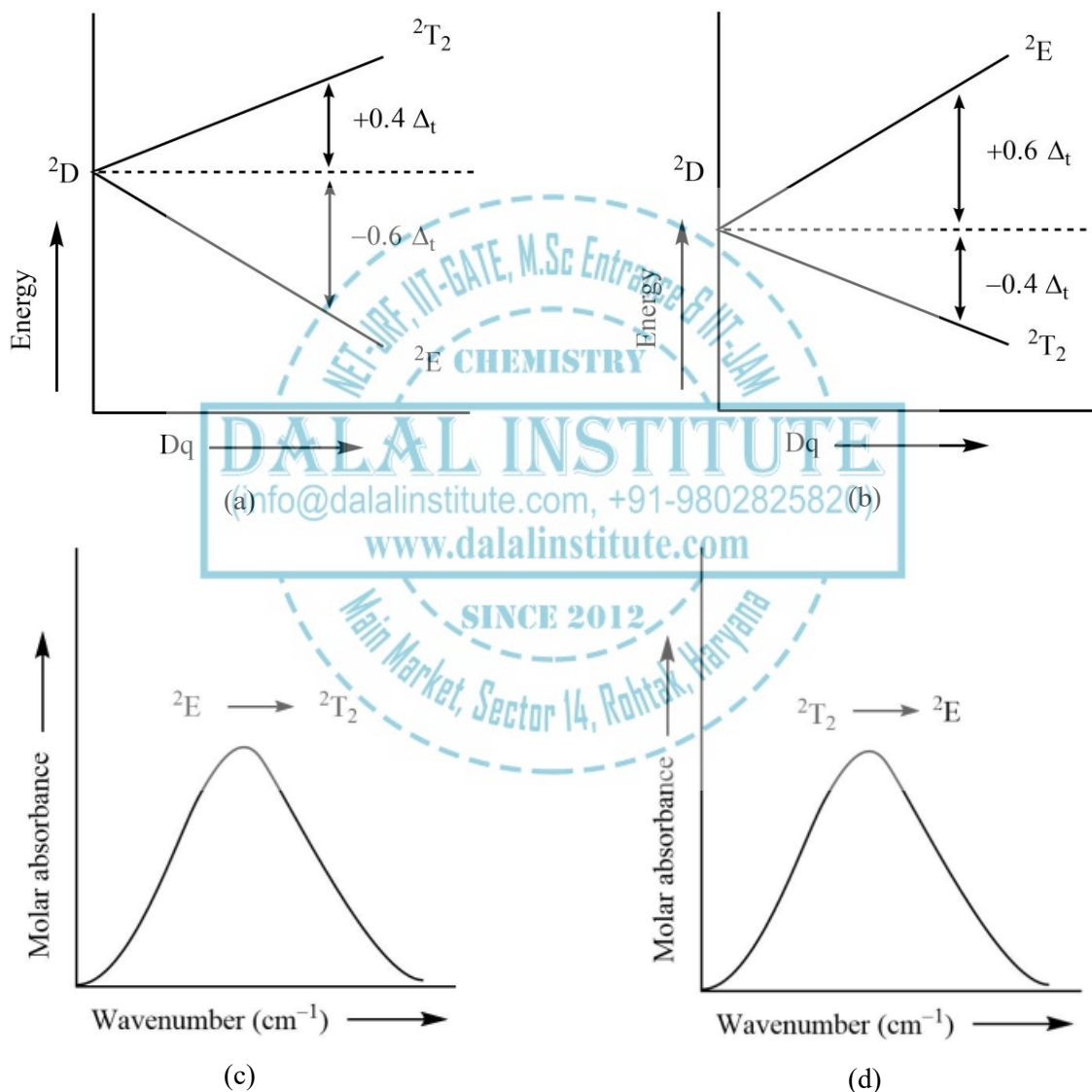


Figure 18. The splitting pattern of  ${}^2D$  state in tetrahedral complexes with (a)  $d^1$ -configuration and (b)  $d^9$ -configuration; and the corresponding electronic spectra of (c)  $ML_4$  ( $d^1$ ) and (d)  $ML_4$  ( $d^9$ ).

iii) Spectra of  $d^4$  and  $d^6$  octahedral complexes:

The ground state term symbol for  $d^4$  and  $d^6$  complexes is  $^5D$ ; but the splitting pattern of their  $^5D$  states is just the opposite of each other, which can be attributed to the electron-hole inverse relationship or simply the hole formalism. In other words, a  $d^6$  metal has an electron vacancy or “hole” in its  $d$ -subshell and thus can be considered as the inverse of the  $d^4$  arrangement. Therefore, despite having identical ground state term symbol  $^5D$  (split into  $^5T_{2g}$  and  $^5E_g$  in the octahedral field), the energy order of Mulliken states in  $d^6$  configuration will be just the inverse of what is in  $d^4$  system.

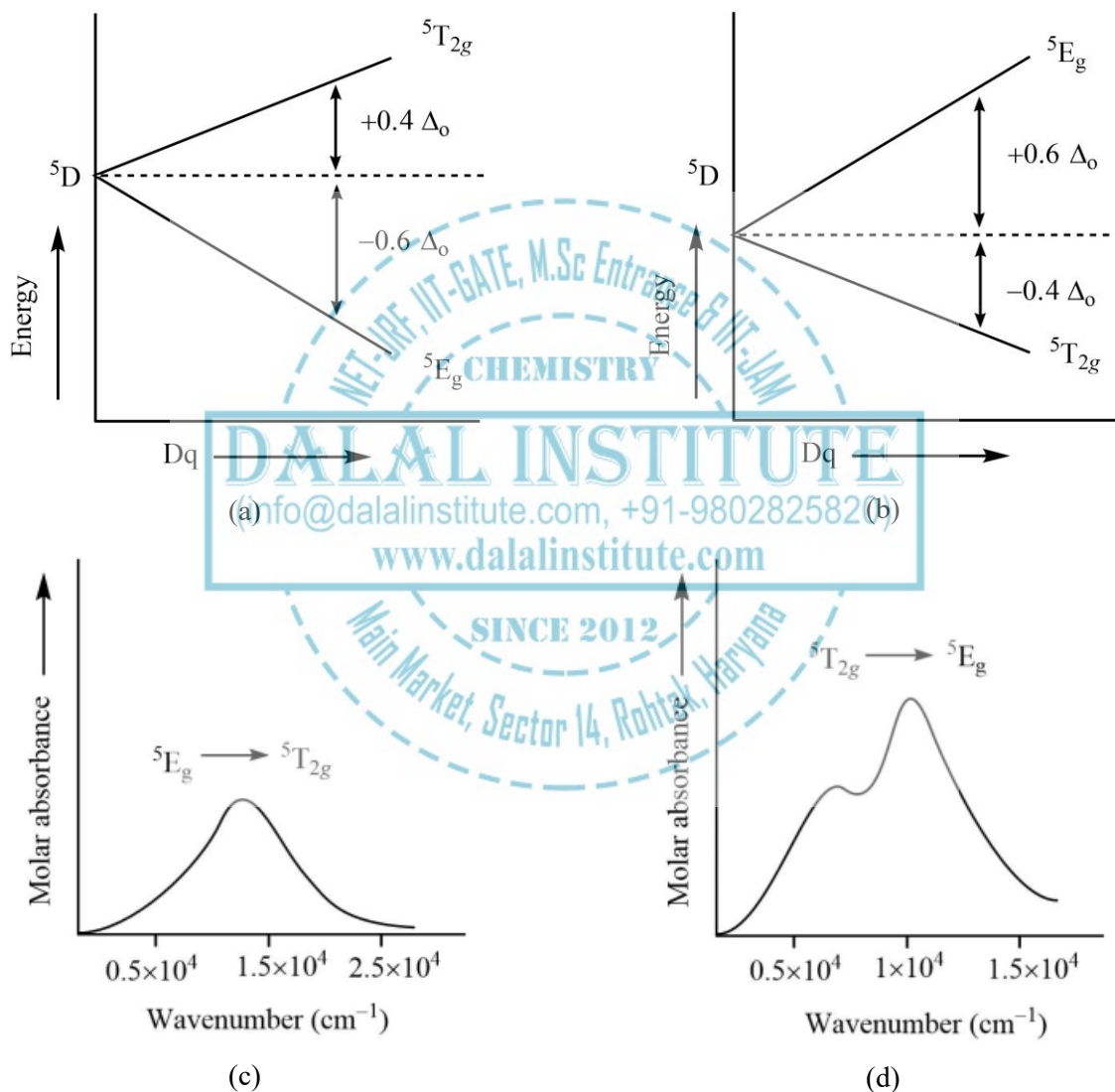


Figure 19. The splitting pattern of  $^5D$  state in octahedral complexes with (a)  $d^4$ -configuration and (b)  $d^6$ -configuration; and the corresponding electronic spectra of (c)  $[\text{Cr}(\text{H}_2\text{O})_6]^{2+}$  and (d)  $[\text{Fe}(\text{H}_2\text{O})_6]^{2+}$ .

iv) Spectra of  $d^4$  and  $d^6$  tetrahedral complexes:

In addition to the electron-hole inverse relationship for  $d^4$  and  $d^6$  octahedral complexes, an inverse relationship for octahedral-tetrahedral crystal field symmetries also exists. This is simply because the crystal fields of these two symmetries produce the inverse splitting pattern of the  $d$ -subshell. Therefore, despite having identical ground state term symbol  $^5D$  (split into  $^5T_2$  and  $^5E$  in the tetrahedral field), the energy order of Mulliken states in the tetrahedral field will be just the inverse of what is in octahedral systems. However, it is worthy to note that the subscript “g” or “u” cannot be used due to the lack of the center of symmetry.

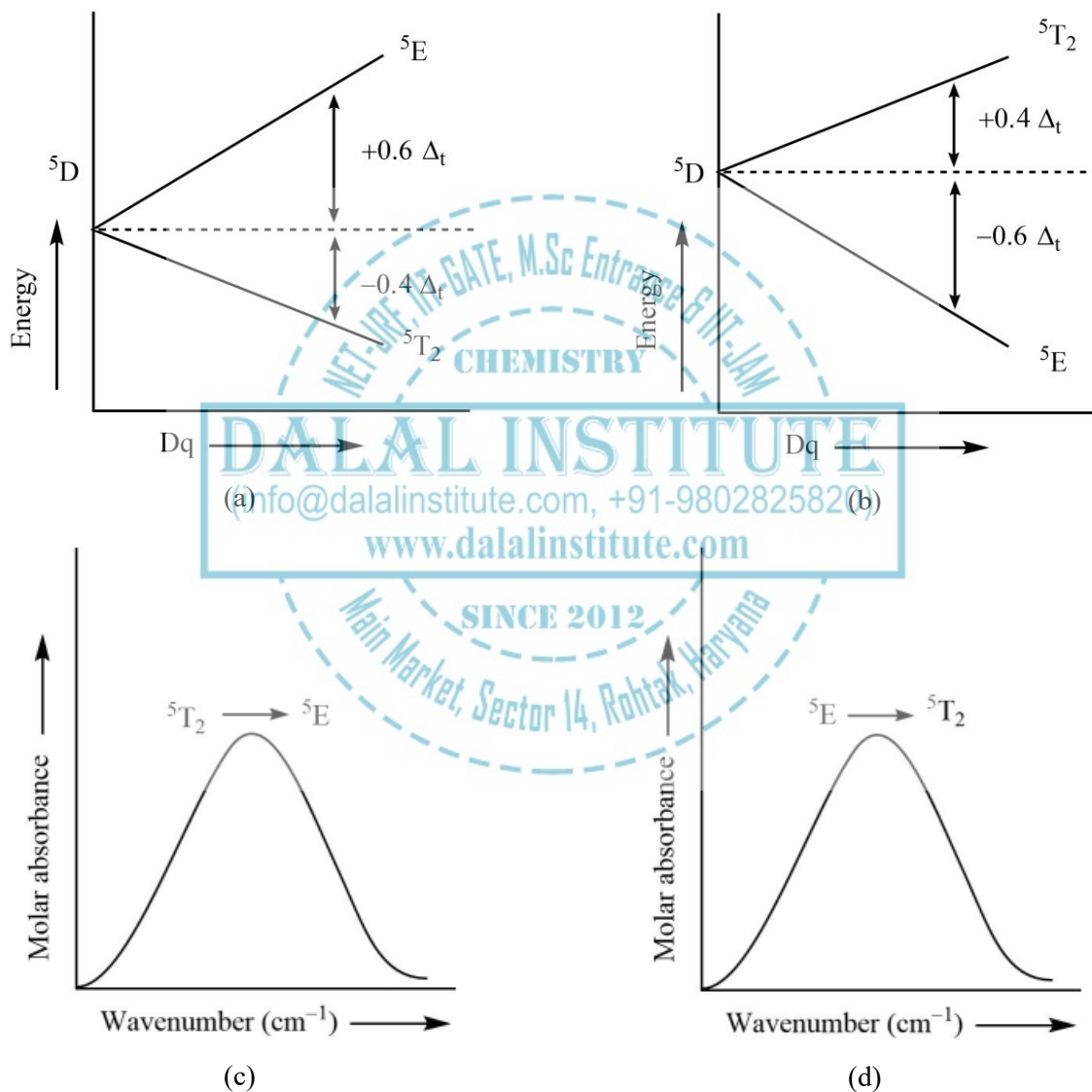


Figure 20. The splitting pattern of  $^5D$  state in tetrahedral complexes with (a)  $d^4$ -configuration and (b)  $d^6$ -configuration; and the corresponding electronic spectra of (c)  $ML_4 (d^4)$  and (d)  $ML_4 (d^6)$ .

## 2. $d^2$ , $d^8$ , $d^3$ , $d^7$ systems:

For the “F” Orgel diagram, the left side contains  $d^2$  and  $d^7$  tetrahedral and  $d^3$  and  $d^8$  octahedral complexes. The right side contains  $d^3$  and  $d^8$  tetrahedral and  $d^2$  and high spin  $d^7$  octahedral complexes. The lowest energy absorption band on the left side of the spectrum is  $A_{2g}(F) \rightarrow T_{2g}(F)$  while on the right side of the spectrum it is  $T_{1g}(F) \rightarrow T_{2g}(F)$  transition. The difference in energy between these two states is solely attributable to electron-electron repulsions. The two free ion electronic states are separated by an energy difference  $15B$ , where  $B$  is the Racah parameter that acts as a measure of electron-electron repulsions. The value of  $B$  can be calculated experimentally in a very similar manner as the value of ligand-field splitting  $\Delta$  is obtained.

For instance, in an octahedral  $d^2$  complex, there are three ways of arranging the two  $d$  electrons. One is  $t_{2g}^2$ , second is  $t_{2g}^1 e_g^1$  and the last is  $e_g^2$ . These are the three electronic states under consideration and are one should use the right-hand side of the diagram. Moreover, the energy gap between each state is equal to  $\Delta$  since it requires the promotion of one electron from  $t_{2g}$  to  $e_g$ . It is clear from the Orgel diagram that there are four states: two  $T_{1g}$  states, one  $T_{2g}$  state, and one  $A_{2g}$  state. The spin multiplicities are omitted in the diagram that allows it to be generalized for  $d^8$  complexes. The subscript  $g$  and  $u$  should be omitted if the same diagram is to be used to generalize the spectra of tetrahedral counterparts. It is also worthy to note that the ordering of the second and third transition on the right-hand side is reversed after the crossover point.

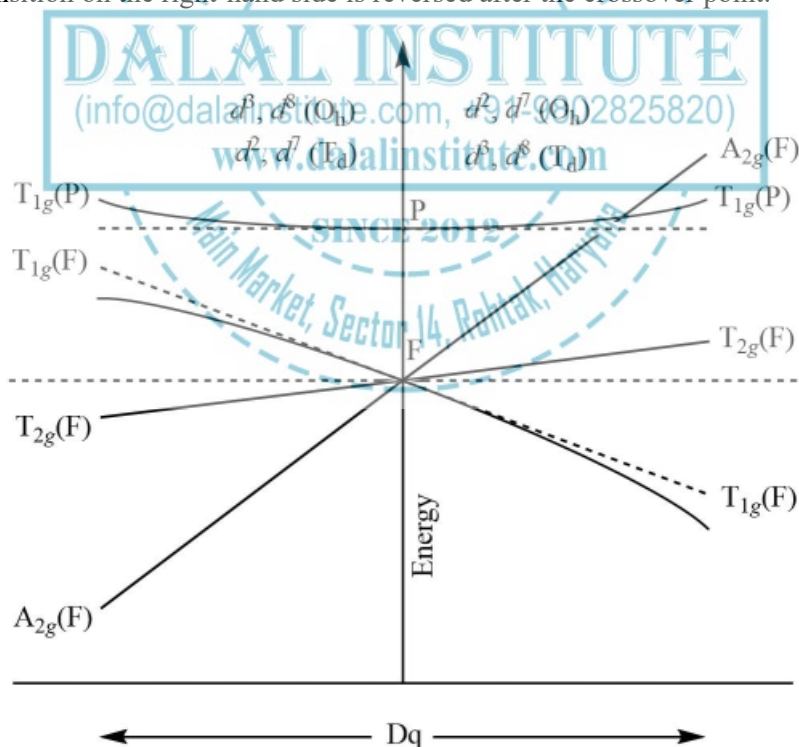


Figure 21. Orgel diagram for  $d^2$ ,  $d^8$ ,  $d^3$ ,  $d^7$  complexes in octahedral ( $O_h$ ) and tetrahedral ( $T_d$ ) crystal fields.

i) Spectra of  $d^2$  and  $d^8$  octahedral complexes:

The ground state term symbol for  $d^2$  and  $d^8$  complexes is  ${}^3F$ ; but the splitting pattern of their  ${}^3F$  states is just the opposite of each other, which can be attributed to the electron-hole inverse relationship or simply the hole-formalism. In other words, a  $d^8$  metal has two electron vacancies or “holes” in its  $d$ -subshell and thus can be considered as the inverse of the  $d^2$  arrangement. Therefore, despite having identical ground state term symbol  ${}^3F$  (split into  ${}^3A_{2g}$ ,  ${}^3T_{2g}$  and  ${}^3T_{1g}$  in the octahedral field), the energy order of Mulliken states in  $d^8$ -configuration complexes will be just the inverse of what is in  $d^2$  system.

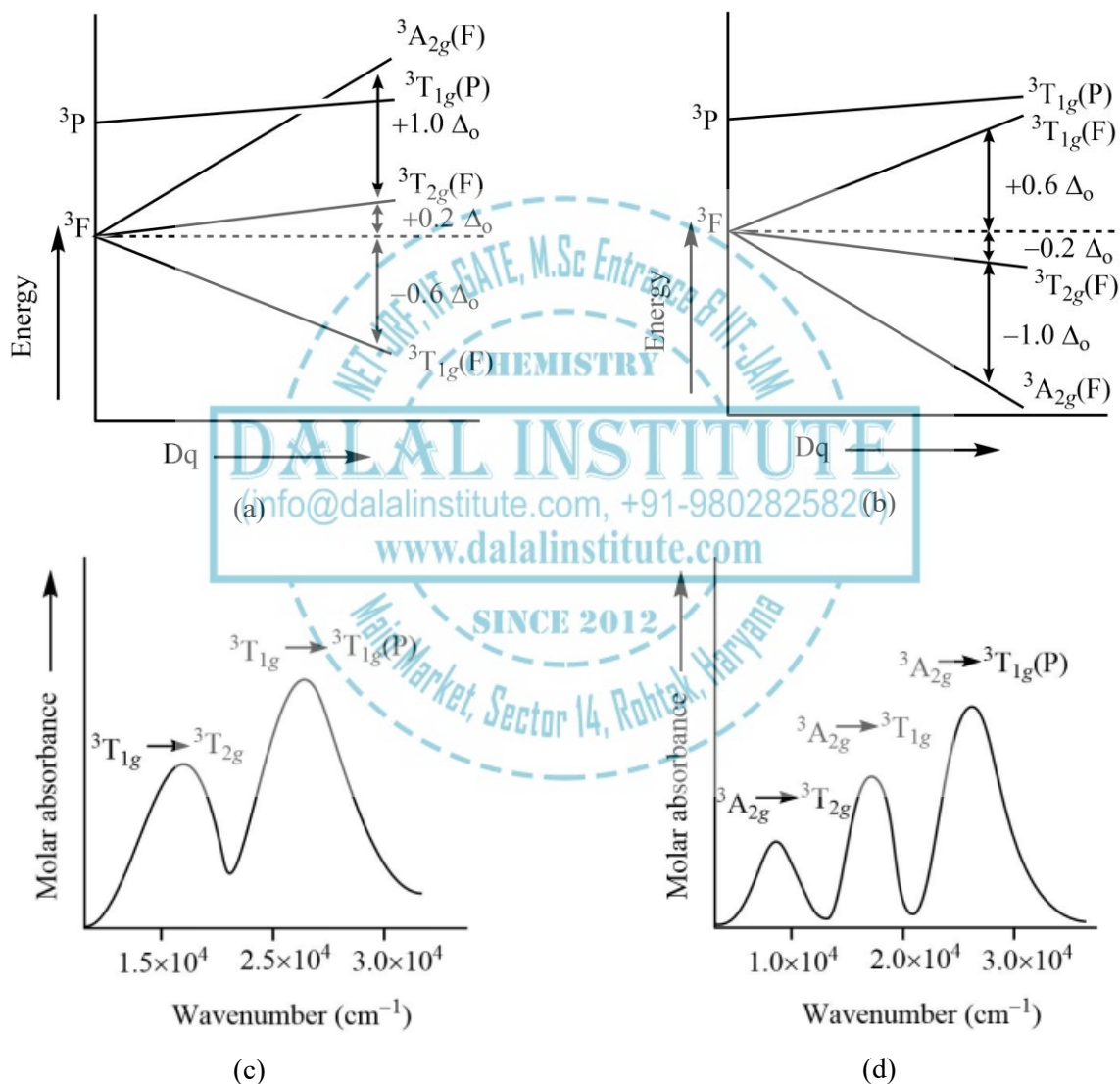


Figure 22. The splitting pattern of  ${}^3F$  state in octahedral complexes with (a)  $d^2$ -configuration and (b)  $d^8$ -configuration; and the corresponding electronic spectra of (c)  $[V(H_2O)_6]^{3+}$  and (d)  $[Ni(H_2O)_6]^{2+}$ .

ii) Spectra of  $d^2$  and  $d^8$  tetrahedral complexes:

In addition to the electron-hole inverse relationship for  $d^2$  and  $d^8$  octahedral complexes, an inverse relationship for octahedral-tetrahedral crystal field symmetries also exists. This is simply because the crystal fields of these two symmetries produce the inverse splitting pattern of the  $d$ -subshell. Therefore, despite having identical ground state term symbol  $^3F$  (split into  $^3A_2$ ,  $^3T_2$  and  $^3T_1$  tetrahedral field), the energy order of Mulliken states in the tetrahedral field will be just the inverse of what is in octahedral systems. However, it is worthy to note that the subscript “g” or “u” cannot be used due to the lack of the center of symmetry.

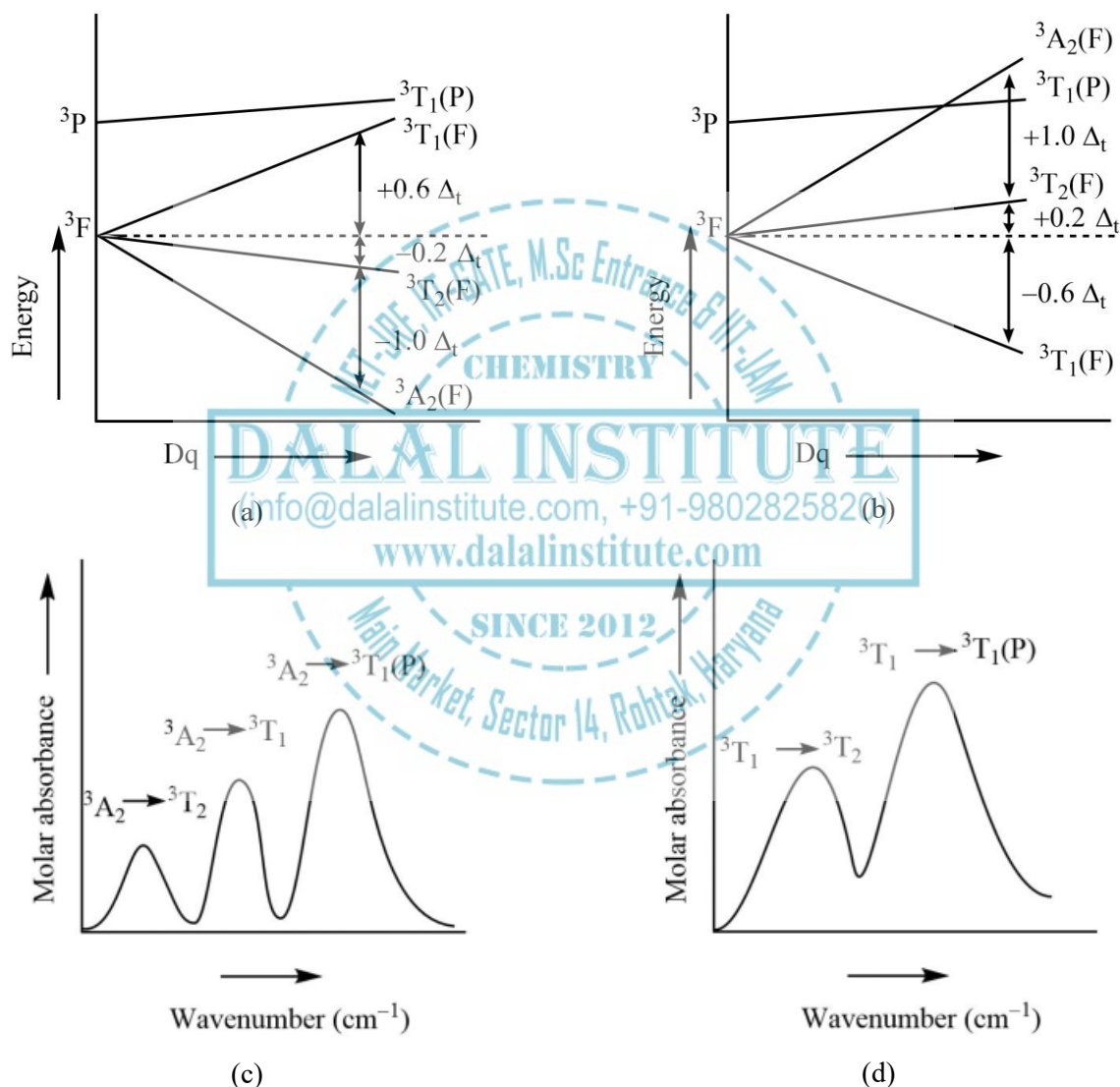


Figure 23. The splitting pattern of  $^3F$  state in tetrahedral complexes with (a)  $d^2$ -configuration and (b)  $d^8$ -configuration; and the corresponding electronic spectra of (c)  $ML_4 (d^2)$  and (d)  $ML_4 (d^8)$ .

iii) Spectra of  $d^3$  and  $d^7$  octahedral complexes:

The ground state term symbol for  $d^3$  and  $d^7$  complexes is  ${}^4F$ ; but the splitting pattern of their  ${}^4F$  states is just the opposite of each other, which can be attributed to the electron-hole inverse relationship or simply the hole formalism. In other words, a  $d^7$  metal has an electron vacancy or “hole” in its  $d$ -subshell and thus can be considered as the inverse of the  $d^3$  arrangement. Therefore, despite having identical ground state term symbol  ${}^4F$  (split into  ${}^4A_{2g}$ ,  ${}^4T_{2g}$  and  ${}^4T_{1g}$  in the octahedral field), the energy order of Mulliken states in  $d^7$  configuration will be just the inverse of what is in  $d^3$  system.

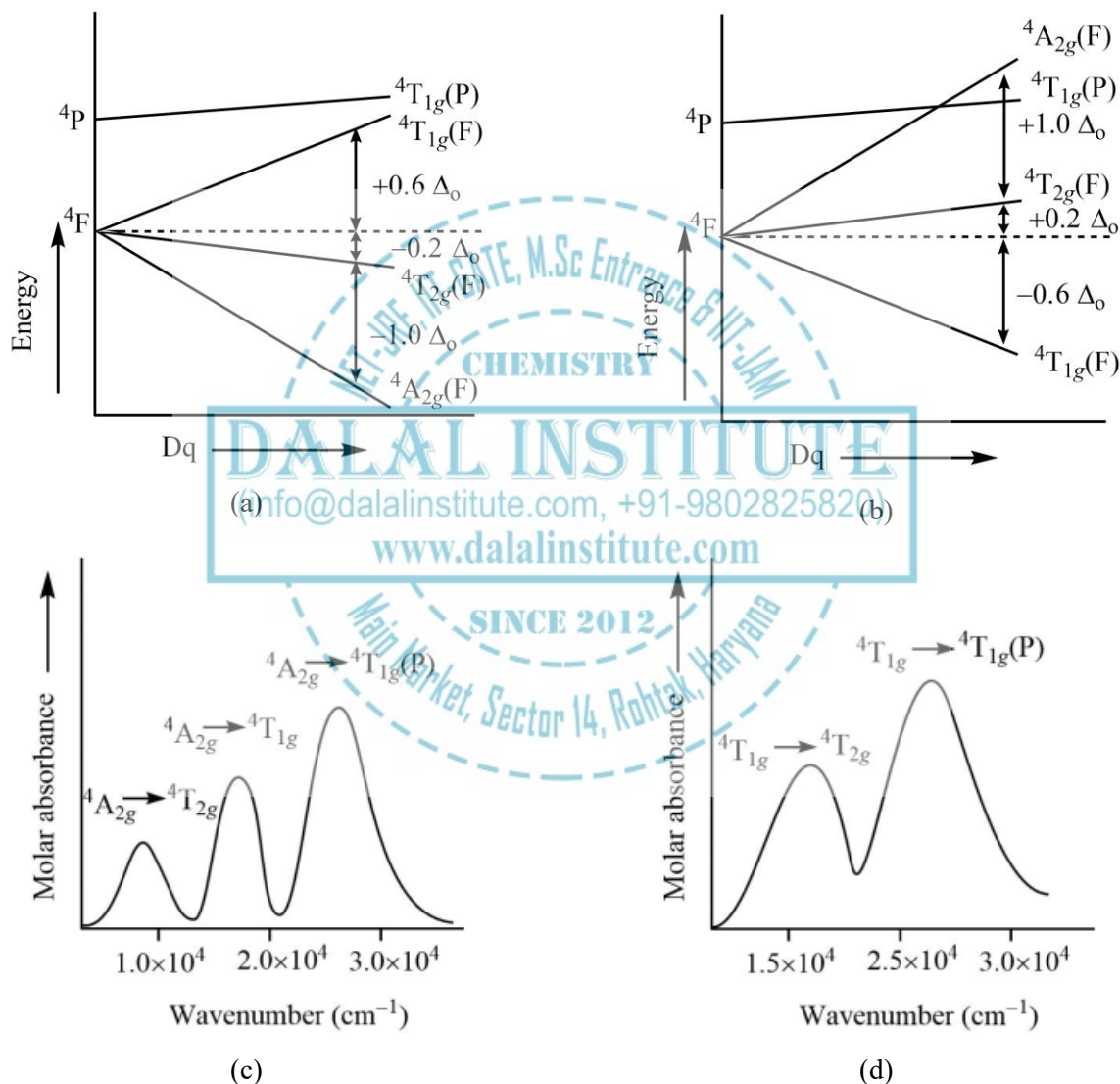


Figure 24. The splitting pattern of  ${}^4F$  state in octahedral complexes with (a)  $d^3$ -configuration and (b)  $d^7$ -configuration; and the corresponding electronic spectra of (c)  $[\text{Cr}(\text{H}_2\text{O})_6]^{3+}$  and (d)  $[\text{Co}(\text{H}_2\text{O})_6]^{2+}$ .

iv) Spectra of  $d^3$  and  $d^7$  tetrahedral complexes:

In addition to the electron-hole inverse relationship for  $d^3$  and  $d^7$  octahedral complexes, an inverse relationship for octahedral-tetrahedral crystal field symmetries also exists. This is simply because the crystal fields of these two symmetries produce the inverse splitting pattern of the  $d$ -subshell. Therefore, despite having identical ground state term symbol  $^4F$  (split into  $^4A_2$ ,  $^4T_2$  and  $^4T_1$  in the tetrahedral field), the energy order of Mulliken states in the tetrahedral field will be just the inverse of what is in octahedral systems. However, it is worthy to note that the subscript “g” or “u” cannot be used due to the lack of the center of symmetry.

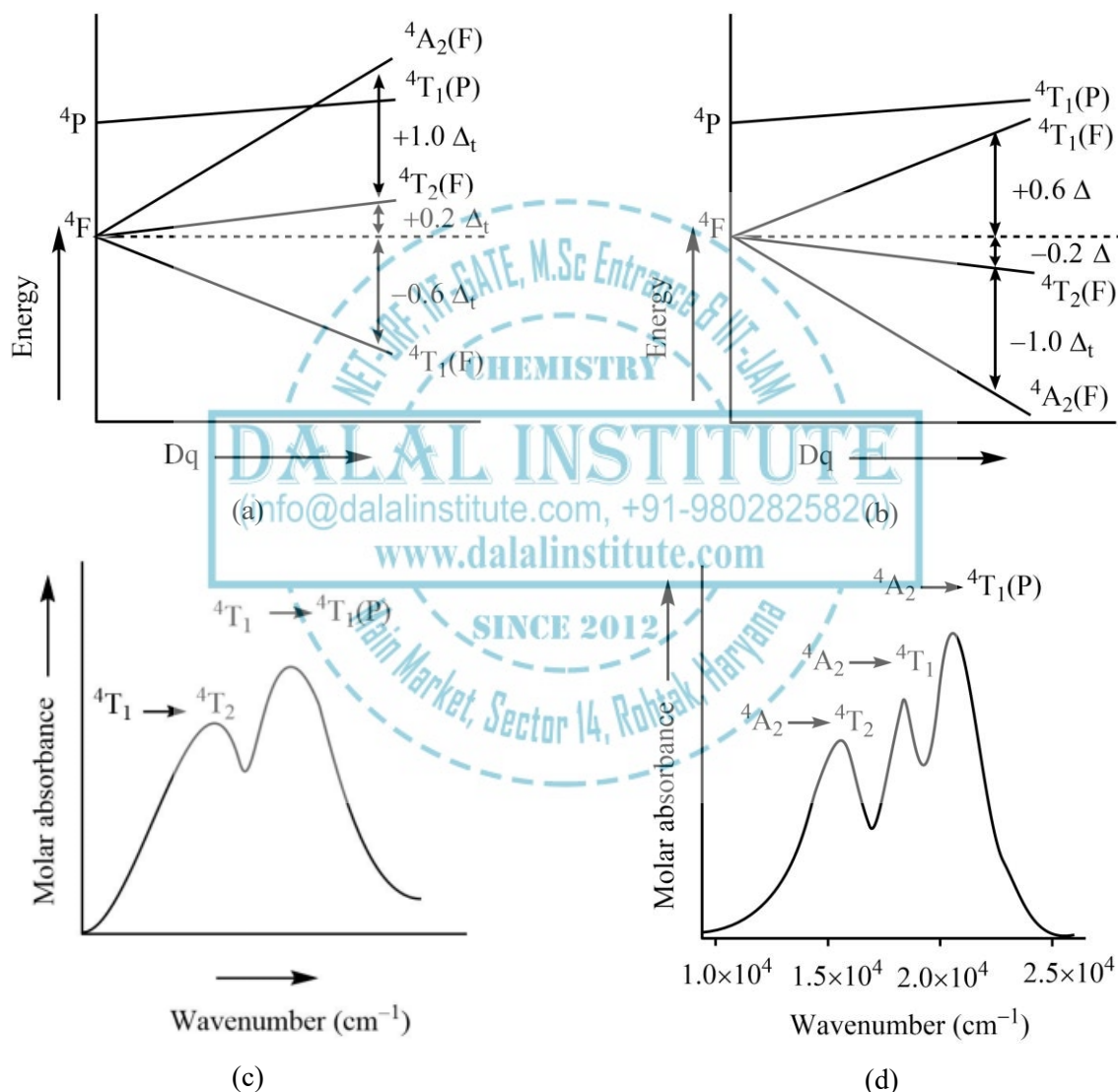


Figure 25. The splitting pattern of  $^4F$  state in tetrahedral complexes with (a)  $d^3$ -configuration and (b)  $d^7$ -configuration; and the corresponding electronic spectra of (c)  $ML_4$  ( $d^3$ ) and (d)  $[CoCl_4]^{2-}$  ( $d^7$ ).

3.  $d^5$  systems:

Orgel diagrams we have studied so far include only spin allowed transitions. However, in the case of  $d^5$ -configuration, this is not possible as there is only one electronic state with a multiplicity of six,  ${}^6A_{1g}$ . Therefore, all the transitions must occur with a change in the spin multiplicity and are spin forbidden for octahedral as well as tetrahedral complexes. The lowest energy absorption band of the spectrum is  ${}^6A_{1g}(S) \rightarrow {}^4T_{1g}(G)$  in octahedral; while in the tetrahedral complex, it is  ${}^6A_1(S) \rightarrow {}^4T_1(G)$  transition. The difference in energy between these two states is also attributable to electron-electron repulsions and B, the Racah parameter that acts as a measure of electron-electron repulsions.

The electronic configuration for ground state term symbol is  $t_{2g}^3 e_g^2$  with five unpaired electrons having parallel spins and any promotion or rearrangement of the electrons would lead to a lower multiplicity state. Moreover, if we combine this fact perfect octahedral complexes like  $[\text{Mn}(\text{H}_2\text{O})_6]^{2+}$ , the absorption intensities become very weak due to the additional selection rule of Laporte forbiddance. This makes  $[\text{Mn}(\text{H}_2\text{O})_6]^{2+}$  pale pink in color but the tetrahedral complexes of  $\text{Mn}^{2+}$  are quite instance due to the absence of the centre of symmetry. The subscript g and u should be omitted if the same diagram is to be used to generalize the spectra of tetrahedral counterparts. It is also worthy to note that the electronic states with symmetry never cross each other but repel each other due to their quantum mechanical mixing.

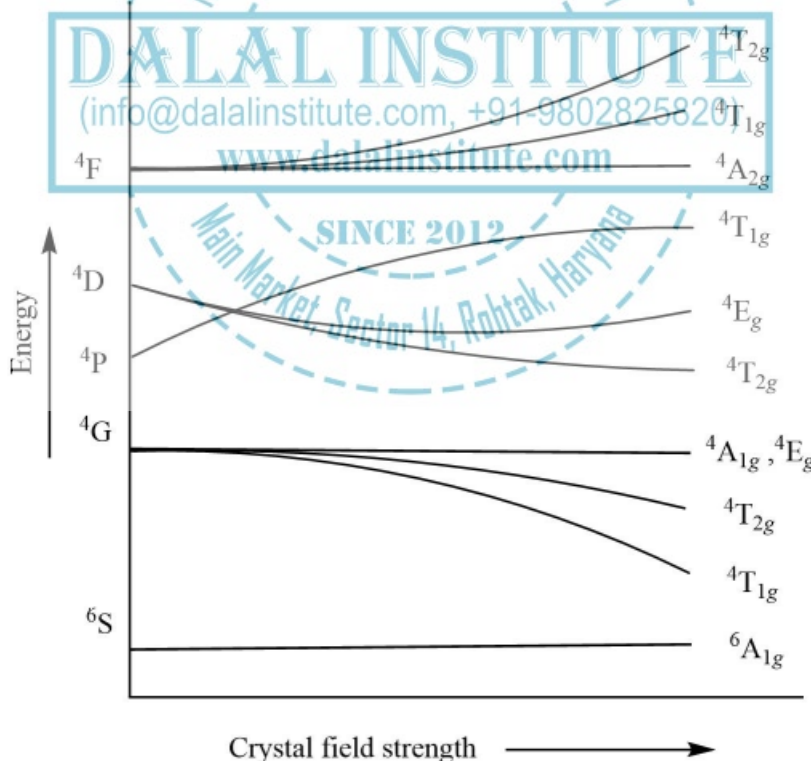


Figure 26. Orgel diagram for  $d^5$  complexes in octahedral ( $O_h$ ) and tetrahedral ( $T_d$ ) crystal fields.

Unlike other electronic configurations, the ground state of  $d^5$  system remains the same but the gerade subscript will be removed i.e.  ${}^6A$ . The same is true for other Mulliken states. In other words, the subscript “g” or “u” cannot be used due to the lack of the center of symmetry.

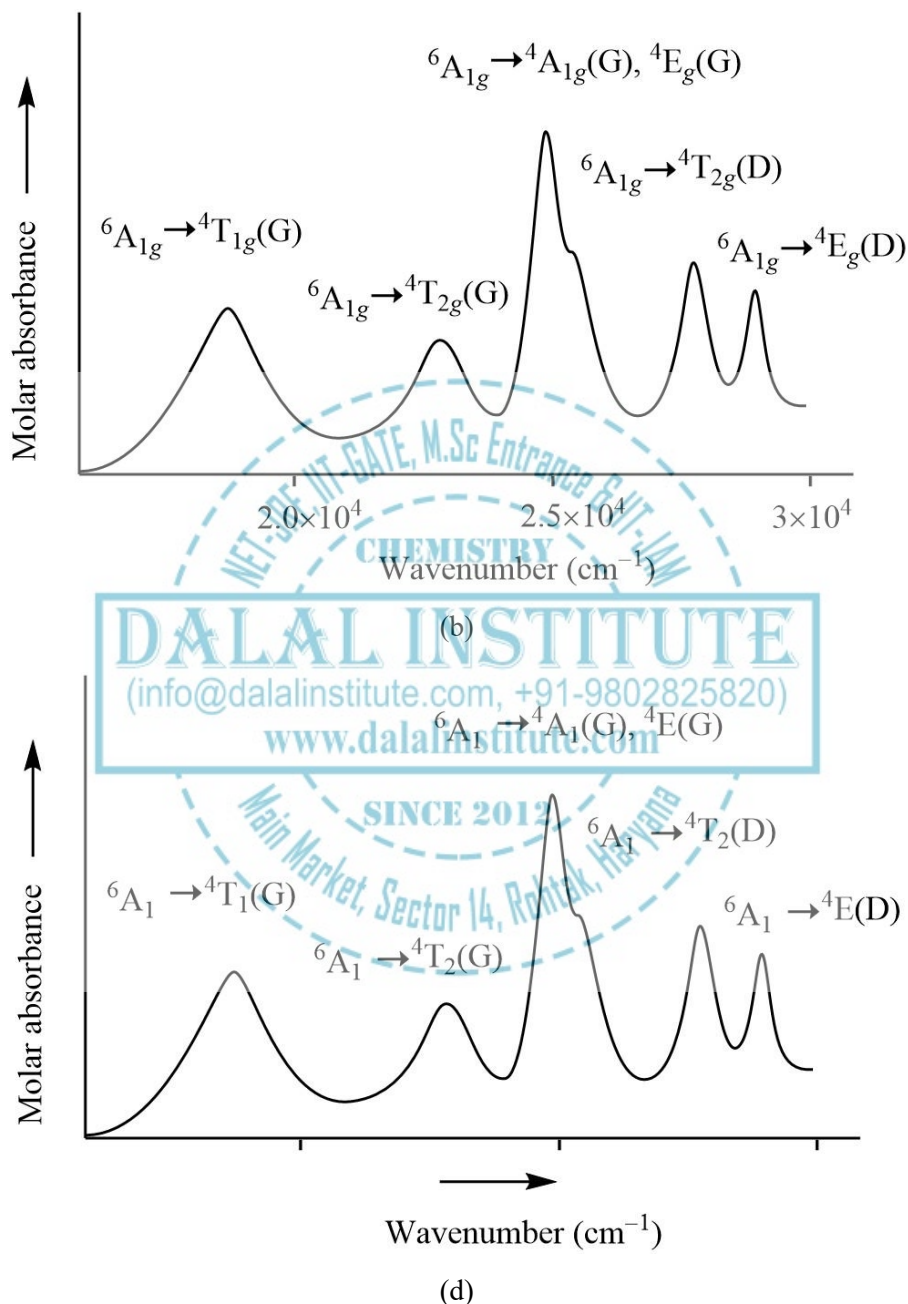


Figure 27. The electronic spectra of (a)  $[\text{Mn}(\text{H}_2\text{O})_6]^{2+}$  and (b)  $[\text{ML}_4]^{d^5}$ .

➤ *Tanabe-Sugano Diagrams*

In 1954, two Japanese scientists, Yukito Tanabe and Satoru Sugano published a paper entitled "On the absorption spectra of complex ions". Earlier than that, very little was available regarding the excited electronic states of transition metal complexes. Tanabe and Sugano used the Hans Bethe's CFT concept and Giulio Racah's linear combinations of Slater integrals (Racah parameters) to rationalize the absorption spectra of the octahedral metal complex in a quantitative frame than what had been accomplished earlier. After a number of spectroscopic experiments, they estimated the values B and C (two of Racah's parameters) for every  $d$ -electronic configuration based on the trends in the UV visible absorption spectrum of isoelectronic transition metals of  $3d$  series. The energy plots of various electronic states of every electron configuration are now called as Tanabe-Sugano or simply the T-S diagrams. In other words, Tanabe-Sugano diagrams are nothing but some special kind of correlation diagrams that can be used in weak as well as strong field complexes. These diagrams are used in transition metal chemistry to forecast the UV-visible absorption spectrum of coordination compounds and the results from these diagrams can also be compared to experimentally obtained spectroscopic data. T-S diagrams can be used qualitatively to approximate the value of crystal field splitting energy ( $\Delta$ ). Unlike Orgel diagrams (applicable to high-spin complexes only), these diagrams can be used for spin-free as well as spin-paired complexes. T-S diagrams can also be exploited to find the size of the ligand field required to cause high-spin–low-spin transitions. In contrast to the Orgel diagrams, the ground state is set as a reference in a T-S diagram. The ground-state-energy is taken to be zero for all ligand field strengths, and the energy of all other states along-with their components are plotted with respect to the ground state term.

In Tanabe-Sugano diagrams, the  $x$ -axis is expressed in terms of the crystal field splitting parameter ( $\Delta$  or  $Dq$ ) divided by the Racah parameter (B). Along  $y$ -axis, the energy,  $E$ , divided by B is taken. Out of three Racah parameters (A, B, and C), which describe various aspects of inter-electronic repulsion, A is an average total inter-electron repulsion whereas B and C correspond with individual  $d$ -electronic repulsions. The value of A is constant for  $d$ -electronic configuration, and therefore, is unnecessary for obtaining relative energies, and so is absent from T-S diagram studies of metal complexes. The parameter C is required only in some special cases. The parameter B is the most significant of all Racah's parameters in transition metals complexes. Moreover, certain lines bend due to the mixing of states with same symmetry. Although transitions between the same spin-multiplicity are allowed, energy profiling of spin-forbidden states is also included in the T-S diagrams, which were absent in Orgel diagrams. All states are usually Labelled on the right side of the diagram; nonetheless, some labels may be allotted on other locations for more clarity in case of complicated T-S diagrams like  $d^6$ . The free ion terms for a specific  $d^n$  configuration are shown in order of increasing energy on the  $y$ -axis of the T-S diagram. The relative of energies free ion terms are obtained using Hund's rules. The splitting of free ion terms has already been discussed in Table 7 and Table 8. Certain T-S diagrams like  $d^4$ ,  $d^5$ ,  $d^6$ , and  $d^7$ ; also have a starlight vertical line at a certain  $Dq/B$  value, which represents a discontinuity in the slopes of the excited-states' terms. This occurs when the pairing energy (P) becomes equal to the crystal field splitting energy. Metal complexes to the left of this vertical line are spin-free, while the complexes to the right are spin-paired. There is no low-spin or high-spin designation for  $d^2$ ,  $d^3$ , or  $d^8$ . The subscript "g" and "u" can be omitted as all designations are gerade.

1.  $d^1, d^9$  systems:i)  $d^1$ -configuration

Metal complexes with  $d^1$ -configuration do not have any inter electronic repulsion and the single electron resides in the  $t_{2g}$  orbital ground state. When  $t_{2g}$  orbital set holds the single electron, six microstates will have  ${}^2T_{2g}$  state energy of  $-4 Dq$ ; and when the electron is promoted to the  $e_g$  orbital, the four microstates will have  ${}^2E_g$  state energy of  $+6 Dq$ . This is in accordance with the single absorption band in a UV-vis experiment; and thus, the transition from  ${}^2T_{2g}$  to  ${}^2E_g$  does not require a Tanabe–Sugano diagram.

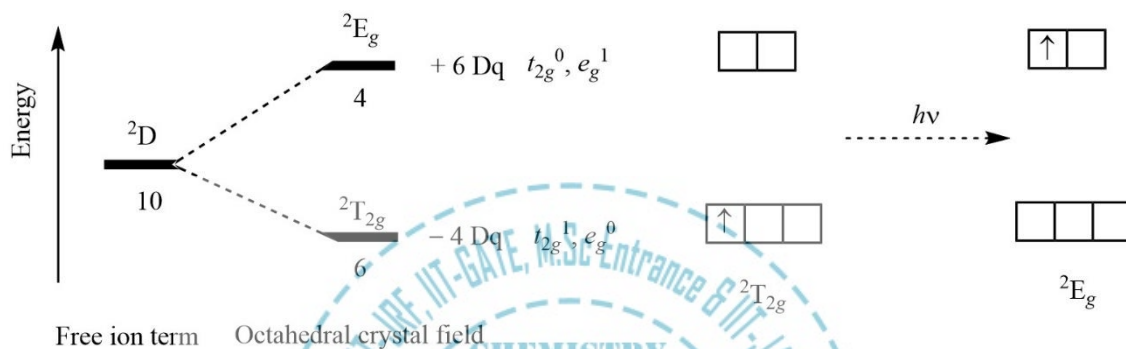


Figure 28. Splitting of free ion term for  $d^1$  complexes in the octahedral crystal field.

ii)  $d^9$ -configuration

In  $d^9$  octahedral metal complexes, the ground state filling of electrons ( $t_{2g}^6 e_g^3$ ) has only four microstates that have  ${}^2E_g$  energy state with  $-6 Dq$ . When the electron from  $t_{2g}$  is promoted to the  $e_g$  orbital set; the new configuration will have six microstates that have  ${}^2T_{2g}$  energy state with  $+4 Dq$ . This could also be described as a positive "hole" that moves from the  $e_g$  to the  $t_{2g}$  orbital set. The sign of  $Dq$  is opposite that for  $d^1$ , with a  ${}^2E_g$  ground state and a  ${}^2T_{2g}$  excited state. Like the  $d^1$  case,  $d^9$  octahedral complexes do not require the Tanabe–Sugano diagram to predict their absorption spectra.

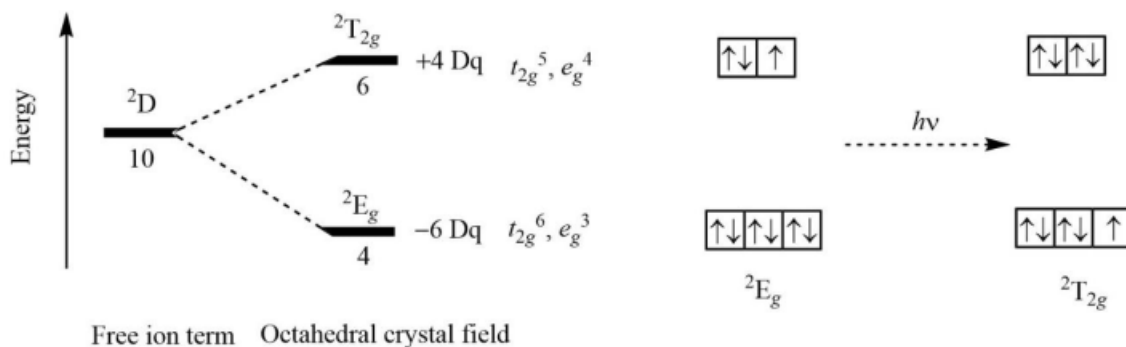


Figure 29. Splitting of free ion term for  $d^9$  complexes in the octahedral crystal field.

2.  $d^2$  systems:

Metal complexes with  $d^2$ -configuration have  ${}^3F$  ground state term symbol in the absence of any crystal field. However, when six ligands approach in octahedral coordination, the ground state term symbol becomes  ${}^3T_{1g}$  and remains as such in the weak field as well as strong ligand field.

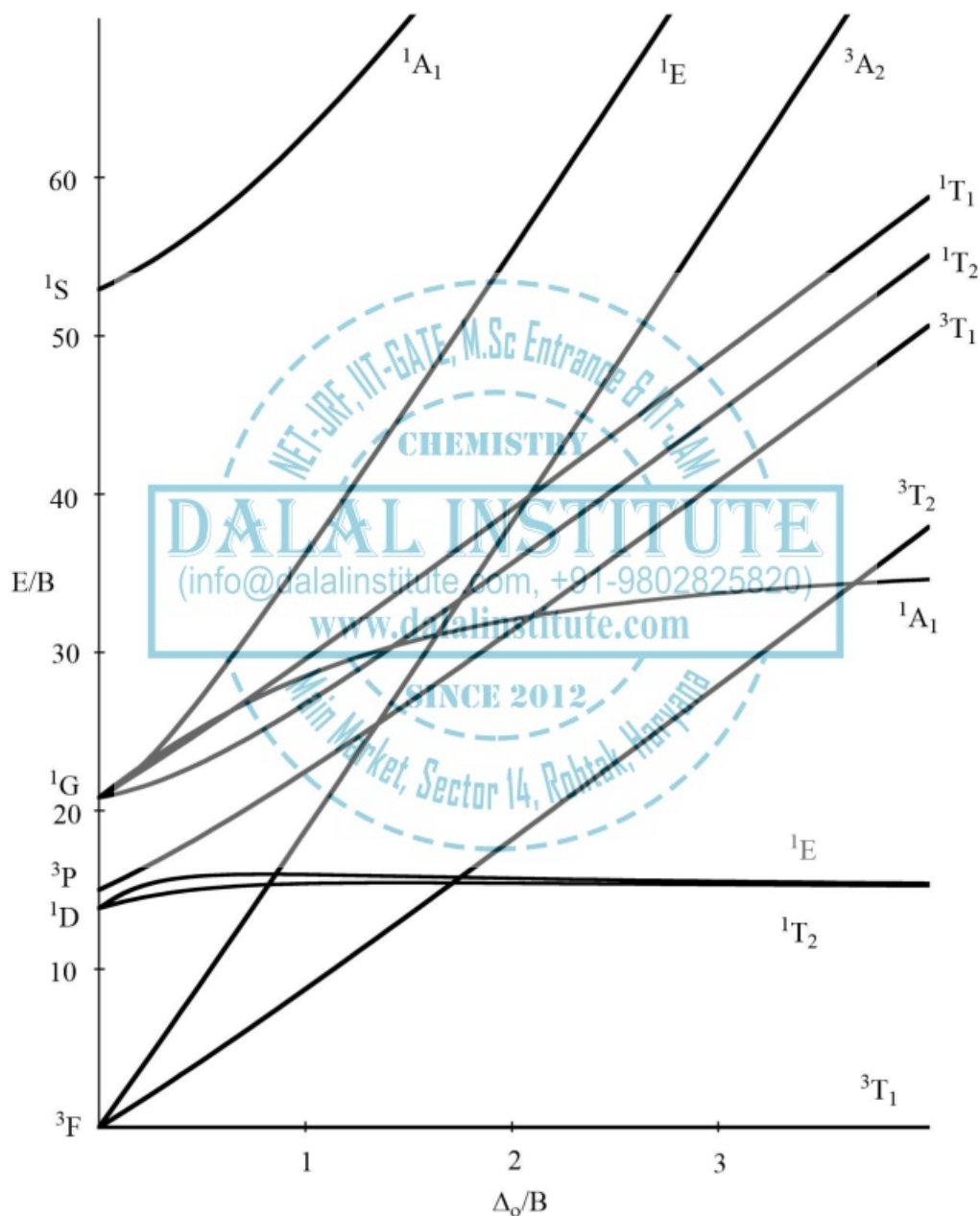


Figure 30. Splitting of free ion terms for  $d^2$  complexes in the octahedral crystal field.

### 3. $d^3$ systems:

Metal complexes with  $d^3$ -configuration have  $^4F$  ground state term symbol in the absence of any crystal field. However, when six ligands approach in octahedral coordination, the ground state term symbol becomes  $^4A_{2g}$  and remains as such in the weak field as well as strong ligand field.

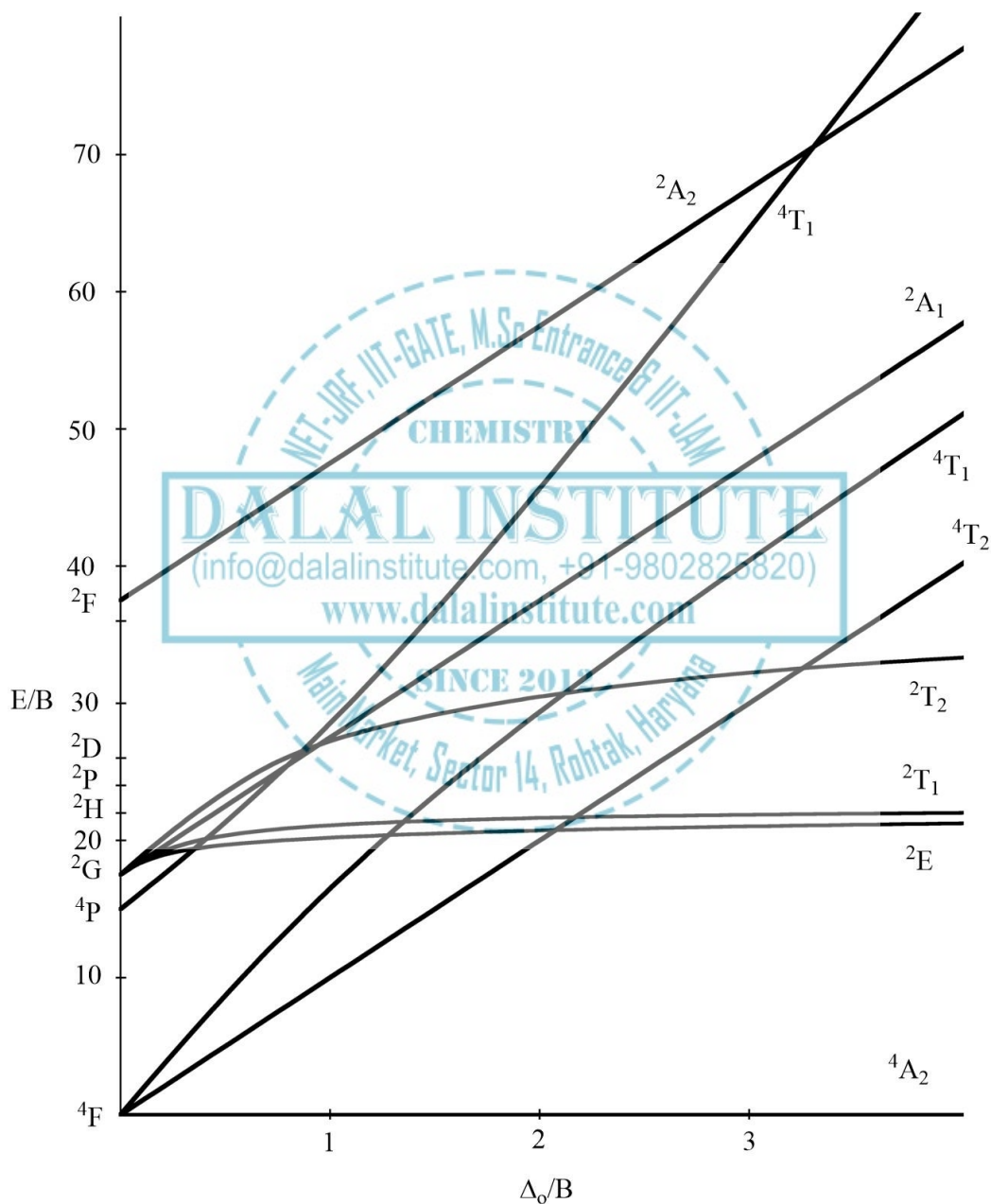


Figure 31. Splitting of free ion terms for  $d^3$  complexes in the octahedral crystal field.

4.  $d^4$  systems:

Metal complexes with  $d^4$ -configuration have  $^5D$  ground state term symbol in the absence of any crystal field. However, when six ligands approach in octahedral coordination, the ground state term symbol becomes  $^5E_g$  in the weak field and  $^3T_{1g}$  in a strong ligand field.

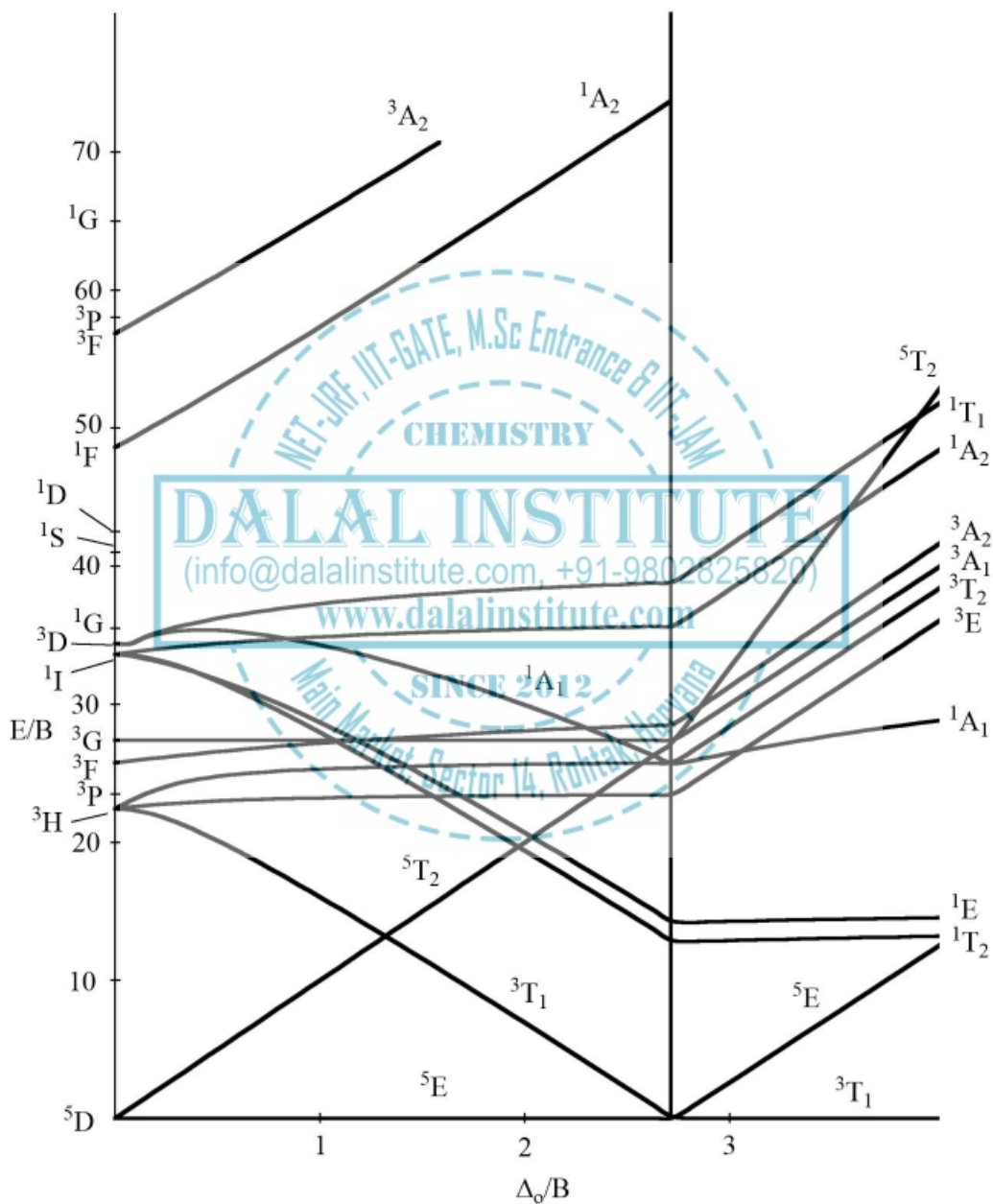


Figure 32. Splitting of free ion terms for  $d^4$  complexes in the octahedral crystal field.

### 5. $d^5$ systems:

Metal complexes with  $d^5$ -configuration have  ${}^6S$  ground state term symbol in the absence of any crystal field. However, when six ligands approach in octahedral coordination, the ground state term symbol becomes  ${}^6A_{1g}$  in weak field and  ${}^2T_{2g}$  in strong ligand field.

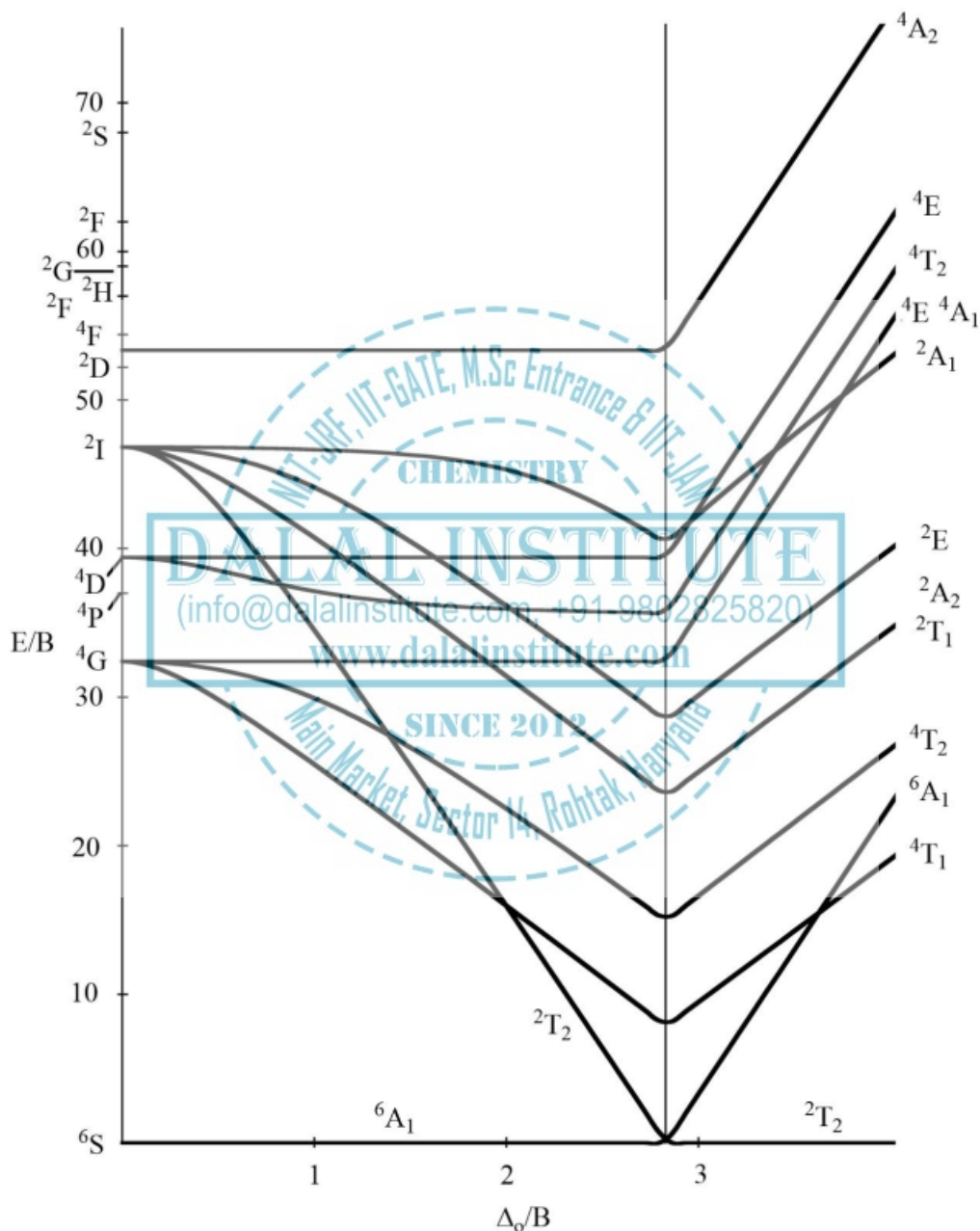


Figure 33. Splitting of free ion terms for  $d^5$  complexes in the octahedral crystal field.

6.  $d^6$  systems:

Metal complexes with  $d^6$ -configuration have  $^5D$  ground state term symbol in the absence of any crystal field. However, when six ligands approach in octahedral coordination, the ground state term symbol becomes  $^1T_{2g}$  in weak and  $^1A_{1g}$  in strong ligand fields.

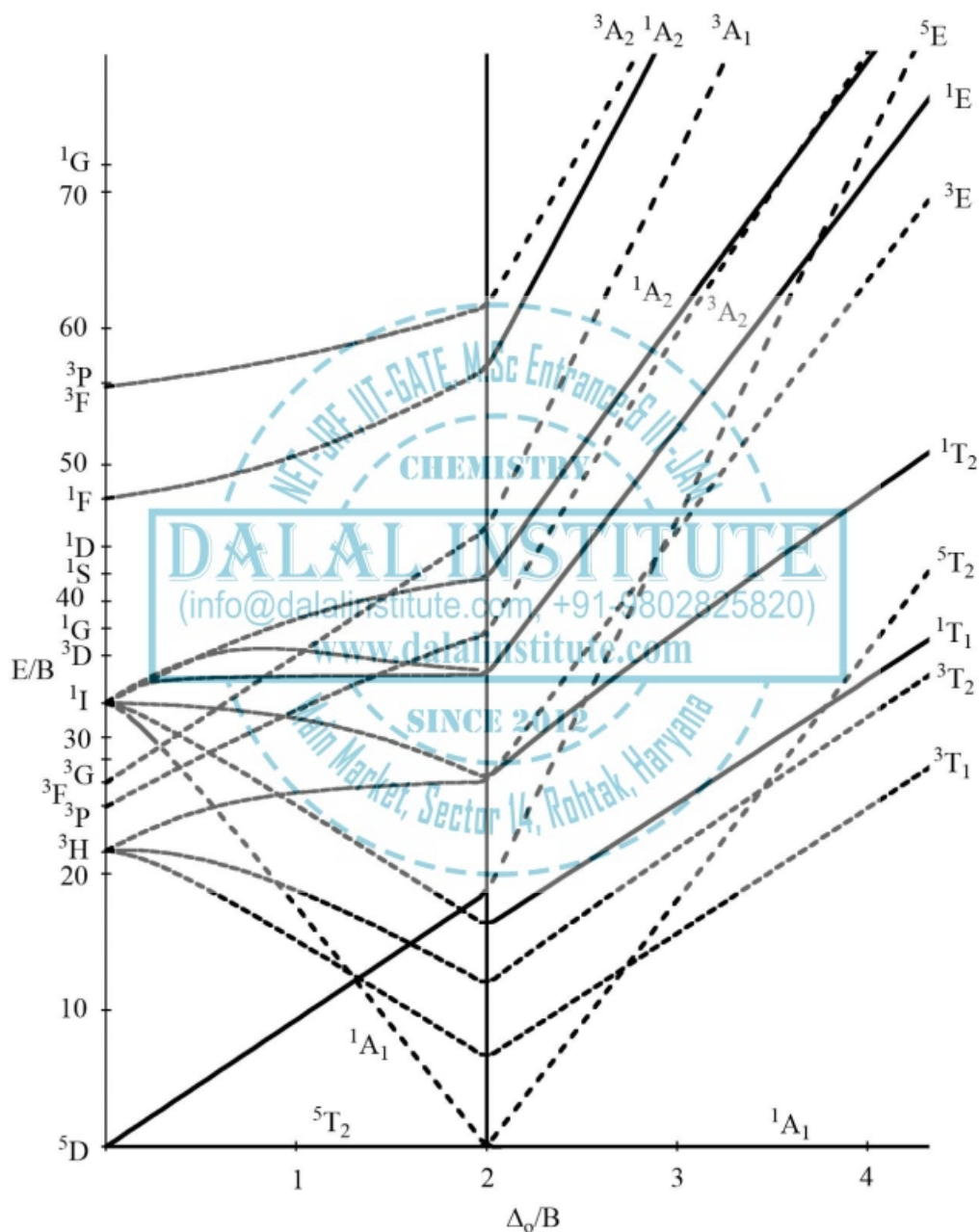


Figure 34. Splitting of free ion terms for  $d^6$  complexes in the octahedral crystal field.

7.  $d^7$  systems:

Metal complexes with  $d^7$ -configuration have  $^4F$  ground state term symbol in the absence of any crystal field. However, when six ligands approach in octahedral coordination, the ground state term symbol becomes  $^4T_{1g}$  in weak  $^2E_g$  in strong ligand fields.

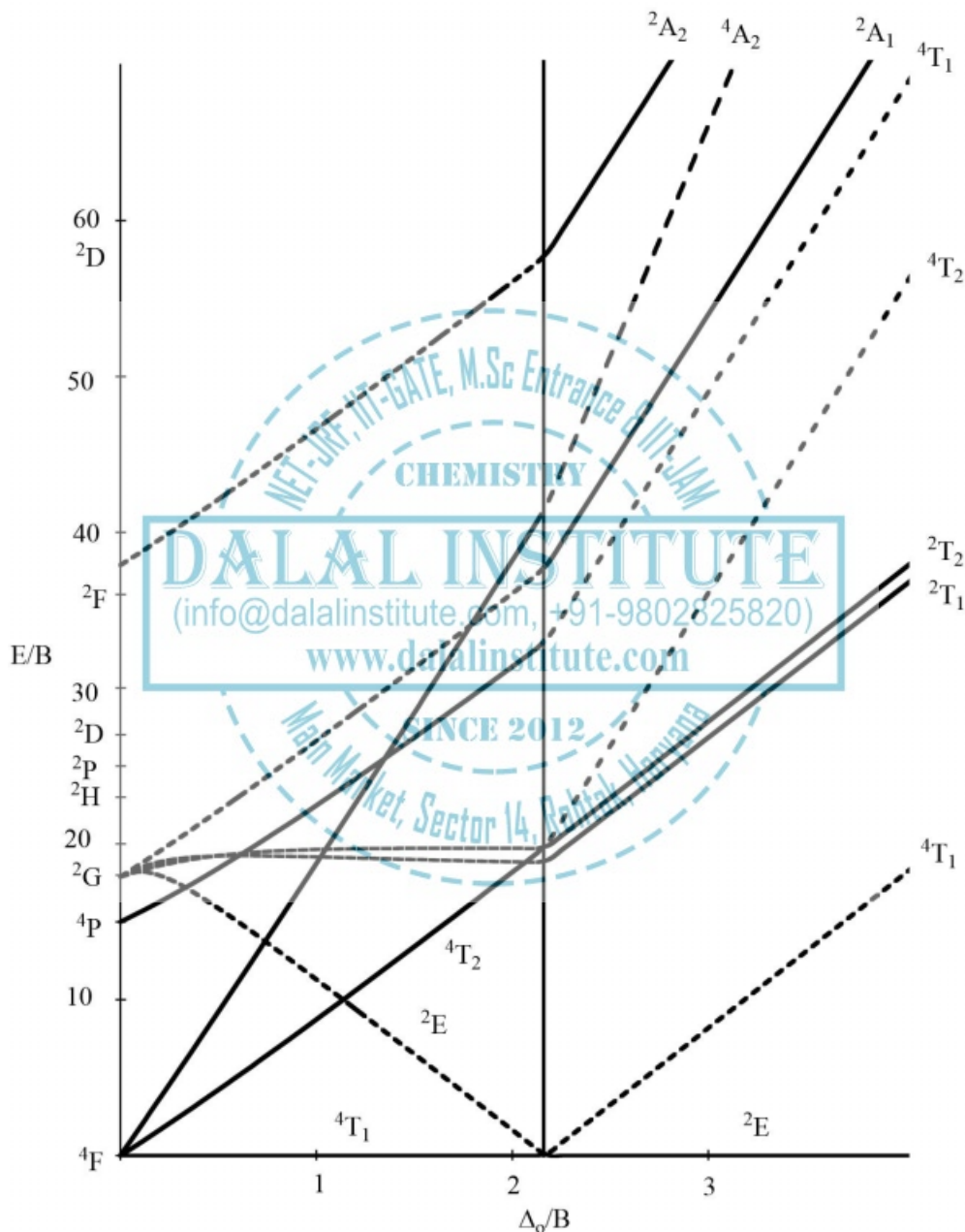


Figure 35. Splitting of free ion terms for  $d^7$  complexes in the octahedral crystal field.

8.  $d^8$  systems:

Metal complexes with  $d^8$ -configuration have  $^3F$  ground state term symbol in the absence of any crystal field. However, when six ligands approach in octahedral coordination, the ground state term symbol becomes  $^3A_{2g}$  and remains as such in weak as well as strong ligand fields.

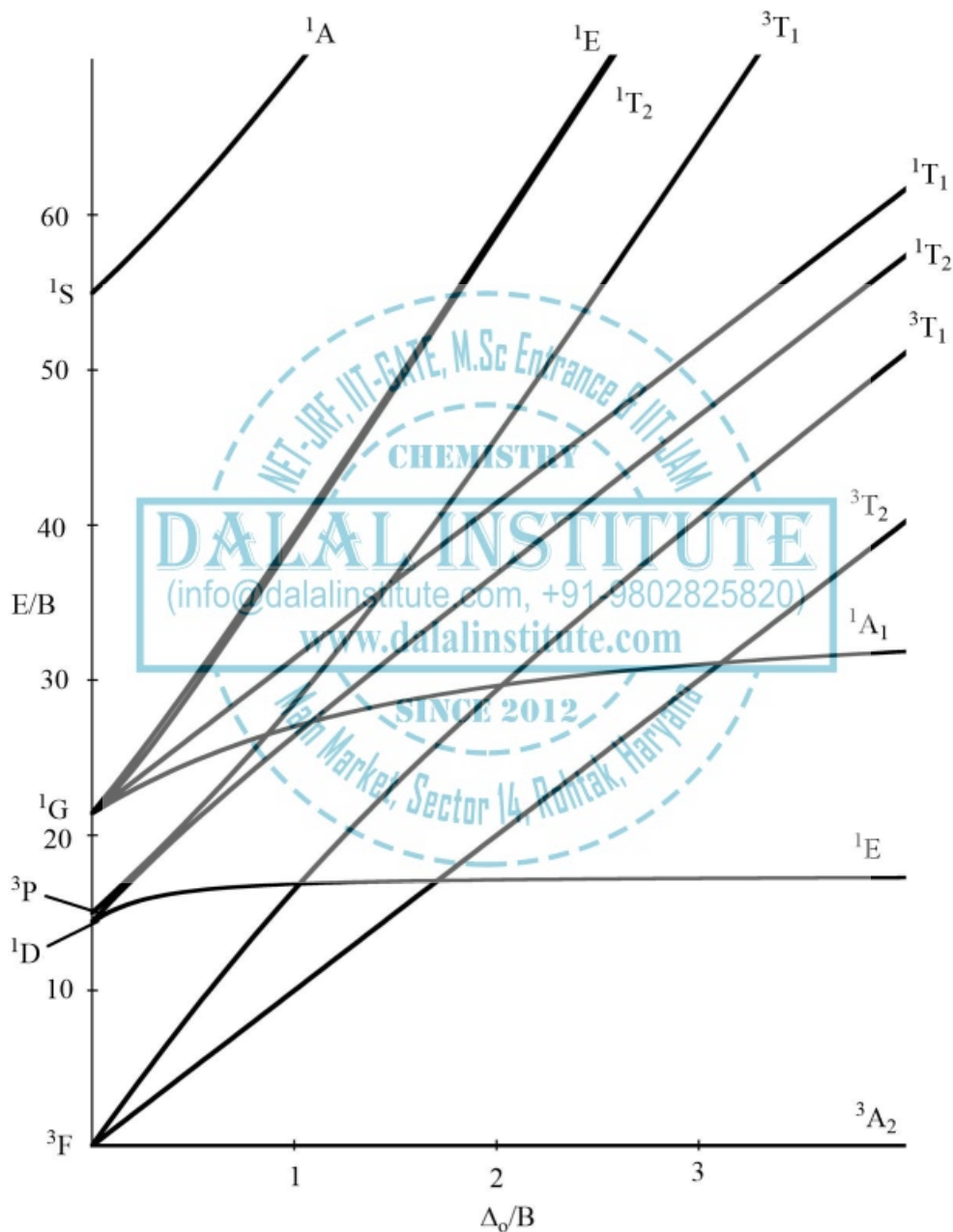


Figure 36. Splitting of free ion terms for  $d^8$  complexes in the octahedral crystal field.

### ❖ Calculation of $Dq$ , $B$ and $\beta$ Parameters

The Orgel diagrams explain how the magnitude of the splitting energy exerted by the ligands on  $d$ -orbitals vary when a free metal ion is approached by a ligand field; and can also act as deciding factor for governing the placement of electrons, just like the inter-electronic repulsion energy. However, if the ligand field splitting energy is greater than the inter-electronic repulsion energy, then Orgel diagrams fail in determining the placement of electrons. In that case, Orgel diagrams are restricted only to the high-spin complexes. Tanabe-Sugano diagrams do not have this restriction and can be applied to the situations when  $\Delta$  is significantly greater than inter-electronic repulsion. Thus, the Tanabe-Sugano diagrams can be utilized in determining electron placements for high-spin and low-spin metal complexes. However, they are limited in the sense that they have only qualitative significance.

Despite that, Tanabe-Sugano and Orgel diagrams are fairly valuable in interpreting UV-vis spectra and can be used to determine the value of crystal field splitting energy ( $Dq$ ), Racah parameter ( $B$ ) and also the nephelauxetic ratio ( $\beta$ ).

#### ➤ $d^1$ Complexes

Metal complexes with  $d^1$ -configuration do not have any inter electronic repulsion and the single electron resides in the  $t_{2g}$  orbital ground state. When  $t_{2g}$  orbital set holds the single electron, six microstates will have  ${}^2T_{2g}$  state energy of  $-4 Dq$ ; and when the electron is promoted to the  $e_g$  orbital, the four microstates will have  ${}^2E_g$  state energy of  $+6 Dq$ . Thus, the only parameter that is needed to be calculated is the magnitude of crystal field splitting energy ( $10 Dq$ ); and the single absorption band in a UV-vis experiment is exactly what we are looking for. Hence, the energy of the transition  ${}^2T_{2g} \rightarrow {}^2E_g$  gives the value of  $\Delta$  directly.

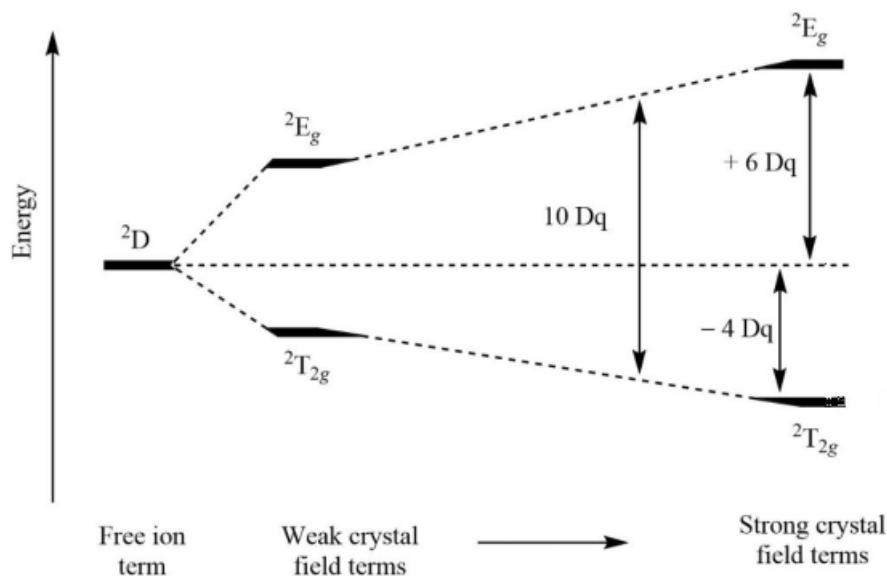


Figure 36. The splitting pattern of free ion term for  $d^1$  complexes in the octahedral crystal field.

Consider the example of  $[\text{Ti}(\text{H}_2\text{O})_6]^{3+}$

**1. Calculation of B:** No need to calculate the Racah parameter.

**2. Calculation of  $\Delta_0$ :** The purple color of the complex ion  $[\text{Ti}(\text{H}_2\text{O})_6]^{3+}$  is due to a broad absorption band at  $20300 \text{ cm}^{-1}$  arising from  ${}^2\text{T}_{2g} \rightarrow {}^2\text{E}_g$  transition. Hence,  $10 \text{ Dq}$  for this complex is  $20300 \text{ cm}^{-1}$ .

**3. Calculation of  $\beta$ :** No need to calculate the nephelauxetic ratio.

➤  **$d^0$  Complexes:**

In  $d^0$  octahedral metal complexes, the ground state filling of electrons ( $t_{2g}^6 e_g^3$ ) has only four microstates that have  ${}^2\text{E}_g$  energy state with  $-6 \text{ Dq}$ . When the electron from  $t_{2g}$  is promoted to the  $e_g$  orbital set; the new configuration will have six microstates that have  ${}^2\text{T}_{2g}$  energy state with  $+4 \text{ Dq}$ . This could also be described as a positive "hole" that moves from the  $e_g$  to the  $t_{2g}$  orbital set. The sign of  $\text{Dq}$  is opposite that for  $d^1$ , with a  ${}^2\text{E}_g$  ground state and a  ${}^2\text{T}_{2g}$  excited state. Like the  $d^1$  case, the only parameter that is needed to be calculated in  $d^0$  complexes is the magnitude of crystal field splitting energy ( $10 \text{ Dq}$ ); and the single absorption band in a UV-vis experiment is exactly what we are looking for. Hence, the energy of the transition  ${}^2\text{E}_g \rightarrow {}^2\text{T}_{2g}$  gives the value of  $\Delta$  directly.

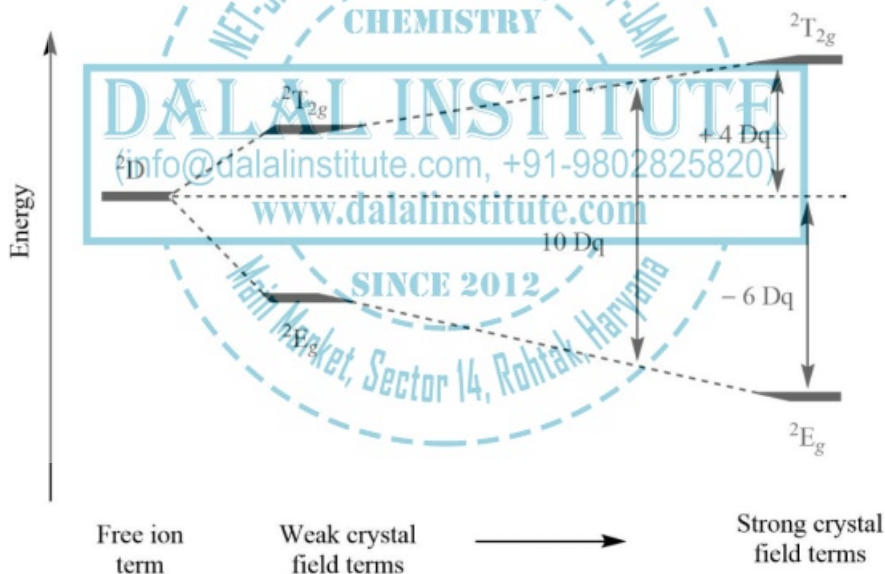


Figure 37. The splitting pattern of free ion term for  $d^0$  complexes in the octahedral crystal field.

Consider the example of  $[\text{Cu}(\text{H}_2\text{O})_6]^{2+}$ .

**1. Calculation of B:** No need to calculate the Racah parameter.

**2. Calculation of  $\Delta_0$ :** In the UV-visible spectra of  $[\text{Cu}(\text{H}_2\text{O})_6]^{2+}$ , the broad band at  $12000 \text{ cm}^{-1}$  is due to spin-allowed  ${}^2\text{E}_g \rightarrow {}^2\text{T}_{2g}$  transition; and hence,  $10 \text{ Dq}$  for this complex is  $12000 \text{ cm}^{-1}$ .

**3. Calculation of  $\beta$ :** No need to calculate the nephelauxetic ratio.

➤  $d^2$  Complexes

Metal complexes with  $d^2$ -configuration have  ${}^3F$  ground state term symbol in the absence of any crystal field. However, when six ligands approach in octahedral coordination, the ground state term symbol becomes  ${}^3T_{1g}$  and remains as such in weak as well as in strong ligand fields. The Orgel and Tanabe-Sugano diagram for  $d^2$ -configuration can be used to estimate the value of crystal field splitting energy for these transition metal complexes.

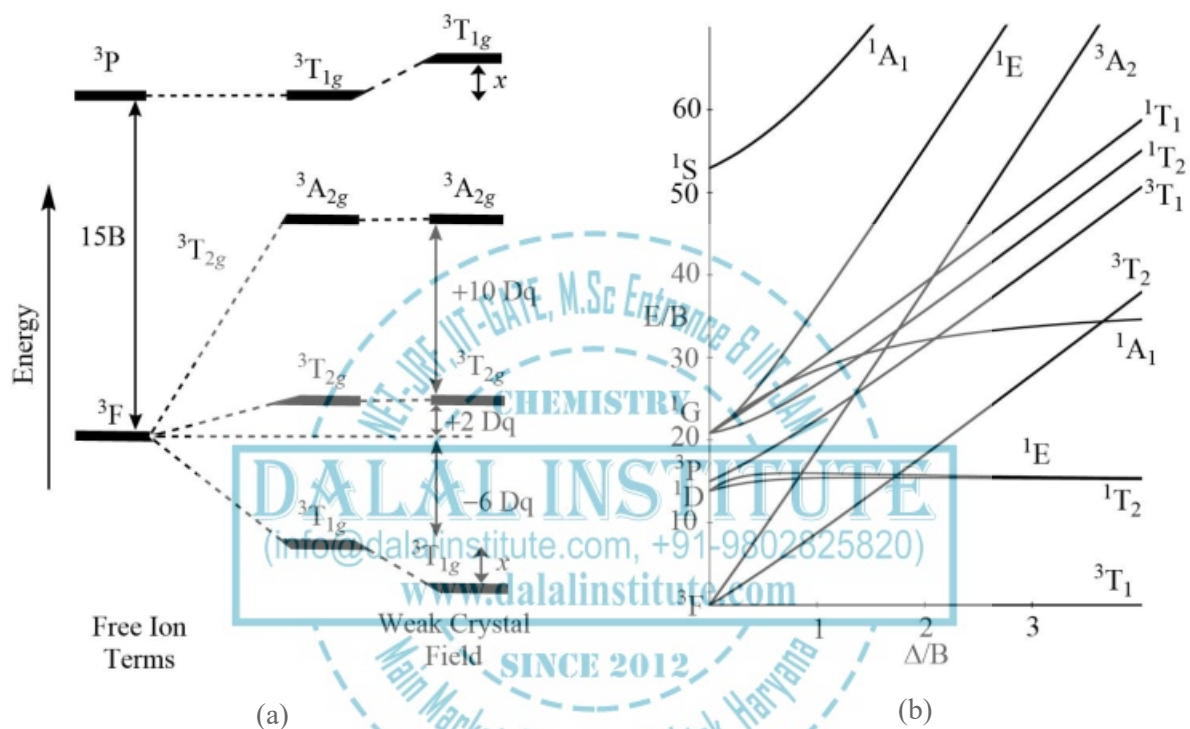


Figure 38. The (a) Orgel and (b) Tanabe-Sugano diagrams for  $d^2$  complexes in the octahedral crystal field.

Consider the example of  $[V(H_2O)_6]^{3+}$ .

**1. Calculation of B:** From the Orgel diagram, it can be clearly seen that the ground state for  $d^2$ -octahedral complexes is  ${}^3T_{1g}$  and there are three main transitions before the crossover point. Moreover, it is worthy to note down that the order of second and third transitions is reversed after the crossover point and only two bands will be observed at or near the crossover point. As the magnitude of the crystal field splitting energy increases, the  ${}^3T_{1g}(F)$  and  ${}^3T_{1g}(P)$  states repel each other more and more with a magnitude of  $x$  energy value.

$$\nu_1 = {}^3T_{1g} \rightarrow {}^3T_{2g}$$

$$\nu_2 = {}^3T_{1g} \rightarrow {}^3A_{2g}$$

$$\nu_3 = {}^3T_{1g} \rightarrow {}^3T_{1g}(P)$$

Which gives

$$v_1 = 8 Dq + x \quad (1)$$

$$v_2 = 18 Dq + x \quad (2)$$

$$v_3 = 15 B + 6 Dq + 2x \quad (3)$$

Adding equation (1) and (2), we get

$$v_2 + v_1 = 18 Dq + x + 8 Dq + x$$

$$v_2 + v_1 = 26 Dq + 2x \quad (4)$$

Subtracting equation (1) and (2), we get

$$v_2 - v_1 = 18 Dq + x - 8 Dq - x$$

$$v_2 - v_1 = 10 Dq \quad (5)$$

Putting the value of  $2x$  from equation (4) in equation (3), we get

$$v_3 = 15 B + 6 Dq + v_2 + v_1 - 26 Dq$$

$$v_3 = 15 B + v_2 + v_1 - 20 Dq \quad (6)$$

Multiplying equation (5) by 2 and putting the value of  $20 Dq$  from equation (5) in equation (6), we get

$$v_3 = 15 B + v_2 + v_1 - 20 Dq$$

$$v_3 = 15 B + v_2 + v_1 - 2v_2 + 2v_1$$

$$15 B = v_3 + v_2 - 3v_1$$

$$B = \frac{v_3 + v_2 - 3v_1}{15} \quad (7)$$

However, only two transitions are observed, this method is difficult to apply in a precise manner and only gives approximations.

From the Tanabe-Sugano diagram, in the UV-visible spectra of  $[V(H_2O)_6]^{3+}$ , two bands are observed with maxima at around  $17500$  and  $26000 \text{ cm}^{-1}$ . There are three possible transitions expected, which include:  $v_1 = {}^3T_{1g} \rightarrow {}^3T_{2g}$ ,  $v_2 = {}^3T_{1g} \rightarrow {}^3T_{1g}(P)$ , and  $v_3 = {}^3T_{1g} \rightarrow {}^3A_{2g}$ ; but only two are observed. The ratio of experimental band energies is:

$$\frac{v_2}{v_1} = \frac{E_2}{E_1} = \frac{E_2/B}{E_1/B} = \frac{26000}{17500} = 1.49$$

Now slide a ruler across the printed diagram (perpendicular to the abscissa) until the ratio of  $E_2/B$  to  $E_1/B$  between lines becomes equivalent to 1.49. In this particular example, this ratio becomes 1.49 when  $\Delta_o/B = 31$ . Stop the ruler movement and find out the values of  $E_2/B$  and  $E_1/B$

$$\frac{E_2}{B} = 43; \quad \frac{E_1}{B} = 27$$

Thus, on the T-S diagram, where  $\Delta_o/B = 31$ ; the value of  ${}^3T_{1g} \rightarrow {}^3T_{2g}$  and  ${}^3T_{1g} \rightarrow {}^3T_{1g}(P)$  i.e.  $E_1/B$  and  $E_2/B$ , are 27 and 43, respectively. The Racah parameter can be found by calculating B from both  $\nu_2$  and  $\nu_1$ .

$$\frac{26000}{B} = 43; \quad \frac{17500}{B} = 27$$

$$B = \frac{26000}{43} = 604 \text{ cm}^{-1}; \quad B = \frac{17500}{27} = 648 \text{ cm}^{-1}$$

$$\text{Average value of Racah parameter (B)} = \frac{604 + 648}{2} = 626 \text{ cm}^{-1}$$

**2. Calculation of  $\Delta_o$ :** Being a weak-complex, the theoretical value of lowest-energy absorption band given by the Orgel diagram is  $8 Dq$  ( ${}^3T_{1g} \rightarrow {}^3T_{2g}$ ); and the experimental value for lowest-energy absorption band is  $17500 \text{ cm}^{-1}$ . Hence, the value of  $10 Dq$  or  $\Delta_o$  can be calculated as:

$$8 Dq = 0.8 \Delta_o = 17500 \text{ cm}^{-1}$$

$$\Delta_o = \frac{17500 \text{ cm}^{-1}}{0.8}$$

$$\Delta_o = 10 Dq = 21875 \text{ cm}^{-1}$$

However, this is just the approximation and a more precise and refined calculation should be carried out using the Tanabe-Sugano diagram. From the average value of the Racah parameter, the ligand field splitting parameter can be found as follows.

$$\frac{\Delta_o}{B} = 31; \quad \frac{\Delta_o}{626 \text{ cm}^{-1}} = 31; \quad \Delta_o = 19406 \text{ cm}^{-1}$$

**3. Calculation of  $\beta$ :** In order to calculate the nephelauxetic ratio, we must have the value of Racah parameter for a free metal ion in its gaseous state. For free  $d^2$  ion like  $V^{3+}$ , it has been observed that  ${}^3P$  state lies  $12925 \text{ cm}^{-1}$  above to the  ${}^3F$  state. Hence,  $15B = 12925 \text{ cm}^{-1}$  or  $B = 862 \text{ cm}^{-1}$ . Now, the value of nephelauxetic ratio can be calculated as

$$\text{Nephelauxetic ratio} = \beta = \frac{B_{\text{complex}}}{B_{\text{free ion}}} = \frac{626 \text{ cm}^{-1}}{862 \text{ cm}^{-1}} = 0.726$$

Hence, inter-electronic repulsion has been decreased during the process of complexation.

➤  $d^8$  Complexes

Metal complexes with  $d^8$ -configuration have  $^3F$  ground state term symbol in the absence of any crystal field. However, when six ligands approach in octahedral coordination, the ground state term symbol becomes  $^3A_{2g}$  and remains as such in weak as well as in strong ligand fields. The Orgel and Tanabe-Sugano diagram for  $d^8$ -configuration can be used to estimate the value of crystal field splitting energy for these transition metal complexes.

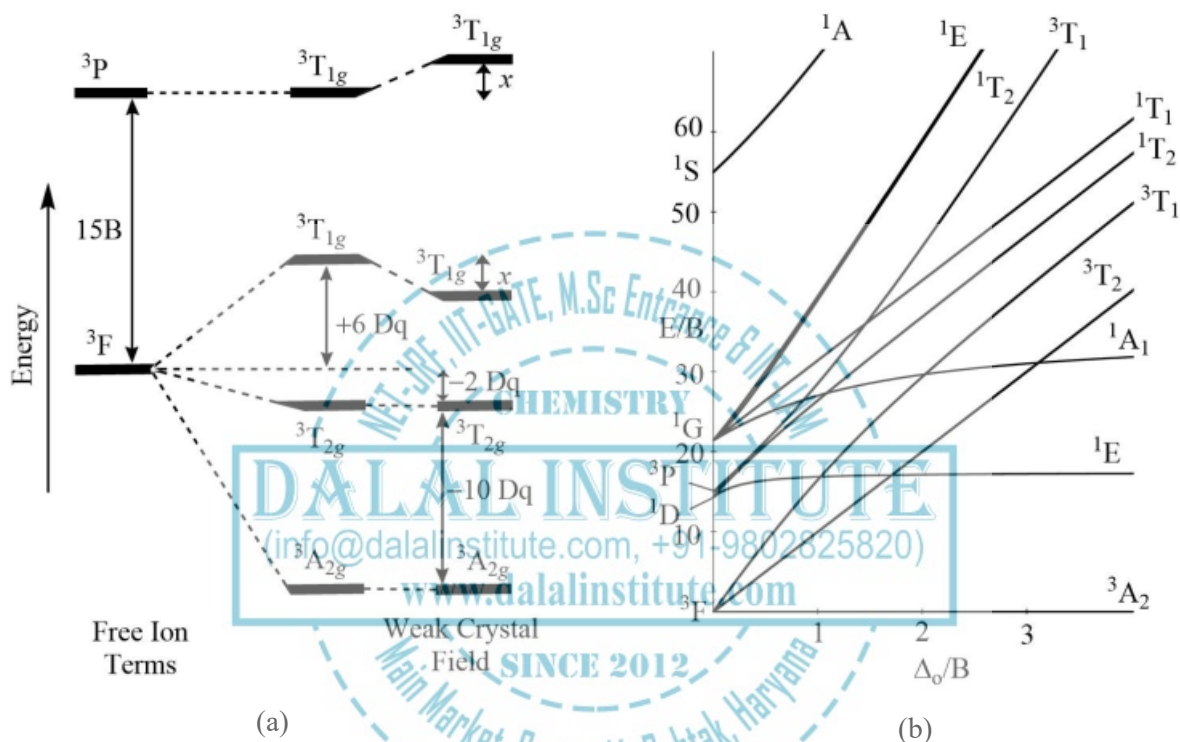


Figure 39. The (a) Orgel and (b) Tanabe-Sugano diagrams for  $d^8$  complexes in the octahedral crystal field.

Consider the example of  $[\text{Ni}(\text{H}_2\text{O})_6]^{2+}$ .

**1. Calculation of B:** From the Orgel diagram, it can be clearly seen that the ground state for  $d^8$ -octahedral complexes is  $^3A_{2g}$  and there are three main transitions. As the magnitude of the crystal field splitting energy increases, the  $^3T_{1g}(\text{F})$  and  $^3T_{1g}(\text{P})$  states repel each other more and more with a magnitude of  $x$  energy value owing to the non-crossing rule of the same symmetry states.

$$\nu_1 = {}^3A_{2g} \rightarrow {}^3T_{2g}$$

$$\nu_2 = {}^3A_{2g} \rightarrow {}^3T_{1g}$$

$$\nu_3 = {}^3A_{2g} \rightarrow {}^3T_{1g}(\text{P})$$

Which gives

$$v_1 = 10 Dq \quad (1)$$

$$v_2 = 18 Dq - x \quad (2)$$

$$v_3 = 15 B + 12 Dq + x \quad (3)$$

Putting value of  $x$  from equation (2) in (3), we get

$$v_3 = 15 B + 12 Dq + 18 Dq - v_2$$

$$v_3 = 15 B + 30 Dq - v_2 \quad (4)$$

Multiplying equation (1) by 3 and putting the value of  $30 Dq$  from equation (1) in (4), we get

$$v_3 = 15 B + 3v_1 - v_2$$

$$15 B = v_3 + v_2 - 3v_1$$

$$B = \frac{v_3 + v_2 - 3v_1}{15} \quad (5)$$

However, this method is applicable only when three transitions are observed. Moreover, this method is difficult to apply in a precise manner and only gives approximations.

From the Tanabe-Sugano diagram, in the UV-visible spectra of  $[\text{Ni}(\text{H}_2\text{O})_6]^{2+}$ , three bands are observed with maxima at around 8500, 14500 and 25300  $\text{cm}^{-1}$ . There are three possible transitions expected, which include:  $v_1 = {}^3A_{2g} \rightarrow {}^3T_{2g}$ ,  $v_2 = {}^3A_{2g} \rightarrow {}^3T_{1g}$ , and  $v_3 = {}^3A_{2g} \rightarrow {}^3T_{1g}(\text{P})$ . The ratio of experimental band energies of  $v_3$  to  $v_2$  is:

$$\frac{v_3}{v_2} = \frac{E_3}{E_2} = \frac{E_3/B}{E_2/B} = \frac{25300}{14500} = 1.74$$

Now slide a ruler across the printed diagram (perpendicular to the abscissa) until the ratio of  $E_2/B$  to  $E_1/B$  between lines becomes equivalent to 1.74. In this particular example, this ratio becomes 1.74 when  $\Delta_0/B = 10$ . Stop the ruler movement and find out the values of  $E_3/B$  and  $E_2/B$  as:

$$\frac{E_3}{B} = 28; \quad \frac{E_2}{B} = 16$$

Thus, on the T-S diagram, where  $\Delta_0/B = 10$ ; the value of  ${}^3A_{2g} \rightarrow {}^3T_{1g}$  and  ${}^3A_{2g} \rightarrow {}^3T_{1g}(\text{P})$  i.e.  $E_2/B$  and  $E_3/B$ , are 28 and 16, respectively. The Racah parameter can be found by calculating  $B$  from second and third i.e. from  $v_3$  and  $v_2$  transitions.

From  $v_3$ , we get

$$\frac{25300}{B} = 28$$

$$B = \frac{25300}{28} = 904 \text{ cm}^{-1}$$

Similarly

$$\frac{14500}{B} = 16$$

$$B = \frac{14500}{16} = 906 \text{ cm}^{-1}$$

Therefore,

$$\text{Average value of Racah parameter (B)} = \frac{904 + 906}{2} = 905 \text{ cm}^{-1}$$

**2. Calculation of  $\Delta_o$ :** Being a weak-complex, the theoretical value of lowest-energy absorption band given by the Orgel diagram is  $10 Dq$  ( ${}^3A_{2g} \rightarrow {}^3T_{2g}$ ); and the experimental value for lowest-energy absorption band is  $8500 \text{ cm}^{-1}$ . Hence, the value of  $10 Dq$  or  $\Delta_o$  can be calculated as

$$10 Dq = 8500 \text{ cm}^{-1}$$

$$\Delta_o = 8500 \text{ cm}^{-1}$$

However, this is just the approximation and a more precise and refined calculation should be carried out using the Tanabe-Sugano diagram. From the average value of the Racah parameter, the ligand field splitting parameter can be found as follows.

$$\frac{\Delta_o}{B} = 10$$

$$\frac{\Delta_o}{905 \text{ cm}^{-1}} = 10$$

$$\Delta_o = 9050 \text{ cm}^{-1}$$

**3. Calculation of  $\beta$ :** In order to calculate the nephelauxetic ratio, we must have the value of the Racah parameter for a free metal ion in its gaseous state. For free  $d^8$  ion like  $\text{Ni}^{2+}$ , it has been observed that  ${}^3P$  state lies  $16200 \text{ cm}^{-1}$  above to the  ${}^3F$  state. Hence,  $15B = 16200 \text{ cm}^{-1}$  or  $B = 1080 \text{ cm}^{-1}$ . Now, the value of nephelauxetic ratio can be calculated as

$$\text{Nephelauxetic ratio} = \beta = \frac{B_{\text{complex}}}{B_{\text{free ion}}} = \frac{905 \text{ cm}^{-1}}{1080 \text{ cm}^{-1}} = 0.838$$

Hence, inter-electronic repulsion has been decreased during the process of complexation.

➤  $d^3$  Complexes

Metal complexes with  $d^3$ -configuration have  $^4F$  ground state term symbol in the absence of any crystal field. However, when six ligands approach in octahedral coordination, the ground state term symbol becomes  $^4A_{2g}$  and remains as such in weak as well as in strong ligand fields. The Orgel and Tanabe-Sugano diagram for  $d^3$ -configuration can be used to estimate the value of crystal field splitting energy for these transition metal complexes.

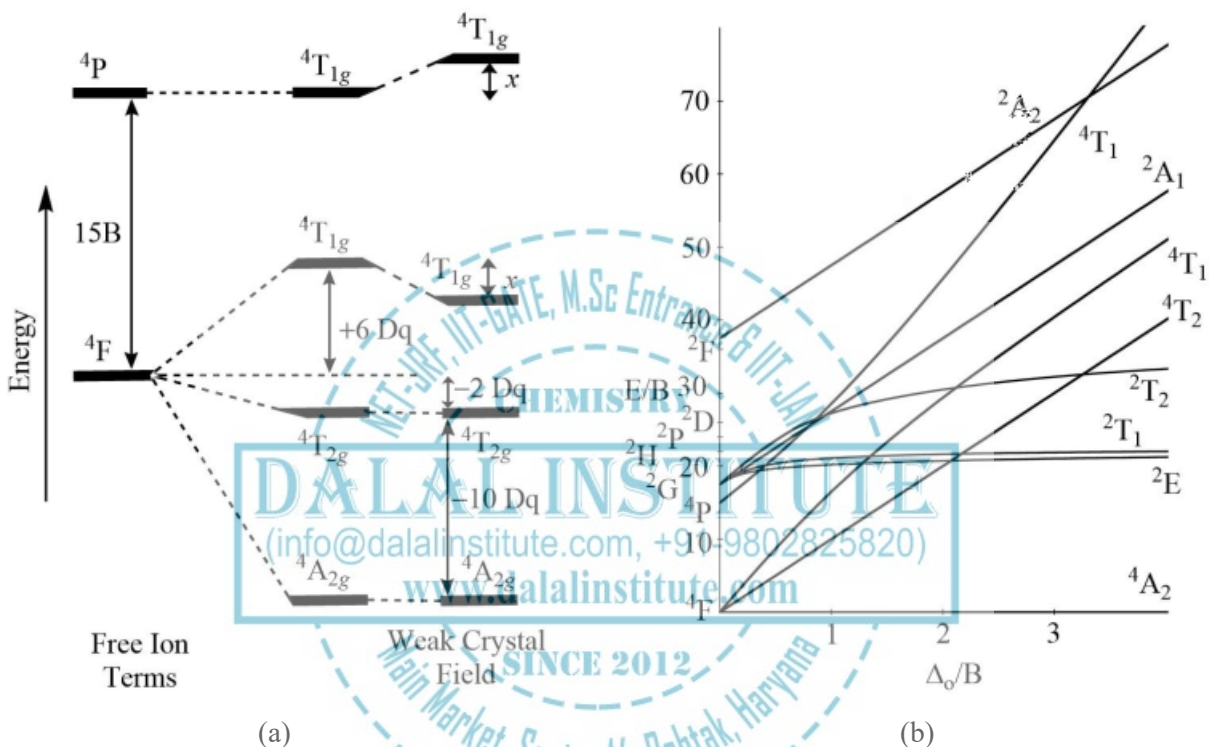


Figure 40. The (a) Orgel and (b) Tanabe-Sugano diagrams for  $d^3$  complexes in the octahedral crystal field.

Consider the example of  $[\text{Cr}(\text{H}_2\text{O})_6]^{3+}$ .

**1. Calculation of B:** From the Orgel diagram, it can be clearly seen that the ground state for  $d^3$ -octahedral complexes is  $^4A_{2g}$  and there are three main transitions. As the magnitude of the crystal field splitting energy increases, the  $^4T_{1g}(\text{F})$  and  $^4T_{1g}(\text{P})$  states repel each other more and more with a magnitude of  $x$  energy value owing to the non-crossing rule of the same symmetry states.

$$v_1 = ^4A_{2g} \rightarrow ^4T_{2g}$$

$$v_2 = ^4A_{2g} \rightarrow ^4T_{1g}$$

$$v_3 = ^4A_{2g} \rightarrow ^4T_{1g}(\text{P})$$

Which gives

$$v_1 = 10 Dq \quad (1)$$

$$v_2 = 18 Dq - x \quad (2)$$

$$v_3 = 15 B + 12 Dq + x \quad (3)$$

Putting the value of  $x$  from equation (2) in (3), we get

$$v_3 = 15 B + 12 Dq + 18 Dq - v_2$$

$$v_3 = 15 B + 30 Dq - v_2 \quad (4)$$

Multiplying equation (1) by 3 and putting the value of  $30 Dq$  from equation (1) in (4), we get

$$\begin{aligned} v_3 &= 15 B + 3v_1 - v_2 \\ 15 B &= v_3 + v_2 - 3v_1 \\ B &= \frac{v_3 + v_2 - 3v_1}{15} \end{aligned} \quad (5)$$

However, this method is applicable only when three transitions are observed. Moreover, this method is difficult to apply in a precise manner and only gives approximations.

From the Tanabe-Sugano diagram, in the UV-visible spectra of  $[\text{Cr}(\text{H}_2\text{O})_6]^{3+}$ , three bands are observed with maxima at around 17000, 24000 and 37000  $\text{cm}^{-1}$ . There are three possible transitions expected, which include:  $v_1 = {}^4A_{2g} \rightarrow {}^4T_{2g}$ ,  $v_2 = {}^4A_{2g} \rightarrow {}^4T_{1g}$ , and  $v_3 = {}^4A_{2g} \rightarrow {}^4T_{1g}(\text{P})$ . The ratio of experimental band energies of  $v_2$  to  $v_1$  is:

$$\frac{v_2}{v_1} = \frac{E_2}{E_1} = \frac{E_2/B}{E_1/B} = \frac{24000}{17000} = 1.41$$

Now slide a ruler across the printed diagram (perpendicular to the abscissa) until the ratio of  $E_2/B$  to  $E_1/B$  between lines becomes equivalent to 1.41. In this particular example, this ratio becomes 1.41 when  $\Delta_o/B = 24$ . Stop the ruler movement and find out the values of  $E_2/B$  and  $E_1/B$  as:

$$\frac{E_2}{B} = 33.90; \quad \frac{E_1}{B} = 24$$

Thus, on the T-S diagram, where  $\Delta_o/B = 24$ ; the value of  ${}^4A_{2g} \rightarrow {}^4T_{1g}$  and  ${}^4A_{2g} \rightarrow {}^4T_{1g}(\text{P})$  i.e.  $E_2/B$  and  $E_3/B$ , are 33.90 and 24, respectively. The Racah parameter can be found by calculating  $B$  from first and second i.e. from  $v_2$  and  $v_1$  transitions.

From  $v_2$ , we get

$$\frac{24000}{B} = 33.90$$

$$B = \frac{24000}{33.90} = 708 \text{ cm}^{-1}$$

Similarly

$$\frac{17000}{B} = 24$$

$$B = \frac{17000}{24} = 708 \text{ cm}^{-1}$$

Therefore,

$$\text{Average value of Racah parameter (B)} = \frac{708 + 708}{2} = 708 \text{ cm}^{-1}$$

**2. Calculation of  $\Delta_o$ :** Being a weak-complex, the theoretical value of lowest-energy absorption band given by the Orgel diagram is  $10 Dq$  ( ${}^4A_{2g} \rightarrow {}^4T_{2g}$ ); and the experimental value for lowest-energy absorption band is  $17000 \text{ cm}^{-1}$ . Hence, the value of  $10 Dq$  or  $\Delta_o$  can be calculated as

$$10 Dq = 17000 \text{ cm}^{-1}$$

$$\Delta_o = 17000 \text{ cm}^{-1}$$

However, this is just the approximation and a more precise and refined calculation should be carried out using the Tanabe-Sugano diagram. From the average value of the Racah parameter, the ligand field splitting parameter can be found as follows.

$$\frac{\Delta_o}{B} = 24$$

$$\frac{\Delta_o}{708 \text{ cm}^{-1}} = 24$$

$$\Delta_o = 16992 \text{ cm}^{-1}$$

**3. Calculation of  $\beta$ :** In order to calculate the nephelauxetic ratio, we must have the value of the Racah parameter for a free metal ion in its gaseous state. For free  $d^3$  ion like  $\text{Cr}^{3+}$ , it has been observed that  ${}^3P$  state lies  $15450 \text{ cm}^{-1}$  above to the  ${}^3F$  state. Hence,  $15B = 15450 \text{ cm}^{-1}$  or  $B = 1030 \text{ cm}^{-1}$ . Now, the value of nephelauxetic ratio can be calculated as:

$$\text{Nephelauxetic ratio} = \beta = \frac{B_{\text{complex}}}{B_{\text{free ion}}} = \frac{708 \text{ cm}^{-1}}{1030 \text{ cm}^{-1}} = 0.687$$

Hence, inter-electronic repulsion has been decreased during the process of complexation.



$$v_3 = {}^4T_{1g} \rightarrow {}^4T_{1g}(P)$$

Which gives

$$v_1 = 8 Dq + x \quad (1)$$

$$v_2 = 18 Dq + x \quad (2)$$

$$v_3 = 15 B + 6 Dq + 2x \quad (3)$$

Adding equation (1) and (2), we get

$$v_2 + v_1 = 18 Dq + x + 8 Dq + x$$

$$v_2 + v_1 = 26 Dq + 2x \quad (4)$$

Subtracting equation (1) and (2), we get

$$v_2 - v_1 = 18 Dq + x - 8 Dq - x$$

$$v_2 - v_1 = 10 Dq \quad (5)$$

Putting the value of  $2x$  from equation (4) in equation (3), we get

$$v_3 = 15 B + 6 Dq + v_2 + v_1 - 26 Dq$$

$$v_3 = 15 B + v_2 + v_1 - 20 Dq \quad (6)$$

Multiplying equation (5) by 2 and putting the value of  $20 Dq$  from equation (5) in equation (6), we get

$$v_3 = 15 B + v_2 + v_1 - 20 Dq$$

$$v_3 = 15 B + v_2 + v_1 - 2v_2 + 2v_1$$

$$15 B = v_3 + v_2 - 3v_1$$

$$B = \frac{v_3 + v_2 - 3v_1}{15} \quad (7)$$

However, only two transitions are observed, this method is difficult to apply in a precise manner and only gives approximations.

From the Tanabe-Sugano diagram, in the UV-visible spectra of  $[\text{Co}(\text{H}_2\text{O})_6]^{2+}$ , two bands are observed with maxima at around 8000, 19600 and 21600  $\text{cm}^{-1}$ . There are three possible transitions expected, which include:  $v_1 = {}^4T_{1g} \rightarrow {}^4T_{2g}$ ,  $v_2 = {}^4T_{1g} \rightarrow {}^4A_{2g}$  and  $v_3 = {}^4T_{1g} \rightarrow {}^4T_{1g}(P)$ . The ratio of experimental band energies is:

$$\frac{v_3}{v_1} = \frac{E_3}{E_1} = \frac{E_3/B}{E_1/B} = \frac{21600}{8000} = 2.70$$

Now slide a ruler across the printed diagram (perpendicular to the abscissa) until the ratio of  $E_3/B$  to  $E_1/B$  between lines becomes equivalent to 2.70. In this particular example, this ratio becomes 2.70 when  $\Delta_o/B = 9.5$ . Stop the ruler movement and find out the values of  $E_2/B$  and  $E_1/B$  as:

$$\frac{E_3}{B} = 22; \quad \frac{E_1}{B} = 8.2$$

Thus, on the T-S diagram, where  $\Delta_o/B = 31$ ; the value of  ${}^3T_{1g} \rightarrow {}^3T_{2g}$  and  ${}^3T_{1g} \rightarrow {}^3T_{1g}(P)$  i.e.  $E_1/B$  and  $E_3/B$ , are 8.2 and 22, respectively. The Racah parameter can be found by calculating B from both  $\nu_2$  and  $\nu_1$ .

$$\frac{21600}{B} = 22; \quad \frac{8000}{B} = 8.2$$

$$B = \frac{21600}{22} = 982 \text{ cm}^{-1}; \quad B = \frac{8000}{8.2} = 976 \text{ cm}^{-1}$$

$$\text{Average value of Racah parameter (B)} = \frac{982 + 976}{2} = 979 \text{ cm}^{-1}$$

**2. Calculation of  $\Delta_o$ :** Being a weak-complex, the theoretical value of lowest-energy absorption band given by the Orgel diagram is  $8 Dq$  ( ${}^3T_{1g} \rightarrow {}^3T_{2g}$ ); and the experimental value for lowest-energy absorption band is  $8000 \text{ cm}^{-1}$ . Hence, the value of  $10 Dq$  or  $\Delta_o$  can be calculated as

$$8 Dq = 0.8 \Delta_o = 8000 \text{ cm}^{-1}$$

$$\Delta_o = \frac{8000 \text{ cm}^{-1}}{0.8}$$

$$\Delta_o = 10 Dq = 10000 \text{ cm}^{-1}$$

However, this is just the approximation and a more precise and refined calculation should be carried out using the Tanabe-Sugano diagram. From the average value of the Racah parameter, the ligand field splitting parameter can be found as follows.

$$\frac{\Delta_o}{B} = 9.5; \quad \frac{\Delta_o}{979 \text{ cm}^{-1}} = 9.5; \quad \Delta_o = 9300 \text{ cm}^{-1}$$

**3. Calculation of  $\beta$ :** In order to calculate the nephelauxetic ratio, we must have the value of the Racah parameter for a free metal ion in its gaseous state. For free  $d^7$  ion like  $\text{Co}^{2+}$ , it has been observed that  ${}^3P$  state lies  $16755 \text{ cm}^{-1}$  above to the  ${}^3F$  state. Hence,  $15B = 16755 \text{ cm}^{-1}$  or  $B = 1117 \text{ cm}^{-1}$ . Now, the value of nephelauxetic ratio can be calculated as:

$$\text{Nephelauxetic ratio} = \beta = \frac{B_{\text{complex}}}{B_{\text{free ion}}} = \frac{979 \text{ cm}^{-1}}{1117 \text{ cm}^{-1}} = 0.876$$

Hence, inter-electronic repulsion has been decreased during the process of complexation.

➤ *d<sup>4</sup> Complexes*

Metal complexes with *d<sup>4</sup>*-configuration have <sup>5</sup>D ground state term symbol in the absence of any crystal field. However, when six ligands approach in octahedral coordination, the ground state term symbol becomes <sup>5</sup>E<sub>g</sub> in the weak field; and becomes <sup>3</sup>T<sub>1g</sub> when the ligand field becomes sufficiently strong. The Orgel and Tanabe-Sugano diagram for *d<sup>4</sup>*-configuration can be used to estimate the value of crystal field splitting energy for these complexes.

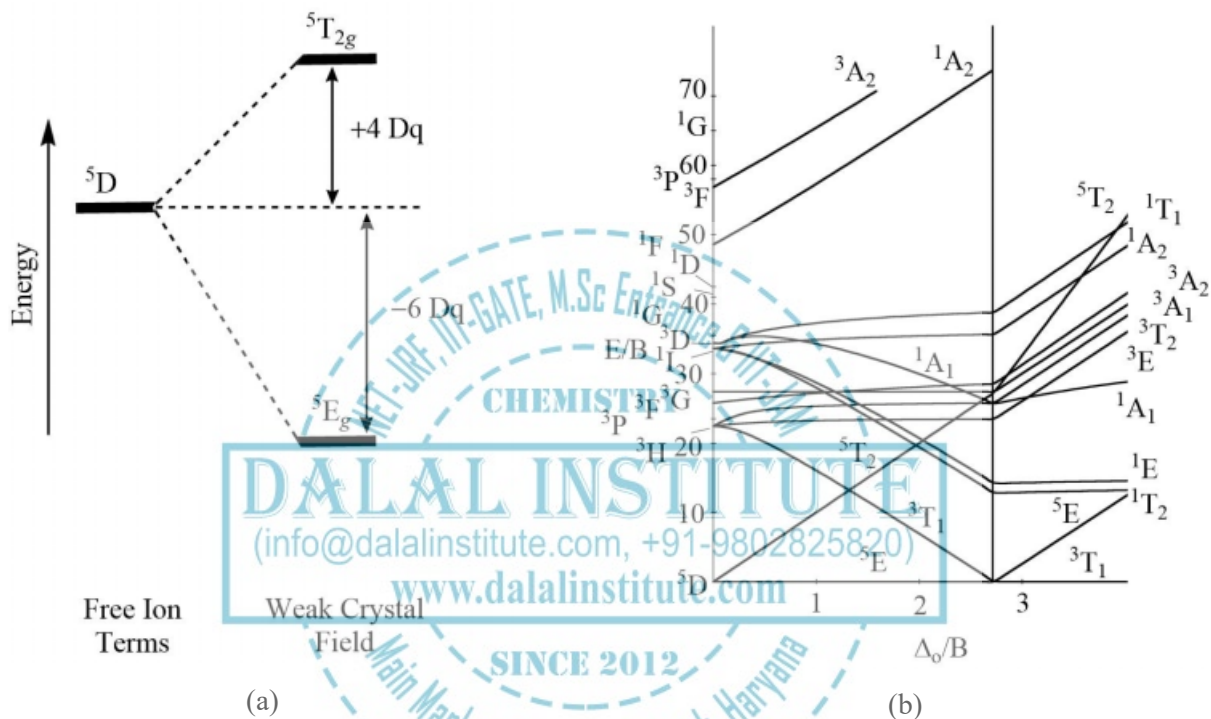


Figure 42. The (a) Orgel and (b) Tanabe-Sugano diagrams for *d<sup>4</sup>* complexes in the octahedral crystal field.

Consider the example of  $[\text{Mn}(\text{CN})_6]^{3-}$

**1. Calculation of B:** From the Tanabe-Sugano diagram, it can clearly be seen that the spin-allowed *d-d* transitions in low-spin *d<sup>4</sup>* metal complexes are <sup>3</sup>T<sub>1g</sub> → <sup>3</sup>E<sub>g</sub>, <sup>3</sup>T<sub>1g</sub> → <sup>3</sup>T<sub>2g</sub>, <sup>3</sup>T<sub>1g</sub> → <sup>3</sup>A<sub>1g</sub> and <sup>3</sup>T<sub>1g</sub> → <sup>3</sup>A<sub>2g</sub>. In the UV-visible absorption spectra of  $[\text{Mn}(\text{CN})_6]^{3-}$ , three bands are observed; one strong band with maxima at around 27000 and other two bands at 29000 and 34000 cm<sup>-1</sup>. Moreover, the bands at 21800 and 43500 cm<sup>-1</sup> can be ignored as they correspond to charge transfer transitions. Thus, the ratio of experimental energies is

$$\frac{\nu_2}{\nu_1} = \frac{E_2}{E_1} = \frac{E_2/B}{E_1/B} = \frac{29000 \text{ cm}^{-1}}{27000 \text{ cm}^{-1}} = 1.07$$

Now slide a ruler across the printed diagram (perpendicular to the abscissa) until the ratio of E<sub>2</sub>/B to E<sub>1</sub>/B i.e. the ratio between the lines corresponding to the first two spin-allowed transitions becomes equivalent

to 1.07. In this particular example, this ratio becomes 1.07 when  $\Delta_o/B = 40$ . Stop the ruler movement and find out the values of  $E_2/B$  and  $E_1/B$ .

$$\frac{E_2}{B} = 38; \quad \frac{E_1}{B} = 35$$

Thus, on the T-S diagram, where  $\Delta_o/B = 40$ ; the value of  ${}^3T_{1g} \rightarrow {}^3T_{2g}$  and  ${}^3T_{1g} \rightarrow {}^3E_g$  i.e.  $E_2/B$  and  $E_1/B$ , are 38 and 35, respectively. The Racah parameter can be found by calculating B from both  $\nu_2$  and  $\nu_1$ .

$$\frac{29000 \text{ cm}^{-1}}{B} = 38; \quad \frac{27000 \text{ cm}^{-1}}{B} = 35$$

$$B = \frac{29000 \text{ cm}^{-1}}{38} = 763 \text{ cm}^{-1}; \quad B = \frac{27000 \text{ cm}^{-1}}{35} = 771 \text{ cm}^{-1}$$

$$\text{Average value of Racah parameter (B)} = \frac{763 \text{ cm}^{-1} + 771 \text{ cm}^{-1}}{2} = 767 \text{ cm}^{-1}$$

**2. Calculation of  $\Delta_o$ :** The only parameter that is needed to be sought for the calculation of the magnitude of crystal field splitting energy (10 Dq) in weak field complexes is the single absorption band in a UV-vis experiment. Hence, the energy of the transition  ${}^5E_g \rightarrow {}^5T_{2g}$  should give the value of  $\Delta$  directly. In other words, the lowest energy absorption band in  $d^4$  high-spin complexes is equal to the crystal field splitting energy. However, the magnitude of crystal field splitting energy for high-spin  $d^4$  complexes cannot be obtained accurately from the Orgel diagram as the Jahn-Teller distortion reduces the symmetry from perfectly octahedral to a tetragonal geometry. The effect of Jahn-Teller distortion will be discussed later in this chapter. Furthermore, the practical applicability of the Tanabe-Sugano diagram in the high-spin region (before  $\Delta_o/B = 27$ ) is strongly doubted because only one spin allowed transition is present, and it is a fact that two minimum spin-allowed transitions are required for the ratio calculation.

Being a strong-field complex, the theoretical value of crystal field splitting energy in  $[\text{Mn}(\text{CN})_6]^{3-}$  cannot be given by the Orgel diagram; hence, we are bound to use Tanabe-Sugano diagram. From the average value of the Racah parameter, what we have deduced earlier, the ligand field splitting parameter can be found as follows.

$$\frac{\Delta_o}{B} = 40; \quad \frac{\Delta_o}{767 \text{ cm}^{-1}} = 40; \quad \Delta_o = 30680 \text{ cm}^{-1}$$

**3. Calculation of  $\beta$ :** In order to calculate the nephelauxetic ratio, we must have the value of the Racah parameter for a free metal ion in its gaseous state. For free  $d^4$  ion like  $\text{Mn}^{3+}$ , the value of B is found to be  $1140 \text{ cm}^{-1}$ . Now, the value of nephelauxetic ratio can be calculated as

$$\text{Nephelauxetic ratio} = \beta = \frac{B_{\text{complex}}}{B_{\text{free ion}}} = \frac{767 \text{ cm}^{-1}}{1140 \text{ cm}^{-1}} = 0.673$$

Hence, inter-electronic repulsion has been decreased during the process of complexation.

➤  $d^6$  Complexes

Metal complexes with  $d^6$ -configuration have  $^5D$  ground state term symbol in the absence of any crystal field. However, when six ligands approach in octahedral coordination, the ground state term symbol becomes  $^5T_{2g}$  in the weak field; and becomes  $^1A_{1g}$  when the ligand field becomes sufficiently strong. The Orgel and Tanabe-Sugano diagram for  $d^6$ -configuration can be used to estimate the value of crystal field splitting energy for these complexes.

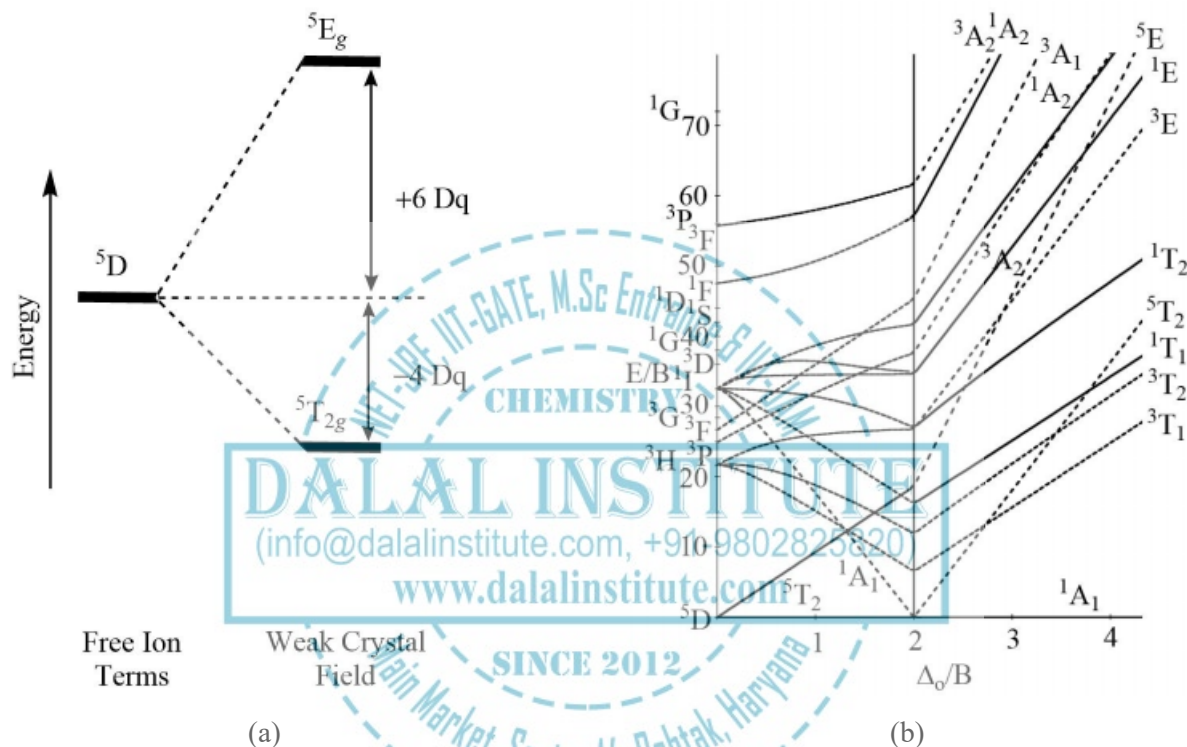


Figure 42. The (a) Orgel and (b) Tanabe-Sugano diagrams for  $d^6$  complexes in octahedral crystal field.

Consider the example of  $[\text{Co}(\text{en})_3]^{3+}$

**1. Calculation of B:** From the Tanabe-Sugano diagram, it can clearly be seen that the spin-allowed  $d-d$  transitions in low-spin  $d^6$  metal complexes are  $^1A_{1g} \rightarrow ^1T_{1g}$  and  $^1A_{1g} \rightarrow ^1T_{2g}$ . In the UV-visible absorption spectra of  $[\text{Co}(\text{en})_3]^{3+}$ , two bands are observed; one strong band with maxima at around 21450 and the other band at  $29450 \text{ cm}^{-1}$ . Therefore, the ratio of experimental band energies is

$$\frac{\nu_2}{\nu_1} = \frac{E_2}{E_1} = \frac{E_2/B}{E_1/B} = \frac{29450 \text{ cm}^{-1}}{21450 \text{ cm}^{-1}} = 1.37$$

Now slide a ruler across the printed diagram (perpendicular to the abscissa) until the ratio of  $E_2/B$  to  $E_1/B$  i.e. the ratio between the lines corresponding to the first two spin-allowed transitions becomes equivalent

to 1.37. In this particular example, this ratio becomes 1.37 when  $\Delta_o/B = 40$ . Stop the ruler movement and find out the values of  $E_2/B$  and  $E_1/B$ .

$$\frac{E_2}{B} = 52; \quad \frac{E_1}{B} = 38$$

Thus, on the T-S diagram, where  $\Delta_o/B = 40$ ; the value of  ${}^1A_{1g} \rightarrow {}^1T_{2g}$  and  ${}^1A_{1g} \rightarrow {}^1T_{1g}$  i.e.  $E_2/B$  and  $E_1/B$ , are 52 and 38, respectively. The Racah parameter can be found by calculating B from both  $\nu_2$  and  $\nu_1$ .

$$\frac{29450 \text{ cm}^{-1}}{B} = 52; \quad \frac{21450 \text{ cm}^{-1}}{B} = 38$$

$$B = \frac{29450 \text{ cm}^{-1}}{52} = 566 \text{ cm}^{-1}; \quad B = \frac{21450 \text{ cm}^{-1}}{38} = 564 \text{ cm}^{-1}$$

$$\text{Average value of Racah parameter (B)} = \frac{566 \text{ cm}^{-1} + 564 \text{ cm}^{-1}}{2} = 565 \text{ cm}^{-1}$$

**2. Calculation of  $\Delta_o$ :** The only parameter that is needed to be sought for the calculation of the magnitude of crystal field splitting energy (10 Dq) in weak-field  $d^6$ -complexes is the single absorption band in a UV-vis experiment. Hence, the energy of the transition  ${}^5T_{2g} \rightarrow {}^5E_g$  should give the value of  $\Delta$  directly. In other words, the lowest energy absorption band in  $d^6$  high-spin complexes is equal to the crystal field splitting energy. However, the magnitude of crystal field splitting energy for high-spin  $d^6$  complexes cannot be obtained accurately from the Orgel diagram as the Jahn-Teller distortion reduces the symmetry from perfectly octahedral to a tetragonal geometry. The effect of Jahn-Teller distortion will be discussed later in this chapter. Furthermore, the practical applicability of the Tanabe-Sugano diagram in the high-spin region (before  $\Delta_o/B = 20$ ) is strongly doubted because only one spin allowed transition is present, and it is a fact that two minimum spin-allowed transitions are required for the ratio calculation.

Being a strong-field complex, the theoretical value of crystal field splitting energy in  $[\text{Co(en)}_3]^{3+}$  cannot be given by the Orgel diagram; hence, we are bound to use Tanabe-Sugano diagram. From the average value of the Racah parameter, what we have deduced earlier, the ligand field splitting parameter can be found as follows.

$$\frac{\Delta_o}{B} = 40; \quad \frac{\Delta_o}{565 \text{ cm}^{-1}} = 40; \quad \Delta_o = 22600 \text{ cm}^{-1}$$

**3. Calculation of  $\beta$ :** In order to calculate the nephelauxetic ratio, we must have the value of the Racah parameter for a free metal ion in its gaseous state. For free  $d^6$  ion like  $\text{Co}^{3+}$ , the value of B is found to be  $1100 \text{ cm}^{-1}$ . Now, the value of nephelauxetic ratio can be calculated as

$$\text{Nephelauxetic ratio} = \beta = \frac{B_{\text{complex}}}{B_{\text{free ion}}} = \frac{565 \text{ cm}^{-1}}{1100 \text{ cm}^{-1}} = 0.514$$

Hence, inter-electronic repulsion has been decreased during the process of complexation.

➤  $d^5$  Complexes

Metal complexes with  $d^5$ -configuration have  ${}^6S$  ground state term symbol in the absence of any crystal field. However, when six ligands approach in octahedral coordination, the ground state term symbol becomes  ${}^6A_{1g}$  in the weak field; and becomes  ${}^2T_{2g}$  when the ligand field becomes sufficiently strong. The Tanabe-Sugano diagram for  $d^5$ -configuration can be used to estimate the value of crystal field splitting energy for these complexes.

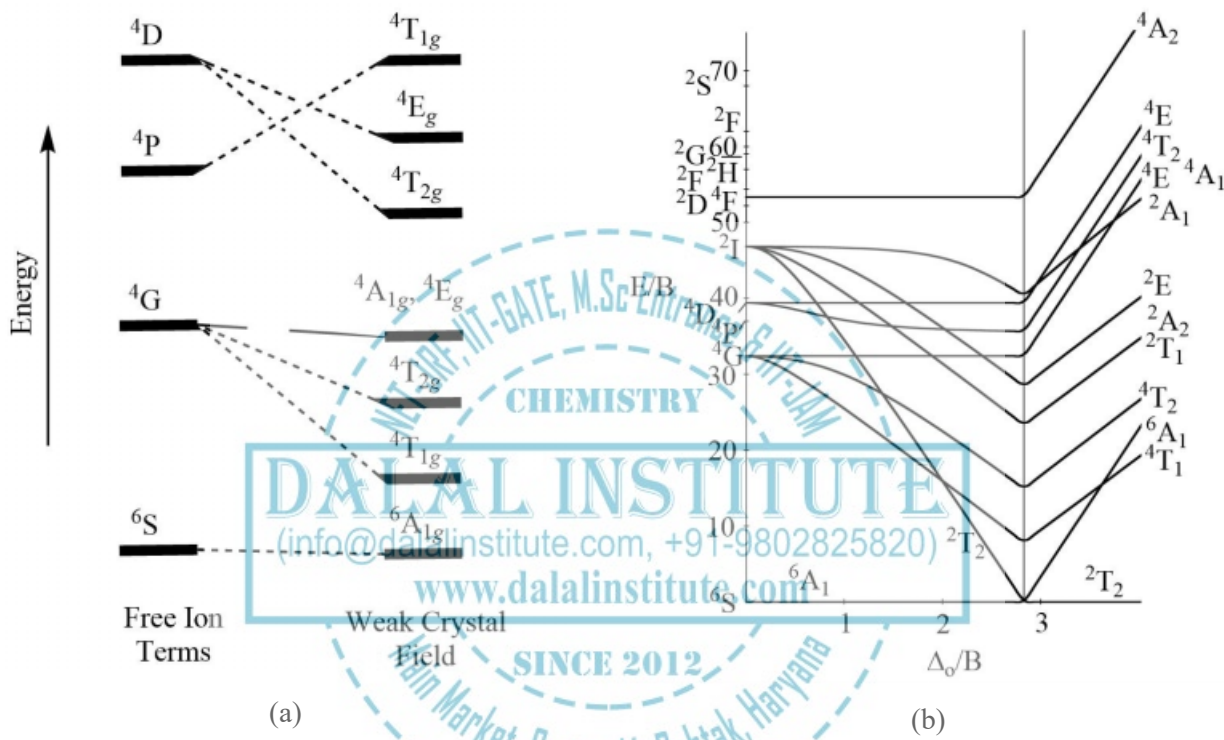


Figure 42. The (a) Orgel and (b) Tanabe-Sugano diagrams for  $d^5$  complexes in the octahedral crystal field.

Consider the example of  $[\text{Mn}(\text{H}_2\text{O})_6]^{2+}$

**1. Calculation of B:** From the Tanabe-Sugano diagram, it can clearly be seen that there is no spin-allowed  $d-d$  transitions in high-spin  $d^5$  metal complexes. However, main spin-forbidden transitions are  ${}^6A_{1g} \rightarrow {}^4T_{1g}(G)$ ,  ${}^6A_{1g} \rightarrow {}^4T_{2g}(G)$ ,  ${}^6A_{1g} \rightarrow {}^4A_{1g}(G)$ ,  ${}^6A_{1g} \rightarrow {}^4E_g(G)$ ,  ${}^1A_{1g} \rightarrow {}^4T_{2g}(D)$  and  ${}^1A_{1g} \rightarrow {}^4E_g(D)$ . In the UV-visible absorption spectra of  $[\text{Mn}(\text{H}_2\text{O})_6]^{2+}$ , the first two bands are observed at around 18600 and the other band at  $22900 \text{ cm}^{-1}$ . Therefore, the ratio of experimental band energies is

$$\frac{\nu_2}{\nu_1} = \frac{E_2}{E_1} = \frac{E_2/B}{E_1/B} = \frac{22900 \text{ cm}^{-1}}{18600 \text{ cm}^{-1}} = 1.23$$

Now slide a ruler across the printed diagram (perpendicular to the abscissa) until the ratio of  $E_2/B$  to  $E_1/B$  i.e. the ratio between the lines corresponding to the first two spin-allowed transitions becomes equivalent

to 1.23. In this particular example, this ratio becomes 1.23 when  $\Delta_o/B = 11$ . Stop the ruler movement and find out the values of  $E_2/B$  and  $E_1/B$ .

$$\frac{E_2}{B} = 29$$

$$\frac{E_1}{B} = 24$$

Thus, on the Tanabe-Sugano diagram, where  $\Delta_o/B = 11$ ; the value of  ${}^6A_{1g} \rightarrow {}^4T_{2g}(G)$  and  ${}^6A_{1g} \rightarrow {}^4T_{1g}(G)$  i.e.  $E_2/B$  and  $E_1/B$ , are 29 and 24, respectively. The Racah parameter can be found by calculating B from both  $\nu_2$  and  $\nu_1$ .

$$\frac{22900 \text{ cm}^{-1}}{B} = 29$$

$$\frac{18600 \text{ cm}^{-1}}{B} = 24$$

$$B = \frac{22900 \text{ cm}^{-1}}{29} = 789 \text{ cm}^{-1}; \quad B = \frac{18600 \text{ cm}^{-1}}{24} = 775 \text{ cm}^{-1}$$

$$\text{Average value of Racah parameter (B)} = \frac{789 \text{ cm}^{-1} + 775 \text{ cm}^{-1}}{2} = 782 \text{ cm}^{-1}$$

**2. Calculation of  $\Delta_o$ :** The magnitude of crystal field splitting energy for high-spin  $d^5$  complexes cannot be obtained accurately from the Orgel diagram as the degeneracy of the ground state term is only one and does not split at all in the octahedral field. Therefore, we are bound to use the Tanabe-Sugano diagram. From the average value of the Racah parameter, what we have deduced earlier, the ligand field splitting parameter can be found as follows.

$$\frac{\Delta_o}{B} = 11$$

$$\frac{\Delta_o}{782 \text{ cm}^{-1}} = 11$$

$$\Delta_o = 8602 \text{ cm}^{-1}$$

**3. Calculation of  $\beta$ :** In order to calculate the nephelauxetic ratio, we must have the value of Racah parameter for a free metal ion in its gaseous state. For free  $d^5$  ion like  $\text{Mn}^{2+}$ , the value of B is found to be  $960 \text{ cm}^{-1}$ . Now, the value of nephelauxetic ratio can be calculated as

$$\text{Nephelauxetic ratio} = \beta = \frac{B_{\text{complex}}}{B_{\text{free ion}}} = \frac{782 \text{ cm}^{-1}}{960 \text{ cm}^{-1}} = 0.814$$

Hence, the inter-electronic repulsion has been decreased during the process of complexation.

### ❖ Effect of Distortion on the $d$ -Orbital Energy Levels

The splitting pattern of five  $d$ -orbitals for different geometries is also different; and therefore, this also induces an evident effect upon the  $d-d$  transitions in a metal ion complex. The UV-visible spectrum arising from these transitions provide information about the structure of these complexes. Hence, the effect of structural distortion upon the energies of the various free ion terms must be studied in detail.

#### ➤ Distortion in Six-Coordinated Complexes

The hexa-coordination of ligands in different metal complexes can be categorized as octahedral, tetragonal, rhombic and trigonal anti-prismatic. If six ligands are supposed to approach the metal center along  $x$ ,  $y$ , and  $z$ -axis (each passing through the two faces of a cube) then the octahedral, tetragonal and rhombic geometries can be represented by the bond length correlation of  $x = y = z$ ,  $x = y \neq z$  and  $x \neq y \neq z$ , respectively. The tetragonal distortions from perfect octahedron occur as the elongation or compression along only one four-fold axis while the rhombic distortions occur as the unequal amount of elongation or compression along two four-fold axes of rotation. Moreover, the trigonal distortions occur as the elongation or compression along one of the four three-fold symmetry axis.

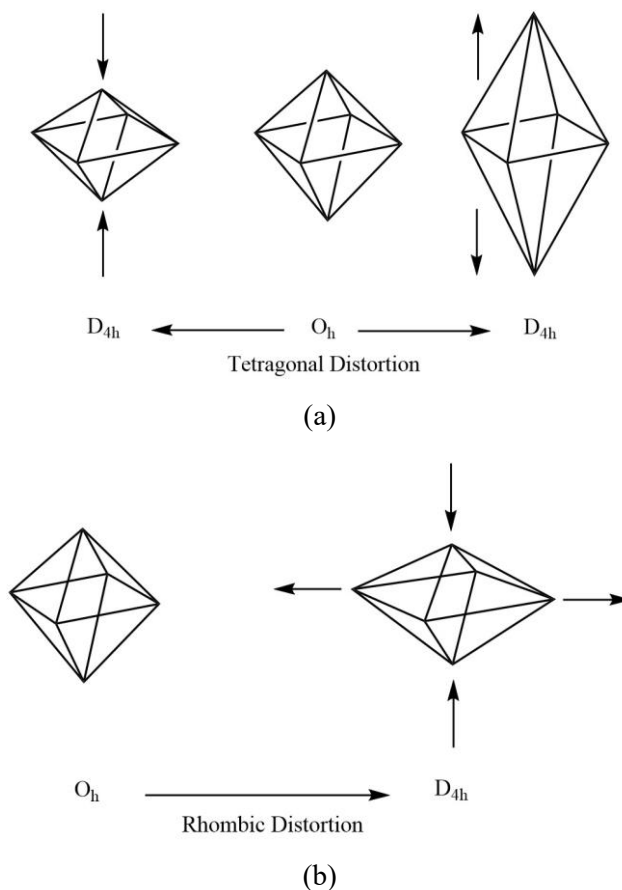


Figure 43. Continued on the next page...

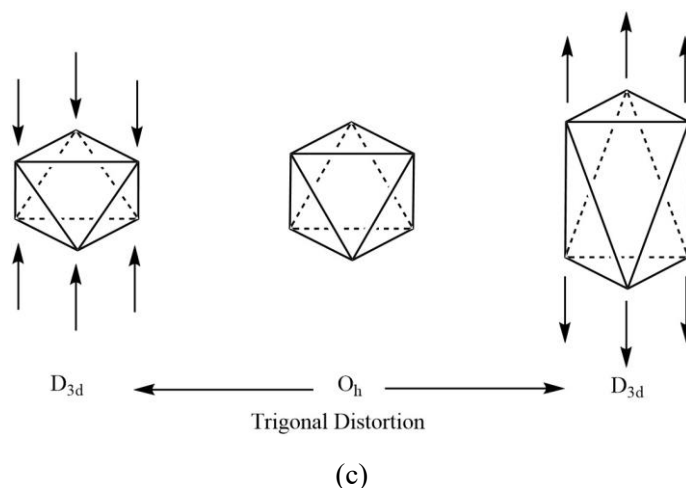


Figure 43. The (a) tetragonal (b) rhombic and (c) trigonal distortion in octahedral metal complexes.

**1. Tetragonal distortion:** As there is no inter-electronic repulsion in the  $d^1$ -complexes, the electronic energy states can be correlated with the splitting pattern of  $d$ -orbital set. Hence, in the case of  $z$ -out tetragonal distortion, the repulsion between metal electrons and ligand electrons will be less for the states comprising of electron density concentrated in orbitals directed toward  $z$ -axis. However, the tetragonal compression along  $z$ -axis will destabilize the electronic states having electron density distribution along or near  $z$ -axis. The effect of tetragonal distortion upon free ion terms of  $d^1$  and  $d^4$ -metal complexes can be shown as:

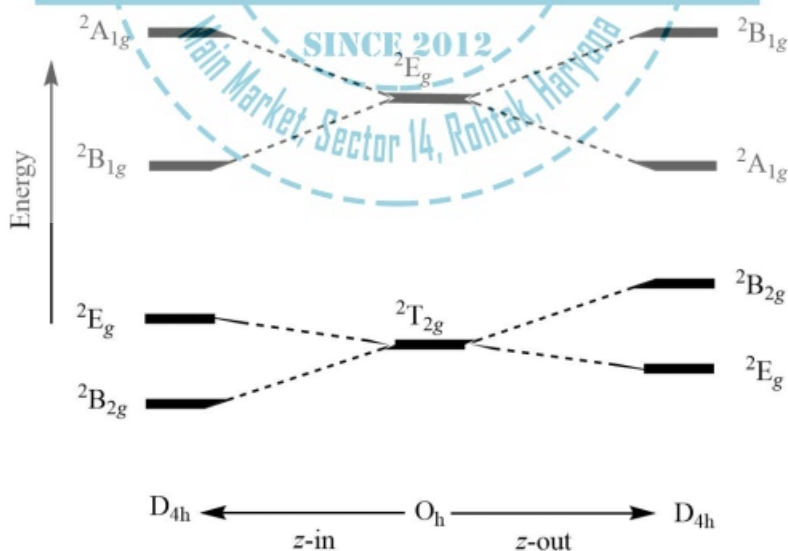


Figure 44. The splitting pattern of  $d$ -orbital energy levels of  $d^1$ -metal complexes undergoing tetragonal distortion.

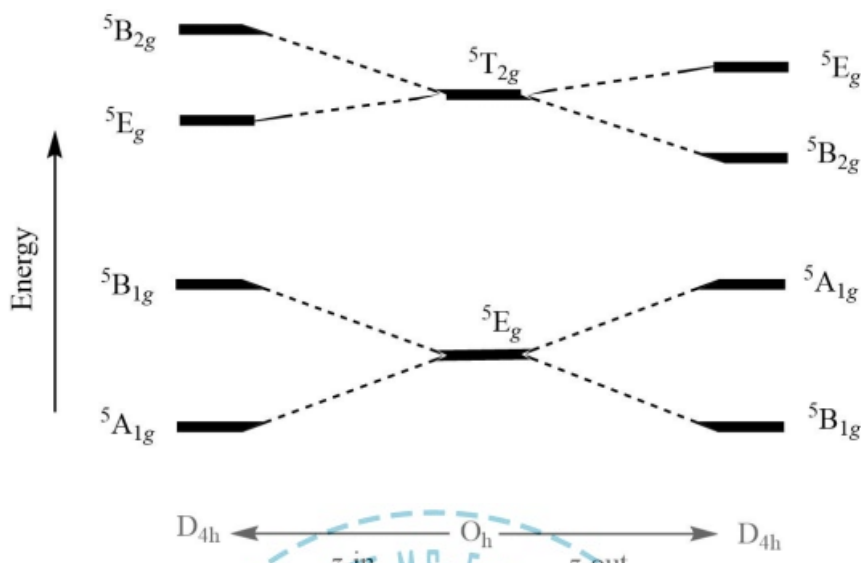


Figure 45. The splitting pattern of  $d$ -orbital energy levels of  $d^4$ -metal complexes undergoing tetragonal distortion.

It is worthy to mention that the homoleptic complexes of  $d^1$ -configuration prefer to undergo tetragonal compression due to Jahn-Teller distortion rather than the elongation. However, the heteroleptic complexes do show a splitting profile shown in the left side of Figure 44, like  $\text{trans}[\text{TiA}_4\text{B}_2]^{3+}$ , if A-type ligands occupy a higher position in the spectrochemical series than B-type.

Apart from the Jahn-Teller distortions, the degeneracy of electronic states of octahedral complexes is also lifted when all the six ligands are not the same. This lowering of symmetry creates additional energy levels. For instance,  $\text{Cr}^{3+}$  is a  $d^3$  system and does not show conventional Jahn-Teller distortion but the complexes like  $\text{trans}[\text{CrA}_4\text{B}_2]^{3+}$  show quite complex UV-visible spectrum which can only be explained in terms of energy levels of  $D_{4h}$  symmetry. Furthermore, chelate metal complexes like  $[\text{Cr}(\text{ox})_3]^{3-}$  and  $[\text{Cr}(\text{en})_3]^{3+}$  are no longer ideal octahedral geometries as their symmetry is lowered down to  $D_3$  point group. However, the UV-visible spectrum of these complexes can successfully be rationalized as if they are arising from a perfectly octahedral complex like  $[\text{CrA}_6]^{3+}$ . This is obviously due to the fact that the extent of perturbation in these chelate complexes is quite small. Nevertheless, if we replace one ethylenediamine with two  $\text{F}^-$  ligands to form  $\text{trans}[\text{Cr}(\text{en})_3]^{3+}$ , the perturbation produced by the differentiation of the ligands is no more intolerable limit for ideal octahedral coordination.

The energy levels for a  $d^3$  system in an octahedral complex and their splitting during tetragonal distortion is shown below.

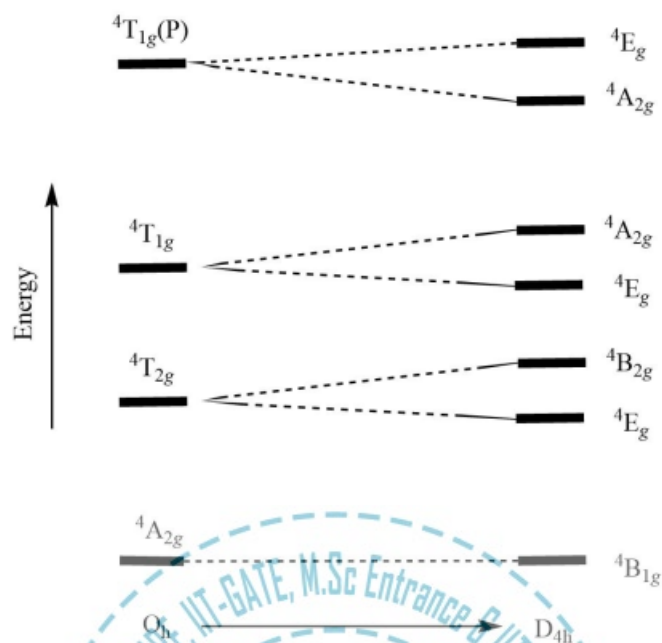


Figure 46. The splitting pattern of  $d$ -orbital energy levels of  $d^3$ -metal complexes in tetragonal distortion.

**2. Rhombic distortion:** The unequal amount of elongation or compression along two four-fold axes of rotation in octahedral complexes produces rhombic distortions. The common examples of rhombic distortion are high-spin Mn(III) and spin-paired Co(III) complex. Owing to more than one  $d$ -electron, we must consider ourselves with electronic states and not simply orbitals. The splitting pattern that occurs in a rhombic field is also shown below.

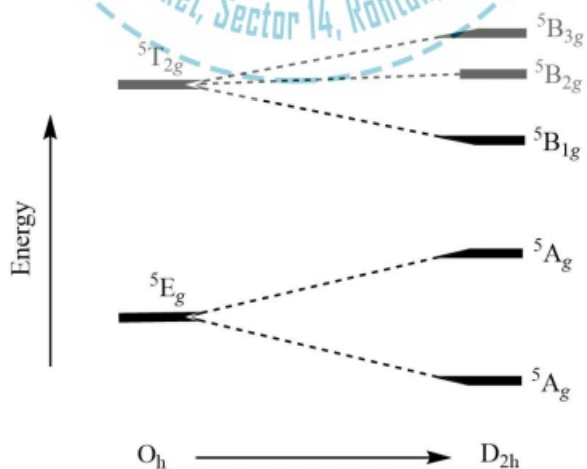


Figure 47. The splitting pattern of  $d$ -orbital energy levels of  $d^4$ -metal complexes in tetragonal distortion.

**3. Trigonal distortion:** The trigonal distortions occur as the elongation or compression along one of the four three-fold symmetry axis. The splitting pattern that occurs in a rhombic field is also shown below.

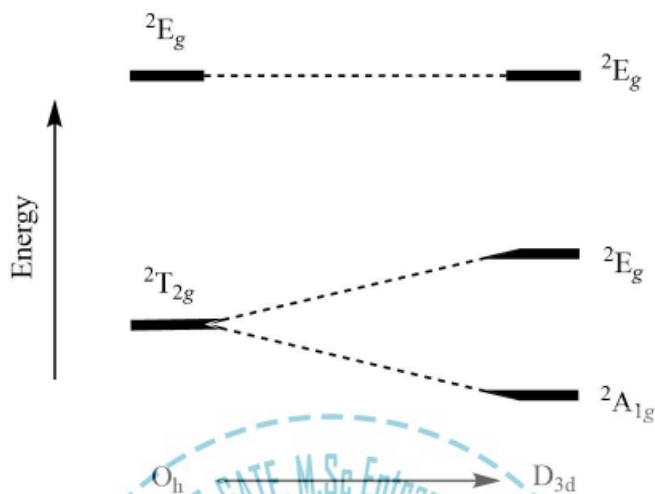


Figure 48. The splitting pattern of  $d$ -orbital energy levels of  $d^1$ -metal complexes in trigonal distortion.

➤ **Distortion in Four-Coordinated Complexes**

The tetra-coordination of ligands in different metal complexes can be categorized mainly as the tetrahedral and square planar. The tetrahedral geometry can be distorted in various ways to produce other four-coordinated structures. For instance, a perfect tetrahedral geometry can be compressed or elongated along two-fold and three-fold axis of symmetry to produce structures having  $D_{2d}$  and  $C_{3v}$  symmetry profiles, respectively. Moreover, the extreme case of compression along one two-fold axis is bound to yield a perfectly flat square-planar structure with  $D_{4h}$  point group.

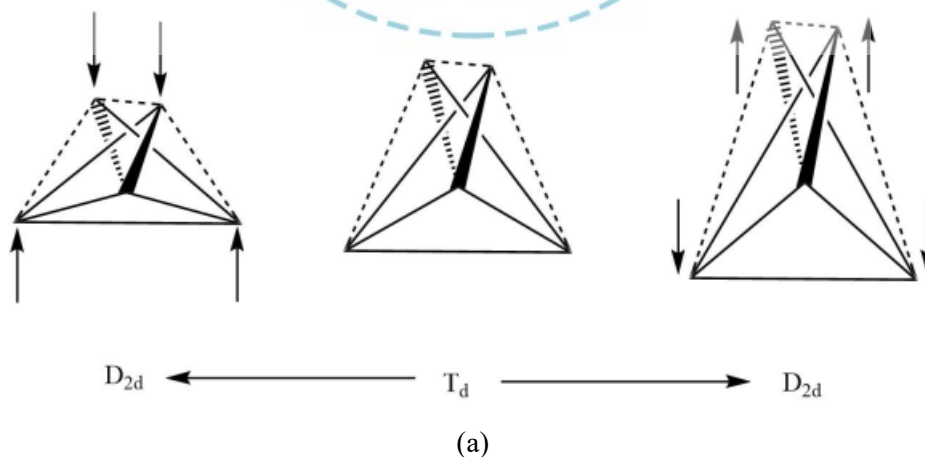


Figure 49. Continued on the next page...

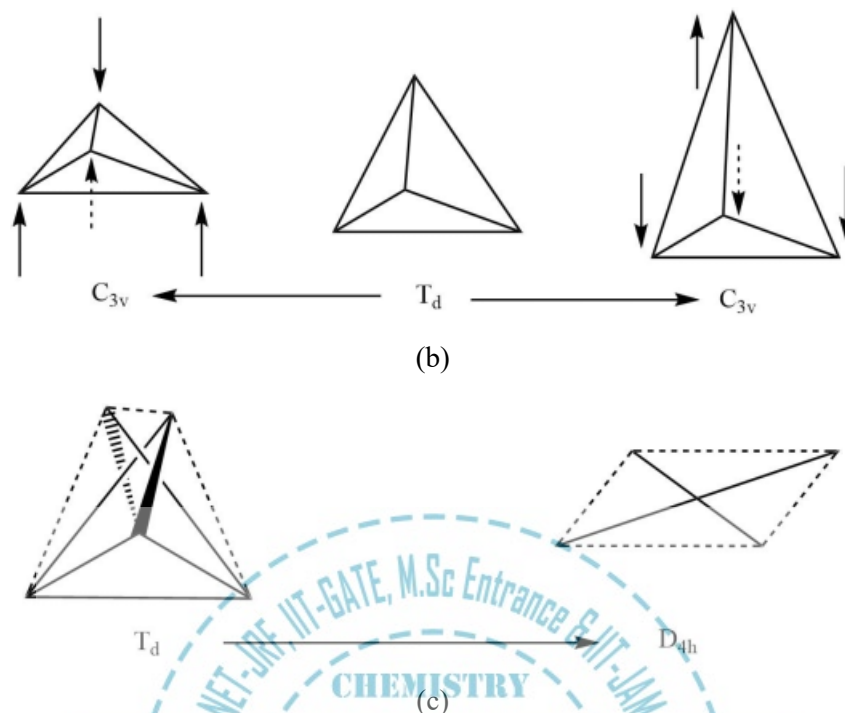


Figure 49. The (a) two-fold (b) three-fold and (c) square-planar distortion in tetrahedral metal complexes.

**1. Two-fold distortion:** The two-fold distortions occur as the elongation or compression along one of the six two-fold symmetry axis. The splitting pattern that occurs in a  $D_{2d}$  crystal field is also shown below.

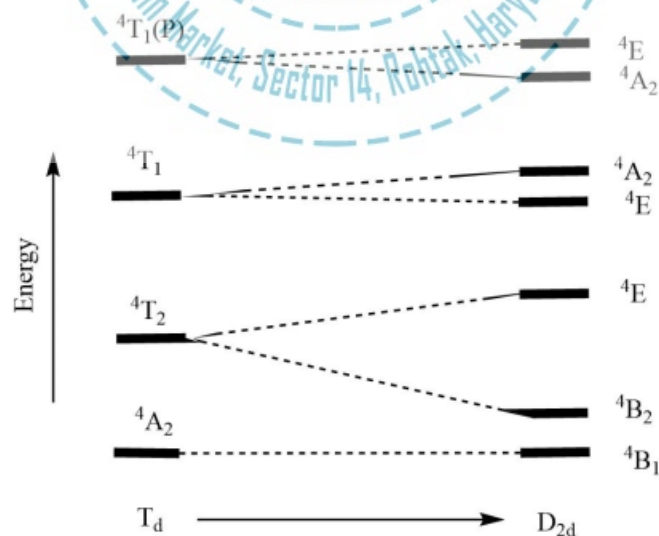


Figure 50. The splitting pattern of  $d$ -orbital energy levels of  $d^7$ -metal complexes in two-fold distortion.

**2. Three-fold distortion:** The three-fold distortions occur as the elongation or compression along one of the four three-fold symmetry axis. The splitting pattern that occurs in a  $C_{3v}$  crystal field is also shown below.

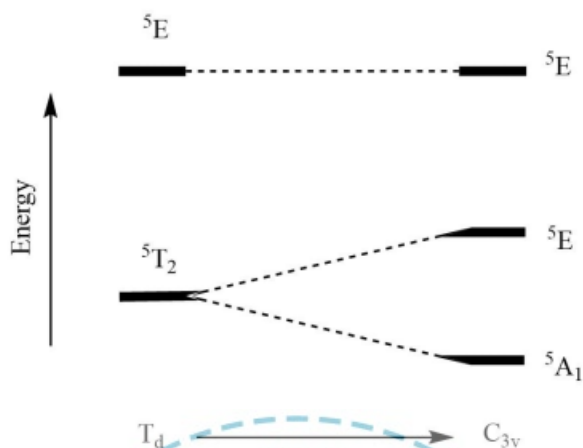


Figure 51. The splitting pattern of  $d$ -orbital energy levels of  $d^4$ -metal complexes in three-fold distortion.

**3. Square-planer distortion:** The square-planer distortions occur as the extreme compression along one of the six two-fold symmetry axis. The splitting pattern that occurs in a  $D_{4h}$  crystal field is shown below.

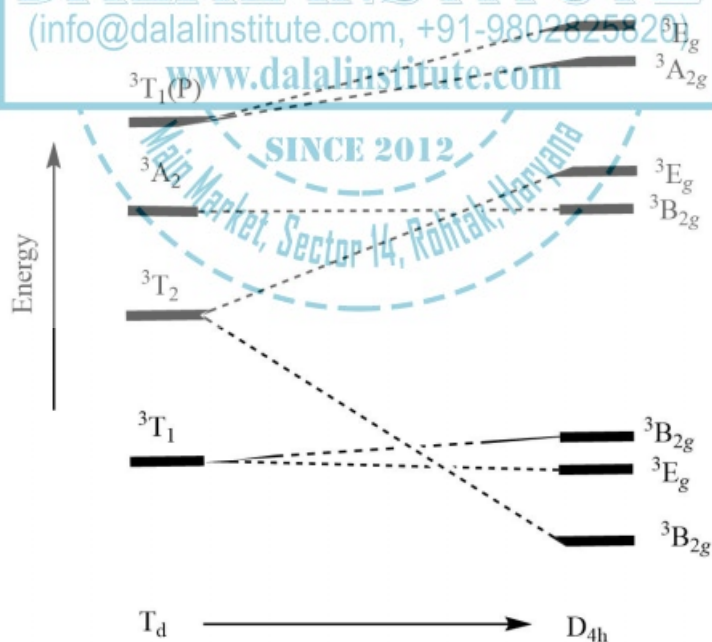


Figure 52. The splitting pattern of  $d$ -orbital energy levels of  $d^8$ -metal complexes in square-planer distortion.

### ❖ Structural Evidence from Electronic Spectrum

The electronic spectrum of transition metal complexes in the near-infrared, visible and ultraviolet region is quite useful in providing the information regarding their structural prototypes. The number of bands, their positions and molar absorptivity values must be considered for any conclusive remarks. Moreover, the spectra in the solution phase should also be checked against the solid-state spectral profile to be sure that no structural alteration has been taken place. These alterations could result in ligand displacement by solvent, ligand rearrangement, or an increase in the coordination number due to solvation. Very reliable information about the ligand environment in transition metal complexes can be found from their electronic spectrum. Some of the main sources of structural information from the UV-visible spectrum of transition metal complexes are given below.

#### ➤ Molar Absorptivity of assigned Bands

The intensities of electronic transitions depend upon the wavefunctions of the ground and excited states; and provide important information about the electronic structure. Ligand field transitions that are forbidden in octahedral complexes may partly be allowed in tetrahedral complexes due to significant  $d-p$  mixing. The intensity of spin-allowed, as well as spin-forbidden  $d-d$  transitions in tetrahedral complexes, is 10-100 times more than in octahedral complexes. However, the values of molar extinction coefficients for  $d-d$  transitions in tetrahedral complexes are still lower than what we observe for charge transfer bands. This is because of the fact that the intensities in the former largely depend upon the ligand contribution to  $e$  and  $t_2$  orbital sets, which is approximately 30% in magnitude. On the other hand, charge transfer transitions occur from an orbital which is largely  $p$  to an orbital with large  $d$ -character. The values for molar extinction coefficients for different types of transitions are given below.

Table 9. The order of magnitude for the molar extinction coefficient for different types of transitions.

Type	Extinction coefficient
$d-d$ spin forbidden, Laporte forbidden ( $O_h$ )	0.1
$d-d$ spin forbidden, Laporte allowed ( $T_d$ )	1
$d-d$ spin allowed, Laporte forbidden ( $O_h$ )	10
$d-d$ spin allowed, Laporte allowed ( $T_d$ )	100
Charge transfer, spin allowed and Laporte allowed	1000

Therefore, as the asymmetry around metal center increases, the intensity of various bands is also enhanced and a superficial shortlisting between tetrahedral and octahedral coordination can be done just on the basis of intensity and number of bands observed. It should also be noted that many complexes that ideally belong to a non-centrosymmetric point group usually have only a small asymmetric contribution to the crystal

field. On the basis of the magnitude of this asymmetric contribution, the intensity lies between that of a truly centrosymmetric and a complex with a highly asymmetric crystal field, such as a square-pyramidal or distorted tetrahedral complex. If geometric distortion is so small that it is in the range of vibrational amplitudes, the intensities of the spectral band would not be much greater than those in typical centrosymmetric compounds. For example, peak intensities in tris-chelate complexes of ethylenediamine are not much more intense than their hexa-ammine counterparts. When asymmetry is the result of a difference in the ligand type on either side of the metal, the deviation depends on how different the ligands actually are. The bands in the spectrum of a complex such as the  $\text{cis-Co}[(\text{NH}_3)_4\text{Cl}_2]^+$  ion are two to three times as intense as those in the corresponding trans complex; and thus, the two isomers can be distinguished on the basis of intensity only. Tetrahedral complexes can easily be distinguished from hexa-coordinated counterparts on the basis of the intensity of the bands. The complex  $\text{Ni}\{\text{OP}[\text{N}(\text{CH}_3)_2]_3\}_4\text{Cl}_2$  could have tetrahedral or distorted octahedral geometries but the similarity of its electronic spectrum to that of  $[\text{NiCl}_4]^{2-}$  implied that this was the first cationic, tetrahedral nickel(II) complex ever synthesized. Further confirmation of the structure comes from the similarity of its x-ray powder diffraction patterns with tetrahedral zinc(II) complexes.

Consistent structural information can be obtained from the electronic spectra of Co(II) complexes. Hexa-coordinated complexes of Co(II) are usually high-spin and the Orgel diagram for  $d^7$ -configuration should be used to assign different peaks. The ground state is  ${}^4T_{1g}$  and a considerable magnitude of spin-orbit coupling is expected in  ${}^4T_{1g}(\text{F}) \rightarrow {}^4T_{2g}(\text{F})$ ,  ${}^4T_{1g}(\text{F}) \rightarrow {}^4A_{2g}(\text{F})$  and  ${}^4T_{1g}(\text{F}) \rightarrow {}^4T_{1g}(\text{P})$  transitions. Being a two-electron transition  ${}^4T_{1g}(\text{F}) \rightarrow {}^4A_{2g}(\text{F})$ , its intensity is pretty low and hardly observed. The electronic spectrum of octahedral  $[\text{Co}(\text{H}_2\text{O})_6]^{2+}$  and tetrahedral  $[\text{CoCl}_4]^{2-}$  are shown in the following figure.

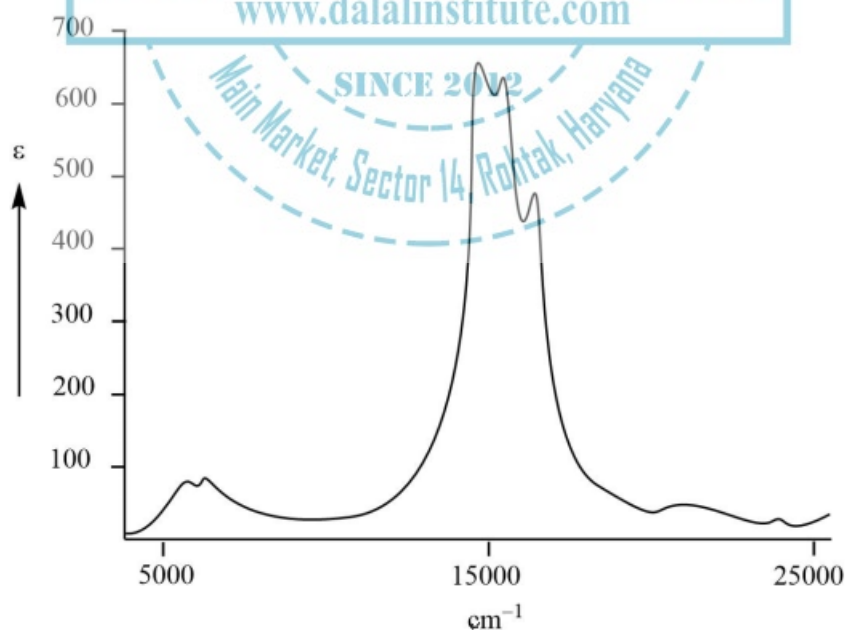


Figure 53. Electronic spectrum of tetrahedral  $[\text{CoCl}_4]^{2-}$ .

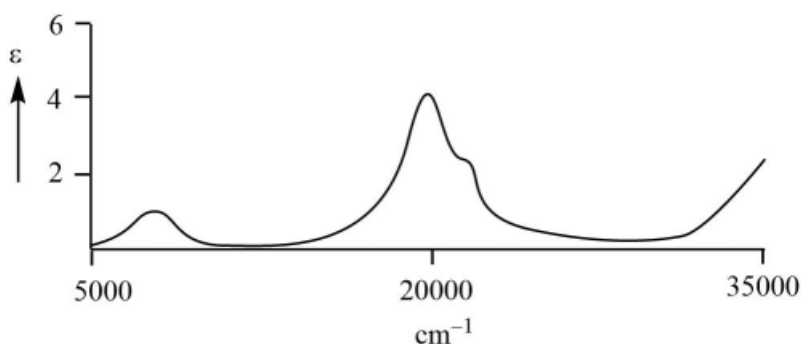


Figure 54. Electronic spectrum of octahedral  $[\text{Co}(\text{H}_2\text{O})_6]^{2+}$ .

Tanabe and Sugano diagram for  $d^7$ -configuration has to be used to explain the electronic spectrum of tetrahedral complexes of Co(II) which are always high-spin in nature. The absorption at  $15000\text{ cm}^{-1}$  may be attributed to  ${}^4\text{A}_2(\text{F}) \rightarrow {}^4\text{T}_1(\text{P})$  and fine structure can be explained in terms of to spin-orbital coupling of the T electronic state. The presence of spin-orbital interaction also permits some quartet  $\rightarrow$  doublet transitions to happen. The other peak shown is assigned to  ${}^4\text{A}_2(\text{F}) \rightarrow {}^4\text{T}_1(\text{F})$  transition while the expected  ${}^4\text{A}_2(\text{F}) \rightarrow {}^4\text{T}_2(\text{F})$  transition is predicted to result in a peak at  $3000\text{--}4500\text{ cm}^{-1}$ . However, most of the UV-visible spectrophotometers cannot record them as they are out of detectable range and usually overlap with the infrared bands of attached ligands. On the other hand, the main peak in the UV-visible spectrum of  $[\text{Co}(\text{H}_2\text{O})_6]^{2+}$  is at about  $20000\text{ cm}^{-1}$  and is allocated to the  ${}^4\text{T}_{1g}(\text{F}) \rightarrow {}^4\text{T}_{1g}(\text{P})$  transition. The shoulder owes to the lifting of degeneracy due to spin-orbital coupling in the excited  ${}^4\text{T}_{1g}(\text{P})$  state. The second band at  $8350\text{ cm}^{-1}$  is ascribed to  ${}^4\text{T}_{1g}(\text{F}) \rightarrow {}^4\text{T}_{2g}(\text{F})$  transition.

#### ➤ *Splitting Pattern of Assigned Bands*

The splitting pattern of absorption peaks provides useful information not only on the symmetry but also on the relative  $\sigma$  and  $\pi$  bonding nature of the attached ligands. The effects of decreased ligand-field symmetry in a mixed ligand metal complex can easily be explained by the analysis of UV-visible spectra of the  $[\text{Co}(\text{en})_3]^{3+}$ ,  $\text{cis-}[\text{Co}(\text{en})_2\text{F}_2]^{1+}$  and  $\text{trans-}[\text{Co}(\text{en})_2\text{F}_2]^{1+}$ . Although the complex  $[\text{Co}(\text{en})_3]^{3+}$  belongs to  $D_3$  point group symmetry, its ligand field pretty close to  $O_h$  symmetry. Therefore, the Tanabe-Sugano diagram for  $d^6$ -configuration should be used to interpret the electronic spectrum which is comprised of two symmetric bands due to the  ${}^1\text{A}_{1g} \rightarrow {}^1\text{T}_{1g}$  and  ${}^1\text{A}_{1g} \rightarrow {}^1\text{T}_{2g}$  transitions, respectively. The spectrum of  $\text{cis-}[\text{Co}(\text{en})_2\text{F}_2]^{1+}$  is somewhat similar to what is observed for  $[\text{Co}(\text{en})_3]^{3+}$ ; however, both bands are broader and slightly shifted to lower energy value. In case of  $\text{trans-}[\text{Co}(\text{en})_2\text{F}_2]^{1+}$ , the lower energy band is obviously split into two components; and the peak intensities are slightly lesser than those of  $\text{cis-}[\text{Co}(\text{en})_2\text{F}_2]^{1+}$  and  $[\text{Co}(\text{en})_3]^{3+}$  which obviously comply with the fact that the former complex does possess a center of symmetry so that the electronic transitions are formally Laporte forbidden.

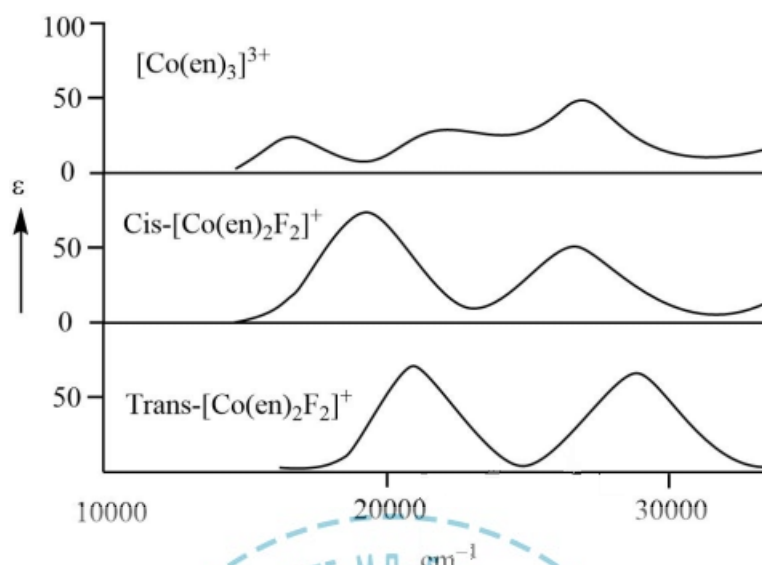


Figure 55. Electronic spectrum of trans-[Co(en)<sub>2</sub>F<sub>2</sub>]<sup>1+</sup>, cis-[Co(en)<sub>2</sub>F<sub>2</sub>]<sup>1+</sup> and [Co(en)<sub>3</sub>]<sup>3+</sup> in aqueous solution.

The main cause of the splitting of bands in trans-[Co(en)<sub>2</sub>F<sub>2</sub>]<sup>1+</sup> is the loss of degeneracy of excited states due to the lowering of ligand-field symmetry; which can be explained in terms of the effect of an increasing tetragonal component of the ligand field on the <sup>1</sup>T<sub>1g</sub> and <sup>1</sup>T<sub>2g</sub> states. The whole schematic is shown in the energy level diagram given below. The two lower energy peaks of trans-[Co(en)<sub>2</sub>F<sub>2</sub>]<sup>1+</sup> may be ascribed to the <sup>1</sup>A<sub>1g</sub> → <sup>1</sup>E<sub>g</sub> and <sup>1</sup>A<sub>1g</sub> → <sup>1</sup>A<sub>2g</sub> transitions, respectively. It is worthy to note that both excited states in the tetragonal field, <sup>1</sup>E<sub>g</sub> and <sup>1</sup>A<sub>2g</sub>, are the components of <sup>1</sup>T<sub>1g</sub> state of O<sub>h</sub>-symmetry. Moreover, as the splitting of <sup>1</sup>T<sub>2g</sub> state is quite insignificant, the two corresponding transitions (<sup>1</sup>A<sub>1g</sub> → <sup>1</sup>E<sub>g</sub> and <sup>1</sup>A<sub>1g</sub> → <sup>1</sup>B<sub>2g</sub>) are not resolved even in the trans complex.

Now, the angular overlap method states that it is the “holohedrized” symmetry that governs the energy levels in a complex; or in other words, *d*-orbital energies depend on the sum of the effects of the ligands along each axis. Therefore, the magnitude of the tetragonal component in the ligand field of the trans-complex is twice that what is active in the cis counterpart. This gives rise to much more overlapping transitions in the spectrum of cis-[Co(en)<sub>2</sub>F<sub>2</sub>]<sup>1+</sup> and no clear splitting of the bands can be resolved. Even though it is not evident in the solution spectra, the sign of ligand field splitting in cis-isomer is different than the trans-isomers. The energy level diagram given in this section is actually for the situation in which the in-plane ligand field is stronger than the axial field, just like in the case of trans-[Co(en)<sub>2</sub>F<sub>2</sub>]<sup>1+</sup> complex. The degree of the splitting is correlated to the difference in σ and π-bonding ability of the in-plane and axial ligands. Thus, the peak splitting profile for mixed-ligand complexes offers a powerful means of obtaining metal-ligand bonding parameters.

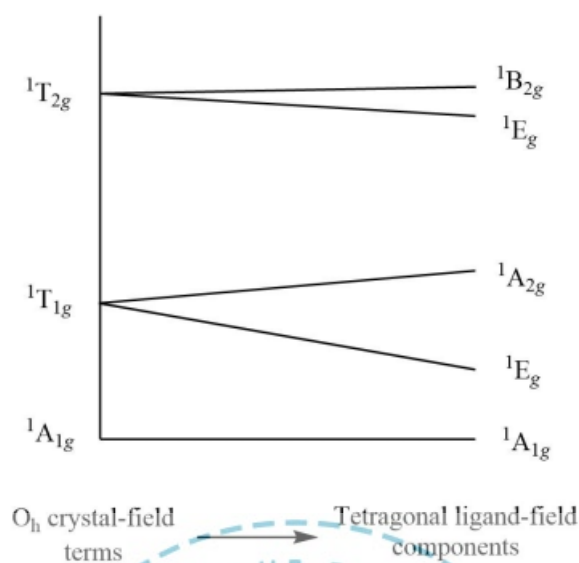


Figure 56. The splitting pattern of  ${}^1T_{1g}$  and  ${}^1T_{2g}$  terms of octahedral  $\text{Co}^{3+}$  complex in increasing the tetragonal ligand field.

In order to analyze the system in a precise manner, the assignment of different bands must be done properly; and if possible, this is best achieved by recording single-crystal polarized spectra. The average position of the split components of the  ${}^1T_{1g}$  is approximately  $18000\text{ cm}^{-1}$  and of  ${}^1T_{2g}$  is  $26000\text{ cm}^{-1}$  for  $\text{trans-}[\text{Co}(\text{en})_2\text{F}_2]^{1+}$ . These values of band positions are rather similar to those of  $\text{cis-}[\text{Co}(\text{en})_2\text{F}_2]^{1+}$  and give a ligand field splitting  $21000\text{ cm}^{-1}$ .

This result is also supported by “the rule of average environment” which states that the magnitude of ligand field splitting in a mixed-ligand complex is around the weighted average of the octahedral ligand fields associated with a complete set of each ligand. For example, the value of crystal field splitting in  $\text{MA}_n\text{B}_{6-n}$  complex can be given as:

$$\Delta = \frac{[n\Delta(\text{MA}_6) + (6 - n)\Delta(\text{MB}_6)]}{6}$$

Putting the values of crystal field splitting values of  $[\text{Co}(\text{en})_3]^{3+}$  and  $[\text{CoF}_6]^{3-}$  in the above equation, we get the expected magnitude of  $\Delta$  for  $[\text{Co}(\text{en})_2\text{F}_2]^{1+}$ .

$$\Delta = \frac{[4(23000) + 2(13000)]}{6} = 19667\text{ cm}^{-1}$$

Which is pretty close to the experimentally observed value of  $21000\text{ cm}^{-1}$  and therefore confirms the practical applications in structure determination.

### ❖ Jahn-Teller Effect

*The Jahn-Teller theorem essentially states that any nonlinear molecule system possessing electronic degeneracy will be unstable and will undergo distortion to form a system of lower symmetry as well as lower energy and thus the degeneracy will be removed.*

This effect describes the geometrical distortion of molecules and ions that is associated with electronically degenerate configurations. A configuration is said to be electronically degenerate if more than one sites are available for the filling of a single electron. The Jahn-Teller effect is generally encountered in octahedral transition metal complexes. The phenomenon is much more common in hexacoordinated complexes of bivalent copper. The  $d^9$  configuration of  $\text{Cu}^{2+}$  ion yields three electrons in the doubly degenerate  $e_g$  orbitals set, leading to a doubly degenerate electronic state as well. Such complexes distort along one of the molecular four-fold axis (always labeled the  $z$ -axis), which has the effect of removing the orbital and electronic degeneracies and lowering the overall energy. The distortion usually occurs via the elongation the metal-ligand bonds along the  $z$ -axis, but sometimes also occurs as a shortening of the same bonds instead. Moreover, the Jahn-Teller theorem predicts the presence of an unstable geometry only and not the direction of the distortion. When distortion involving elongation occurs to decrease the electrostatic repulsion between the electron-pair on the ligand-attached and any extra electrons in metal orbitals with a  $z$ -component; and hence lowering the energy of the metal complex. Inversion center is retained after  $z$ -out as well as  $z$ -in the distortion. Symmetrical configurations possess electronic degeneracy while the unsymmetrical ones do not. Various symmetrical and unsymmetrical configurations are given below.

Table 10. Symmetrical and Unsymmetrical  $t_{2g}$  and  $e_g$  orbitals.

Symmetrical configurations	Unsymmetrical configurations
$t_{2g}^0, t_{2g}^3, t_{2g}^6$	$t_{2g}^1, t_{2g}^2, t_{2g}^4, t_{2g}^5$
$e_g^0, e_g^4, e_g^2$ (high-spin)	$e_g^1, e_g^3, e_g^2$ (low-spin)

Now, the conditions for different kinds of distortion can be summed up as:

Table 11. Conditions for Jahn-Teller distortion.

Type of distortion	Configuration required
No distortion	$t_{2g}$ (symmetrical) + $e_g$ (symmetrical)
Slight distortion	$t_{2g}$ (unsymmetrical)
Strong distortion	$e_g$ (unsymmetrical)

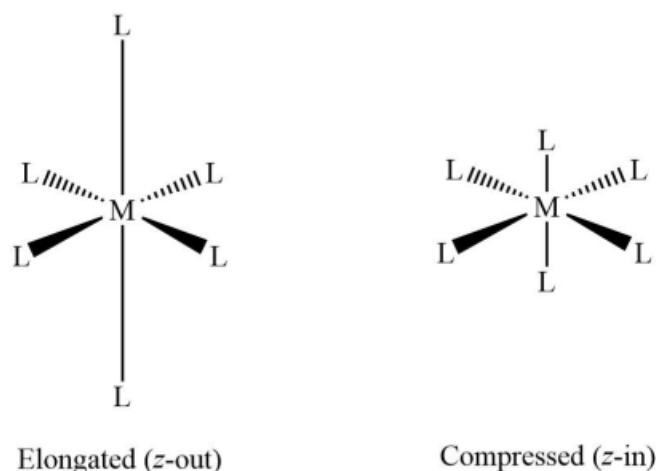


Figure 57. The Jahn-Teller distortions for an octahedral complex.

Let the case of the low-spin  $\text{Co}^{2+}$  octahedral complex. The corresponding electronic configuration is  $t_{2g}^6 e_g^1$ . Owing to the electronically degenerate state, the Jahn-Teller distortion is expected. Now suppose that the single electron of  $e_g$  set is present in  $d_z^2$  orbital; the ligands approaching from  $z$ -axis will feel more repulsion than the ligands coming from  $x$  and  $y$ -axis. Therefore, the bonds along  $z$ -axis will be weaker in comparison to the bond along  $x$  and  $y$ -axis. This results in a tetragonal elongation about  $z$ -axis with two longer and four shorter bonds. This is formally called as  $z$ -out distortion. On the other hand, if the single electron of  $e_g$  set is present in  $d_{x^2-y^2}$  orbital; the ligands approaching from  $x$  and  $y$ -axis will feel more repulsion than the ligands coming from  $z$ -axis. Therefore, the bonds along  $x$  and  $y$ -axis will be weaker in comparison to the bond along  $z$ -axis. This results in a tetragonally flattened octahedral geometry about  $z$ -axis with two shorter and four longer bonds. This is formally called as  $z$ -in distortion.

Consider the following examples

1.  $[\text{Co}(\text{CN})_6]^{4-}$ : It is a low-spin complex with  $t_{2g}^6 e_g^1$  electronic configuration and will undergo strong Jahn-Teller distortion.
2.  $[\text{Cr}(\text{NH}_3)_6]^{3+}$ : It is a high-spin complex with  $t_{2g}^3 e_g^0$  electronic configuration which is completely symmetrical; and therefore, will not show any Jahn-Teller distortion.
3.  $[\text{FeF}_6]^{4-}$ : It is a high-spin complex with  $t_{2g}^4 e_g^2$  electronic configuration and will undergo slight Jahn-Teller distortion.

#### ➤ Energetics of Jahn-Teller Distortion

The Jahn-Teller distortion results in a system of lower symmetry and lower energy. This is actually the opposite of what is expected. Generally, symmetry leads to stability; but the Jahn-Teller effect is actually an exception to this statement. Therefore, it is necessary to discuss the driving force responsible for this behavior. The magnitude of Jahn-Teller effect is larger where the electron density associated with the

degenerate set orbitals is more concentrated. Hence, Jahn-Teller effect plays a significant role in determining the structure of transition metal complexes with active 3d-orbitals. The whole energetics of the Jahn-Teller can be understood by the case study of  $d^9$  and  $d^1$  complexes.

**1.  $\text{Cu}^{2+}$  complexes:** The electronic configuration of free  $\text{Cu}^{2+}$  ion is  $d^9$ ; and in an octahedral environment, it is  $t_{2g}^6 e_g^3$ . Before we put any conclusive remark on the direction or nature of the distortion, we shall find the crystal field stabilization energy for z-out as well as for z-in case.

i) Crystal field stabilization energy for z-out distortion:

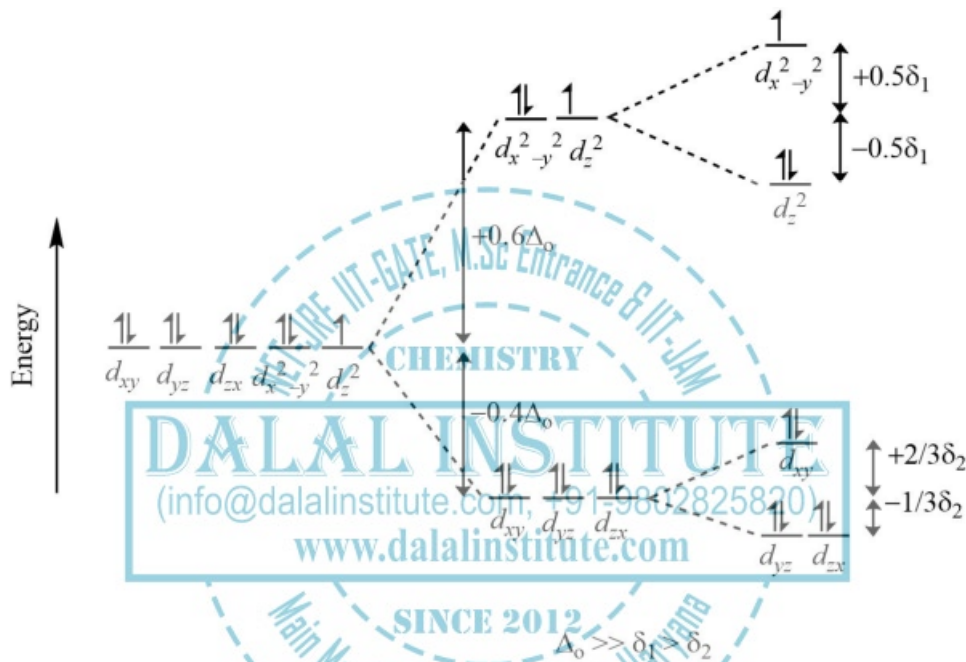


Figure 58. The splitting pattern and filling of  $d$ -orbital set of  $\text{Cu}^{2+}$  in octahedral and subsequently in the tetragonally elongated complex due to Jahn-Teller effect.

CFSE due to distortion = Energy of the distorted complex ( $E_2$ ) – Energy of the complex without distortion ( $E_1$ )

$$E_1 = 6(-0.4\Delta_o) + 3(+0.6\Delta_o)$$

$$E_1 = -0.6\Delta_o$$

$$E_2 = 4(-0.4\Delta_o - \delta_2/3) + 2(-0.4\Delta_o + 2\delta_2/3) + 2(+0.6\Delta_o - \delta_1/2) + 1(+0.6\Delta_o + \delta_1/2)$$

$$E_2 = -0.6\Delta_o - \delta_1/2$$

$$\text{CFSE due to distortion} = E_2 - E_1 = -\delta_1/2$$

Hence, the crystal field stabilization due to z-out distortion is  $-\delta_1/2$ .

ii) Crystal field stabilization energy for z-in distortion:

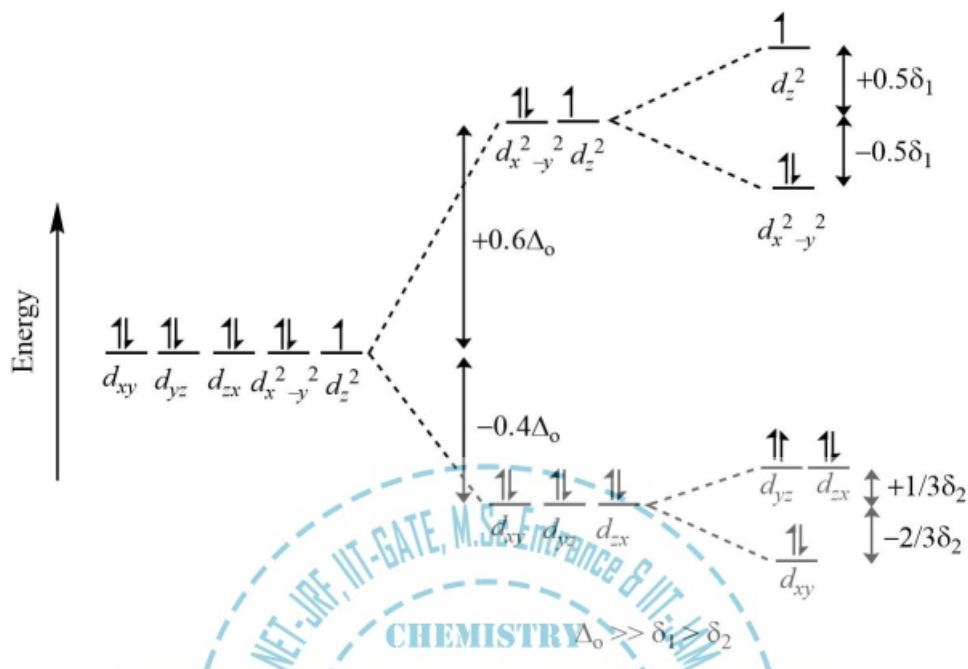


Figure 59. The splitting pattern and filling of  $d$ -orbital set of  $\text{Cu}^{2+}$  in octahedral and subsequently in the tetragonally compressed complex due to Jahn-Teller effect.

(info@dalalinstitute.com, +91-9802825820)

www.dalalinstitute.com

CFSE due to distortion = Energy of the distorted complex ( $E_2$ ) – Energy of the complex without distortion ( $E_1$ )

$$E_1 = 6(-0.4\Delta_o) + 3(+0.6\Delta_o)$$

$$E_1 = -0.6\Delta_o$$

$$E_2 = 4(-0.4\Delta_o - 2\delta_2/3) + 2(-0.4\Delta_o + \delta_2/3) + 2(+0.6\Delta_o - \delta_1/2) + 1(+0.6\Delta_o + \delta_1/2)$$

$$E_2 = -0.6\Delta_o - \delta_1/2$$

$$\text{CFSE due to distortion} = E_2 - E_1 = -\delta_1/2$$

Hence, the crystal field stabilization due to z-in distortion is  $-\delta_1/2$ .

Hence, the magnitude of crystal field stabilization in z-out case is same as that is present in z-in complex. This implies that Jahn-Teller effect cannot predict the direction of the distortion. However, it has been observed that it is the z-out case that dominates in most of the cases. It may depend on the repulsive forces between the  $d$ -electrons and the ligands, so the odd electron will prefer  $d_z^2$ -orbital more than  $d_{x^2-y^2}$  due to the lesser number of ligands it will repel with. Moreover, when a z-in distortion occurs, one can also view it terms of equatorial elongation while z-out will mean the weakening of two axial metal-ligand bonds. In other words, it is easier to weaken two bonds rather stretching four metal-ligand bonds.

**2.  $Ti^{3+}$  complexes:** The electronic configuration of free  $Ti^{3+}$  ion is  $d^1$ ; and in an octahedral environment, it is  $t_{2g}^1 e_g^0$ . Before we put any conclusive remark on the direction or nature of the distortion, we shall find the crystal field stabilization energy for  $z$ -out as well as for  $z$ -in case.

i) Crystal field stabilization energy for  $z$ -out distortion:

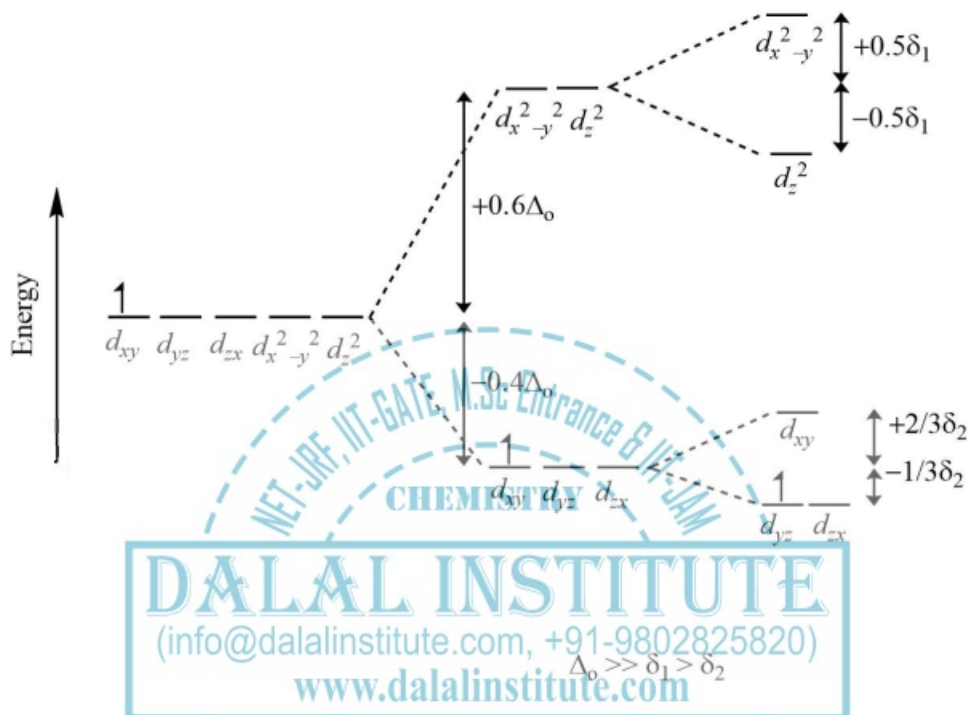


Figure 60. The splitting pattern and filling of  $d$ -orbital set of  $Ti^{3+}$  in octahedral and subsequently in the tetragonally elongated complex due to Jahn-Teller effect.

CFSE due to distortion = Energy of the distorted complex ( $E_2$ ) – Energy of the complex without distortion ( $E_1$ )

$$E_1 = 1(-0.4\Delta_o)$$

$$E_1 = -0.4\Delta_o$$

$$E_2 = 1(-0.4\Delta_o - \delta_2/3)$$

$$E_2 = -0.4\Delta_o - \delta_2/3$$

$$\text{CFSE due to distortion} = E_2 - E_1 = -\delta_2/3$$

Hence, the crystal field stabilization due to  $z$ -out distortion is  $-\delta_2/3$ . Moreover, it is worthy to note that this type of Jahn-Teller distortion is unable to remove the electronic degeneracy completely (the single electron can still be filled in two degenerate orbitals namely  $d_{yz}$  and  $d_{zx}$ ). Therefore, homoleptic octahedral complexes of  $d^1$ -configuration undergoing  $z$ -in distortion are quite rare.

ii) Crystal field stabilization energy for z-in distortion:

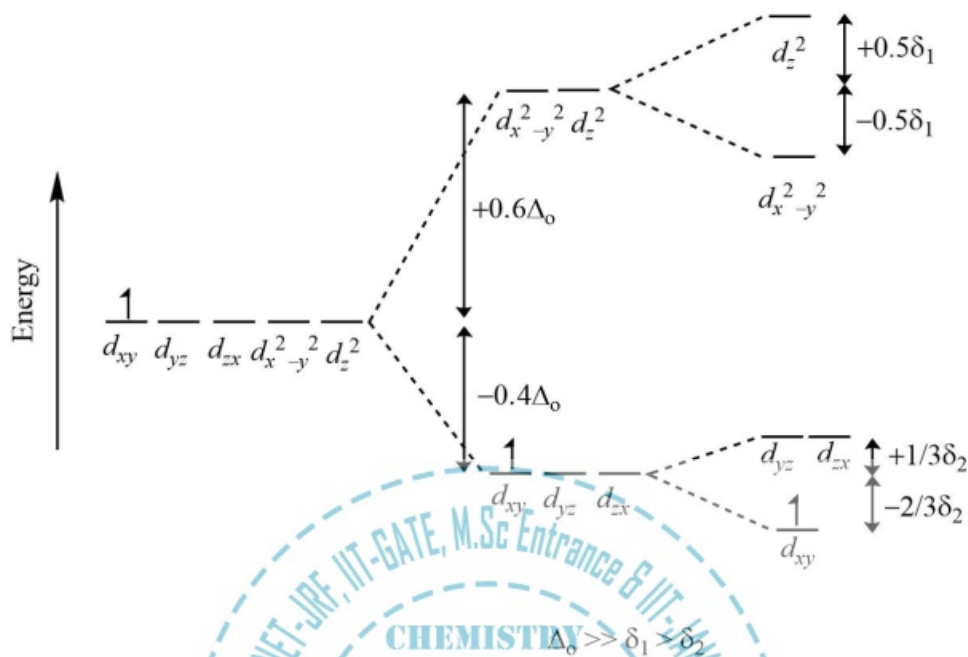


Figure 61. The splitting pattern and filling of  $d$ -orbital set of  $\text{Ti}^{3+}$  in octahedral and subsequently in the tetragonally compressed complex due to the Jahn-Teller effect.

(info@dalalinstitute.com, +91-9802825820)

www.dalalinstitute.com

CFSE due to distortion = Energy of the distorted complex ( $E_2$ ) – Energy of the complex without distortion ( $E_1$ )

$$E_1 = 1(-0.4\Delta_o)$$

$$E_1 = -0.4\Delta_o$$

$$E_2 = 1(-0.4\Delta_o - 2\delta_2/3)$$

$$E_2 = -0.4\Delta_o - 2\delta_2/3$$

$$\text{CFSE due to distortion} = E_2 - E_1 = -2\delta_2/3$$

Hence, the crystal field stabilization due to z-in distortion is  $-2\delta_2/3$ .

Hence, the magnitude of crystal field stabilization in z-out case is half of what is observed in z-in complex. This implies that Jahn-Teller effect can predict the direction of the distortion. However, it is the  $d^1$ -configuration that has been observed to show z-in distortion; otherwise, the z-out case dominates in most of the cases. It may be explained in terms of the repulsive forces between the  $d$ -electrons and the ligands, so the odd electron will prefer  $d_z^2$ -orbital more than  $d_{x^2-y^2}$  due to the lesser number of ligands it will repel with. Nevertheless,  $\text{Ti}^{3+}$  octahedral complexes prefer to undergo z-in due to the greater value of crystal field stabilization energy.

➤ **Effect of Jahn-Teller Distortion on Electronic Spectra**

Jahn-Teller distortions affect the UV-visible spectra of many transition metal complexes in a significant manner and sometimes it is almost impossible to find out the values of the Racah parameter and crystal splitting energy if we do not take it into account. In UV-visible absorption spectroscopy, distortion causes the splitting of bands in the spectrum due to a reduction in symmetry ( $O_h$  to  $D_{4h}$ ). The complexes undergoing Jahn-Teller distortion show an increased number of bands. Consider the following examples:

**1.  $[\text{Cr}(\text{H}_2\text{O})_6]^{2+}$ :** The  $\text{Cr}^{2+}$  ion in aqueous solutions is pale blue and its UV-visible absorption spectrum consists of a weak broad band with a maxima  $14000\text{ cm}^{-1}$ . In normal conditions, this band is expected to provide the value of crystal field splitting value directly (from Orgel-diagram of  $d^4$ -configuration); however, the actual value of  $\Delta_o$  is considerably different. The electronic configuration for high-spin  $\text{Cr}^{2+}$  in the octahedral field is  $t_{2g}^3 e_g^1$ ; and therefore, this complex is bound to undergo strong Jahn-Teller distortion. The energy level diagram and main transitions are shown below.

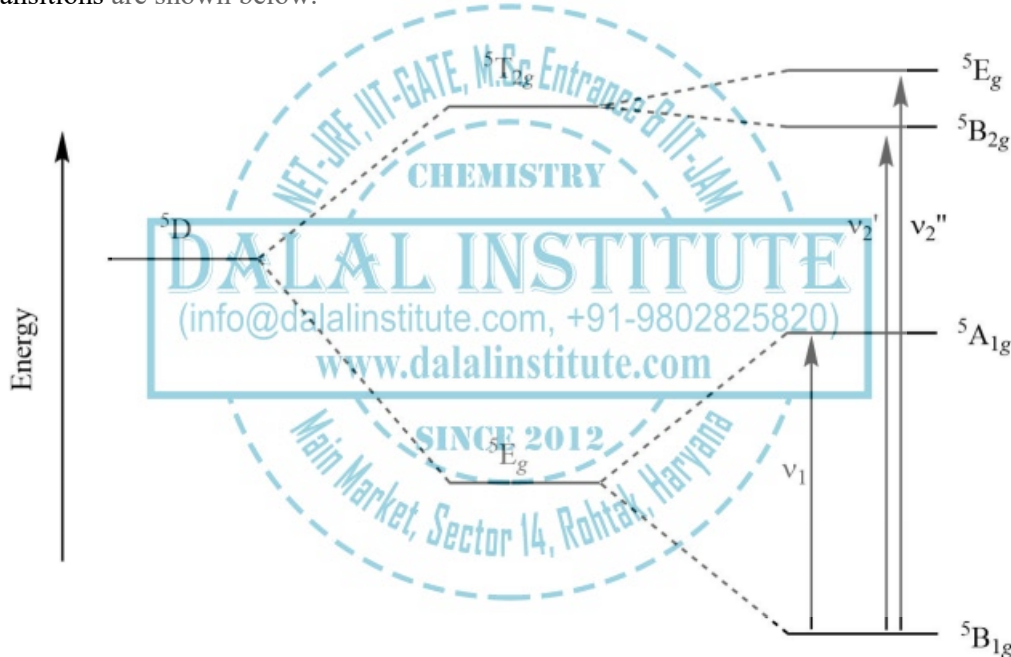
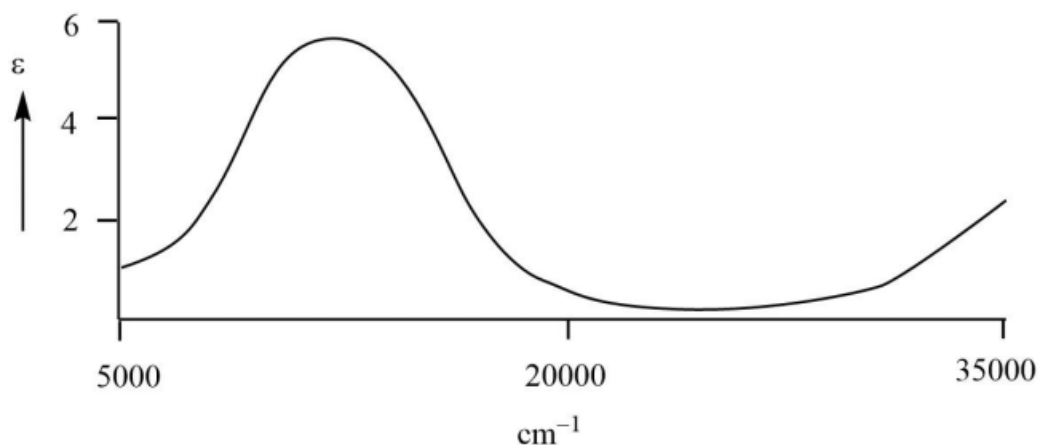


Figure 62. The schematic energy level diagram and prominent transitions in  $[\text{Cr}(\text{H}_2\text{O})_6]^{2+}$ .

The ground state term for a regular octahedral  $[\text{Cr}(\text{H}_2\text{O})_6]^{2+}$  complex would be  ${}^5E_g$  but the ground as well as excited electronic state will undergo a Jahn-Teller distortion. It is worthy to note that the former state shows strong while splitting of later one is weak. Hence, the Tanabe-Sugano diagram cannot be used to describe the energy levels in the complex. The gaussian deconvolution of the overall spectrum has shown that the transition between the split components of the  ${}^5E_g$  level ( ${}^5B_{1g} \rightarrow {}^5A_{1g}$ ) occurs at around  $10000\text{ cm}^{-1}$  and contributes to the low-energy tail of the broad band in aqueous solution.

Figure 63. UV-visible spectra of  $[\text{Cr}(\text{H}_2\text{O})_6]^{2+}$ .

The transitions from the  ${}^5\text{B}_{1g}$  ground state to the components of the  ${}^5\text{T}_{2g}$  state are unresolved and together give rise to the band at around  $14000\text{ cm}^{-1}$ . Now, suppose that the Jahn-Teller effect produces a symmetrical splitting of the  ${}^5\text{E}_g$  state, we can obtain the  $d$ -orbital splitting of the parent octahedral complex from the energy of the  ${}^5\text{B}_{1g} \rightarrow {}^5\text{T}_{2g}$  transition minus half the energy of the  ${}^5\text{B}_{1g} \rightarrow {}^5\text{A}_{1g}$  transition. This gives the estimated value of crystal field splitting value as follows:

$$\Delta_o = [v_2({}^5\text{B}_{1g} \rightarrow {}^5\text{T}_{2g})] - [v_1({}^5\text{B}_{1g} \rightarrow {}^5\text{A}_{1g})]/2$$

$$\Delta_o = 14000 - 10000/2 = 9000\text{ cm}^{-1}$$

Similar results have been observed in the low-temperature spectra of other hydrate complexes with Jahn-Teller distortion.

**2.  $[\text{Fe}(\text{H}_2\text{O})_6]^{2+}$ :** The  $\text{Fe}^{2+}$  ion in aqueous solutions is pale green and its UV-visible absorption spectrum is consisted of a weak broad band with a maxima  $10000\text{ cm}^{-1}$ . The electronic configuration for high-spin  $\text{Fe}^{2+}$  in octahedral field is  $t_{2g}^4 e_g^2$ ; and therefore, this complex is bound to undergo slight Jahn-Teller distortion. The ground state term for a regular octahedral  $[\text{Fe}(\text{H}_2\text{O})_6]^{2+}$  complex would be  ${}^5\text{T}_{2g}$  but the ground as well as excited electronic state will undergo a Jahn-Teller distortion. It is worthy to note that the former state shows strong while splitting of later one is weak.

Hence, the Orgel-diagram can be used to describe the energy levels in the complex. Moreover, as the band is obviously a doublet, we don't need gaussian deconvolution the overall spectrum. The transition from  ${}^5\text{T}_{2g}$  to the split components of the  ${}^5\text{E}_g$  level ( ${}^5\text{B}_{1g}$  and  ${}^5\text{A}_{1g}$ ) are split by an energy difference of around  $2000\text{ cm}^{-1}$ . This contributes to the broadening of the band in aqueous solution. The energy level diagram and main transitions are shown below.

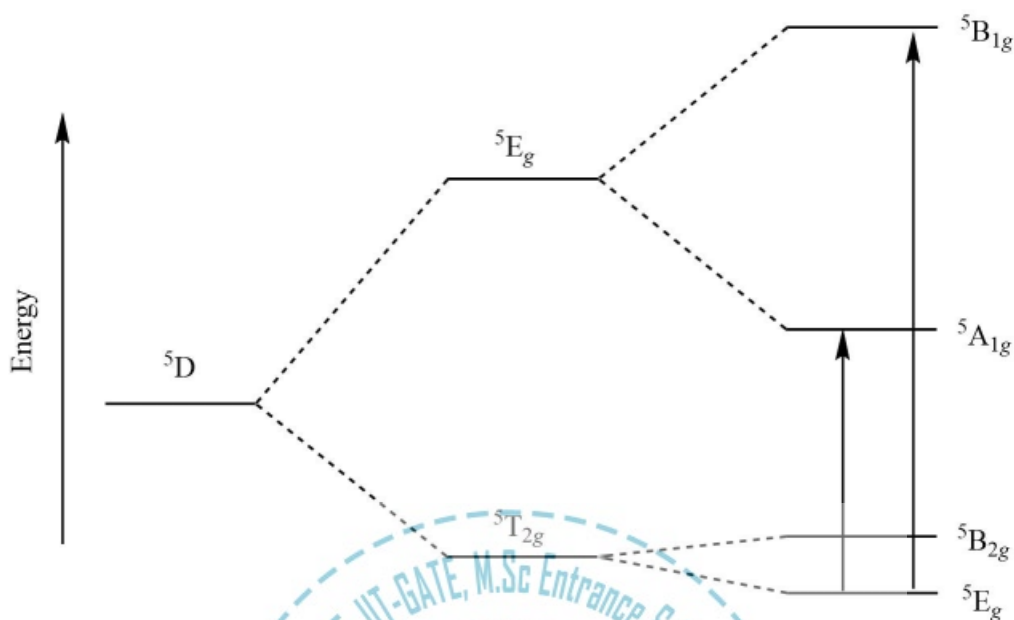


Figure 64. The schematic energy level diagram and prominent transitions in  $[\text{Fe}(\text{H}_2\text{O})_6]^{2+}$ .

The corresponding spectrum is given below.

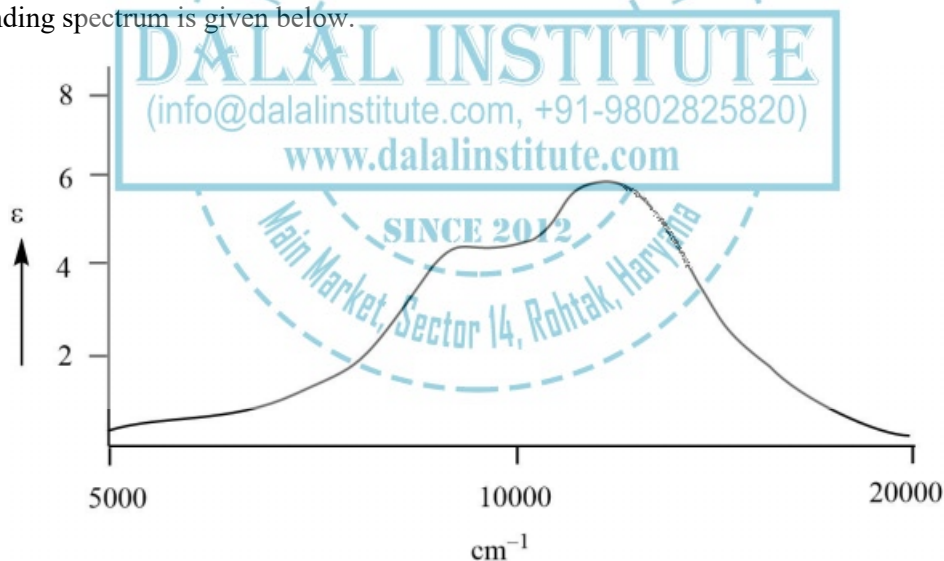


Figure 65. UV-visible spectra of  $[\text{Fe}(\text{H}_2\text{O})_6]^{2+}$ .

Now, suppose that the Jahn-Teller effect produces a symmetrical splitting of the  ${}^5E_g$  state, we can obtain the  $d$ -orbital splitting of the parent octahedral complex from the energy of the  ${}^5T_{2g} \rightarrow {}^5E_g$  transition, and that value, in this case, is  $10000 \text{ cm}^{-1}$ . These results are rather similar to what we have observed in  $[\text{Ti}(\text{H}_2\text{O})_6]^{3+}$ . Both complexes possess Jahn-Teller distortion associated with the electronic degeneracy of  $t_{2g}$  orbital.

➤ **Static and Dynamic Jahn-Teller Distortion**

On the basis of the observed geometry, the Jahn-Teller distortion can be classified in two types as given below.

**1. Static Jahn-Teller distortion:** Some molecules show tetragonal shape under all conditions i.e., in solid state and in solution state; at lower and relatively higher temperatures. This is referred to as static Jahn-Teller distortion. Hence the distortion is strong and permanent. For example, in  $\text{CuF}_2$  lattice

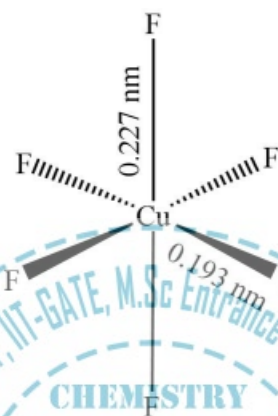


Figure 66. Static Jahn-Teller distortion in  $\text{CuF}_2$  lattice.

**2. Dynamic Jahn-Teller distortion:** If the energy gap between z-out and z-in is smaller than the available thermal energy, the complex ions tend to attain both states, i.e., compressed and elongated. This is known as the "Dynamic Jahn Teller Effect". For examples, consider  $\text{K}_2\text{Pb}[\text{Cu}(\text{NO}_2)_6]$  complex:

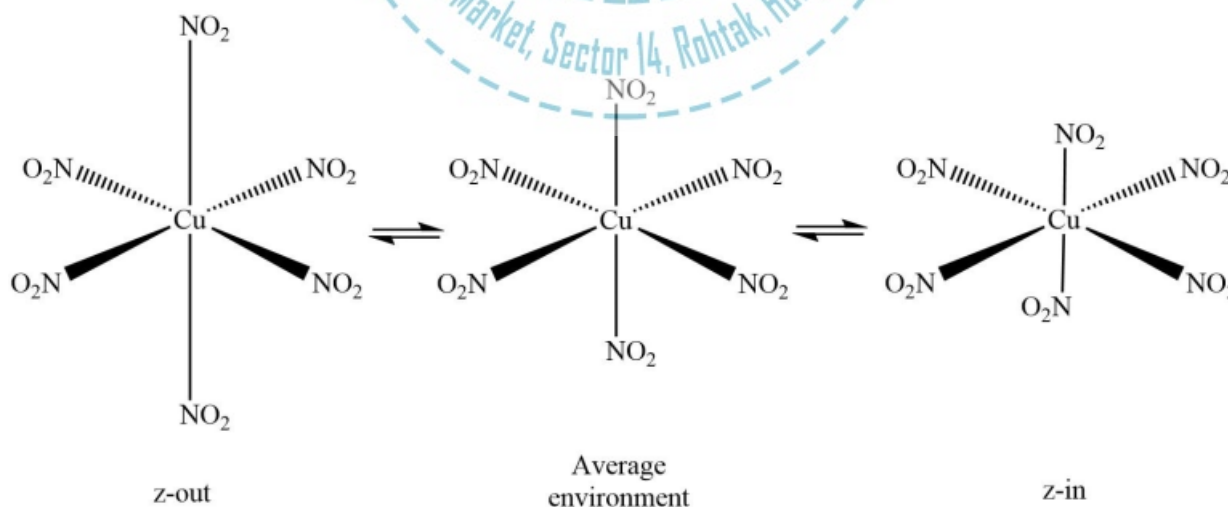


Figure 67. Dynamic Jahn-Teller distortion in  $\text{K}_2\text{Pb}[\text{Cu}(\text{NO}_2)_6]$ .

➤ **Consequences of Jahn-Teller Distortion**

Some of the main consequences of the Jahn-Teller effect in the field of chemical science are given below.

**1. Irving-William series:** Stability of metal complexes with a given ligand follows the order  $Mn^{2+} < Fe^{2+} < Co^{2+} < Ni^{2+} < Cu^{2+} > Zn^{2+}$ . The increase in the stability of the complexes from  $Mn^{2+}$  to  $Zn^{2+}$  is the increase effective nuclear charge. However, the exceptionally greater stability of  $Cu^{2+}$  complexes is the Jahn-Teller distortion.

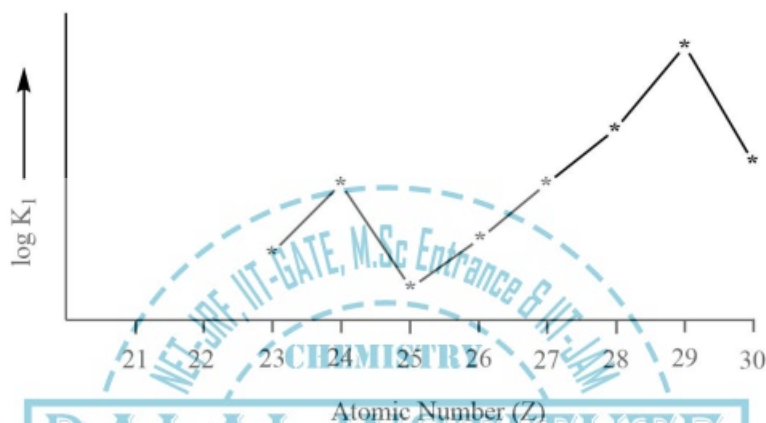


Figure 68. Variation of  $\log K_1$  for the addition of first ethylenediamine.

The sequence is generally quoted only for Mn(II) to Zn(II) as there is little or no data available for the other 3d series transition metal ions as their M(II) oxidation states are not very much stable. Crystal field theory is based on the idea that the interactions between the metal centre and the ligands-attached are purely ionic in nature; this suggests that the stability of the complexes should be related to the charge to radius ratio (ionic potential).

**2. Disproportionation of  $Au^{2+}$  salts:** Bivalent gold is less stable and undergoes disproportionation to form  $Au^{1+}$  and  $Au^{3+}$ . On the other hand, bivalent salts of Cu and Ag ions are quite common and relatively more stable. However, as far as the electronic configuration is concerned, all of the three belong to the same group and are  $d^9$  systems.

Thus, a strong Jahn-Teller distortion is expected. The disproportion of  $Au^{2+}$  can be explained in terms of increasing  $\Delta$  value down the group. Therefore, bivalent salts of gold would have the maximum magnitude of crystal field splitting, which results high destabilization associated with the filling of last electron (in  $d_{x^2-y^2}$ ). This makes  $Au^{2+}$  to undergo either to form  $Au^{3+}$ , a  $d^8$  system; or reduction to  $Au^{1+}$ , a  $d^{10}$  system. The  $d^8$  system ( $Au^{3+}$ ) is usually square-planar in geometry and quite stable as the electron from the  $d_{x^2-y^2}$  is removed. The  $d^{10}$  system ( $Au^{1+}$ ) is of linear geometry and stable due to fully filled configuration.

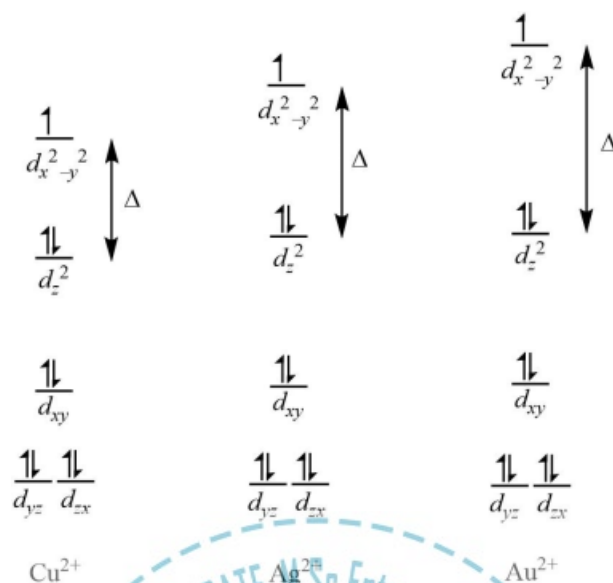


Figure 69. Variation of crystal field splitting energy for tetragonal  $\text{Cu}^{2+}$ ,  $\text{Ag}^{2+}$  and  $\text{Au}^{2+}$ .

**3. Stability order of ethylenediamine complexes of  $\text{Cu}^{2+}$ :** Jahn-Teller distortion is responsible for the stability order of  $[\text{Cu}(\text{en})_3]^{2+}$ ,  $\text{cis-}[\text{Cu}(\text{en})_2(\text{H}_2\text{O})_2]^{2+}$ ,  $\text{trans-}[\text{Cu}(\text{en})_2(\text{H}_2\text{O})_2]^{2+}$ .



Figure 70. Stability order of  $[\text{Cu}(\text{en})_3]^{2+}$ ,  $\text{cis-}[\text{Cu}(\text{en})_2(\text{H}_2\text{O})_2]^{2+}$ ,  $\text{trans-}[\text{Cu}(\text{en})_2(\text{H}_2\text{O})_2]^{2+}$ .

Bivalent copper cannot form  $[\text{Cu}(\text{en})_3]^{2+}$  because the Jahn-Teller distortion induces strain into the ethylenediamine molecule that is added along z-axis. Therefore, the only complex that exists is  $[\text{Cu}(\text{en})_2(\text{H}_2\text{O})_2]^{2+}$ . Similarly,  $\text{cis-}[\text{Cu}(\text{en})_2(\text{H}_2\text{O})_2]^{2+}$  is less stable in comparison than  $\text{trans-}[\text{Cu}(\text{en})_2(\text{H}_2\text{O})_2]^{2+}$ . The extra stability of  $\text{trans-}[\text{Cu}(\text{en})_2(\text{H}_2\text{O})_2]^{2+}$  is because of the non-involvement of longer bonds in chelation.

## ❖ Spectrochemical and Nephelauxetic Series

### ➤ The Spectrochemical Series

The spectrochemical series is a list of ligands arranged on basis of ligand strength and a list of metal ions based on oxidation number, group and its identity.

In crystal field theory, ligands change the difference in energy between the *d*-orbitals ( $\Delta$ ) called the ligand-field splitting parameter or crystal-field splitting parameter for ligands, which is primarily reflected in differences in color of similar metal-ligand complexes. However, there are many ligands which do not form complexes with a particular metal ion and the vice-versa is also true. It clearly means that the value of crystal field splitting energy for these complexes cannot be calculated experimentally. Therefore, an empirical method must be used to find out their  $\Delta$  values. In this method, two empirical parameters have been suggested for different metal ions and ligands.

Table 12. Values of parameters *g* and *f* for different metal centers and ligands.

Metal ion	<i>g</i>	Ligands	<i>f</i>
Co <sup>2+</sup>	9.3	3acac	1.21
Co <sup>3+</sup>	19.0	6H <sub>2</sub> O	1.00
Cr <sup>3+</sup>	17.0	6CH <sub>3</sub> COO <sup>-</sup>	0.96
Cu <sup>2+</sup>	12.0	3en	1.28
Fe <sup>2+</sup>	10.0	6OH <sup>-</sup>	1.70
Mn <sup>2+</sup>	8.5	6Cl <sup>-</sup>	0.80
Ni <sup>2+</sup>	8.9	6F <sup>-</sup>	0.90

Now, on the basis of experimental and empirical results, not only the metal ions but also the ligands can be arranged in the increasing or decreasing order of  $\Delta$ -values. The empirical formula to calculate the magnitude of crystal field splitting energy is given below.

$$\Delta_o = f \times g \times 10^3 \text{ cm}^{-1}$$

i) For [Ni(H<sub>2</sub>O)<sub>6</sub>]<sup>2+</sup>

$$\Delta_o = 8.9 \times 1.00 \times 10^3 \text{ cm}^{-1}$$

$$\Delta_o = 8900 \text{ cm}^{-1}$$

This value is pretty close to what has been observed experimentally (8700 cm<sup>-1</sup>).

ii) For  $[\text{Co}(\text{en})_3]^{3+}$

$$\Delta_o = 19 \times 1.28 \times 10^3 \text{ cm}^{-1}$$

$$\Delta_o = 24320 \text{ cm}^{-1}$$

This experimental value of  $\Delta$  for  $[\text{Co}(\text{en})_3]^{3+}$  is  $23000 \text{ cm}^{-1}$  which is pretty much comparable.

**1. Spectrochemical series of ligands:** The proposal of the spectrochemical series was first given in the year of 1938 by analyzing the results of UV-visible absorption spectra of cobalt complexes. A simple spectrochemical series ordering of ligands from small  $\Delta$  to large  $\Delta$  is given below.

$\text{O}_2^{2-} < \text{I}^- < \text{Br}^- < \text{S}^{2-} < \text{SCN}^-$  (S-bonded)  $< \text{Cl}^- < \text{N}^{3-} < \text{F}^- < \text{NCO}^- < \text{OH}^- < \text{C}_2\text{O}_4^{2-} \approx \text{H}_2\text{O} < \text{NCS}^-$  (N-bonded)  $< \text{CH}_3\text{CN} < \text{py}$  (pyridine)  $< \text{NH}_3 < \text{en}$  (ethylenediamine)  $< \text{bipy}$  (2,2'-bipyridine)  $< \text{phen}$  (1,10-phenanthroline)  $< \text{NO}^{2-} < \text{PPh}_3 < \text{CN}^- < \text{CO}$

Ligands placed on the left side of this spectrochemical series are usually considered as weak-field ligands and cannot cause the electron-pairing within  $3d$  shell and thus form spin-free octahedral complexes. On the other hand, ligands lying at the right end are stronger ligands and form spin-paired octahedral complexes due to forcible pairing of electrons within  $3d$  level and therefore are called low spin ligands. However, it should also be noted that the spectrochemical series is definitely backward from what it should be for a reasonable prediction based on the assumptions of crystal field theory. This deviation from crystal field theory highlights the reliability of the main assumption crystal field theory's that purely ionic bonds exist between metal and ligand. The order of the spectrochemical series can be obtained from the understanding that ligands are frequently classified by their donor or acceptor abilities.

Some, like  $\text{NH}_3$ , are  $\sigma$ -bond donors only, with no orbitals of appropriate symmetry for  $\pi$ -bonding interactions. Bonding by these ligands to metals is relatively simple, using only the  $\sigma$ -bonds to create relatively weak interactions. Another example of a  $\sigma$ -bonding ligand would be ethylenediamine, however, ethylenediamine has a stronger effect than ammonia, generating a larger crystal field split,  $\Delta$ . Ligands that have filled  $p$ -orbitals are potentially  $\pi$ -donors. These types of ligands tend to donate these electrons to the metal along with the  $\sigma$  bonding electrons, exhibiting stronger metal-ligand interactions and an effective decrease of  $\Delta$ . Most halide ligands, as well as  $\text{OH}^-$  and  $\text{H}_2\text{O}$ , are primary examples of  $\pi$ -donor ligands. When ligands have vacant  $\pi^*$  and  $d$  orbitals of suitable energy, there is the possibility of  $\pi$ -backbonding, and the ligands may be  $\pi$ -acceptors. This addition to the bonding scheme increases  $\Delta$ . Ligands that do this very effectively include  $\text{CN}^-$ ,  $\text{CO}$  and many others.

**2. Spectrochemical series of metals:** Like the ligands, different metal ions can also be ordered in increasing  $\Delta$ , and this order is independent of the identity of the ligand to a large extent.

$\text{Mn}^{2+} < \text{Ni}^{2+} < \text{Co}^{2+} < \text{Fe}^{2+} < \text{V}^{2+} < \text{Cu}^{2+} < \text{Fe}^{3+} < \text{Cr}^{3+} < \text{V}^{3+} < \text{Co}^{3+}$

In general, it is almost impossible to claim whether a given ligand will exert a strong or a weak field on a given metal ion. Nevertheless, if we consider the metal ion, it has been observed that the magnitude of ligand field splitting energy increases with increasing oxidation number, and also as we move down the group.

➤ **The Nephelauxetic Series**

The nephelauxetic series is a list of ligands or metal ions ordered on the basis of the strength of their nephelauxetic effect.

In the inorganic studies, the term “nephelauxetic effect” is very frequently used for transition metal complexes. This refers to a decreasing Racah parameter ( $B$ ), a measure of inter-electronic repulsion, that occurs when a free transition-metal ion forms a complex with different types of ligands. The label "nephelauxetic" is for cloud-expanding in the Greek language. The presence of the nephelauxetic effect brings out the drawbacks of crystal field theory, as this suggests a somewhat covalent character in the metal-ligand bonding.

The declining value of the Racah parameter hints that in a metal complex, there is less repulsion between the two electrons in a given doubly occupied metal  $d$ -orbital than what is in the free ion counterpart,  $M^{n+}$ ; which consecutively implies that the orbital size is larger after complexation. Two reasons for electron-cloud-expansion effect may be given; one is that the effective positive charge on the metal is reduced by any negative charge on the ligands, the  $d$ -orbitals can expand a slight manner; the second is the considers the overlapping with ligand orbitals and creation of covalent bonds increases the size of the orbital.

The reduction of  $B$  from its free ion value is normally reported in terms of the nephelauxetic parameter,  $\beta$ , as:

$$\beta = \frac{B'(\text{Complex})}{B(\text{Free ion})}$$

Moreover, it is also observed experimentally that the magnitude of the nephelauxetic parameter always follows a certain order with respect to the nature of the ligands attached. However, there are many ligands which do not form complexes with a particular metal ion and the vice-versa is also true. It clearly means that the value of the Racah parameter for these complexes cannot be calculated experimentally. Therefore, an empirical method must be used to find out their  $B$  values. In this method, two empirical parameters have been suggested for metal ions and ligands.

Table 13. Values of parameters  $k$  and  $h$  for different metal centers and ligands.

Metal ion	$k$	Ligands	$h$
$\text{Co}^{2+}$	0.24	$6\text{CN}^-$	2.0
$\text{Co}^{3+}$	0.35	$3\text{en}$	1.5
$\text{Cr}^{3+}$	0.21	$6\text{H}_2\text{O}$	1.0
$\text{Mn}^{2+}$	0.07	$6\text{NH}_3$	1.4
$\text{Ni}^{2+}$	0.12	$6\text{F}^-$	0.8

The empirical formula to calculate the magnitude of the Racah parameter for any metal ion in complexation is given below.

$$B' = B(1 - kh) \text{ cm}^{-1}$$

Where, B and B' are the Racah parameters for free ion and metal center in complexation, respectively.

i) For  $[\text{Ni}(\text{H}_2\text{O})_6]^{2+}$

$$B' = 1080(1 - 0.12 \times 1.0) \text{ cm}^{-1}$$

$$B' = 950 \text{ cm}^{-1}$$

This value is pretty close to what has been observed experimentally ( $905 \text{ cm}^{-1}$ ).

ii) For  $[\text{Co}(\text{en})_3]^{3+}$

$$B' = 1400(1 - 0.35 \times 1.5) \text{ cm}^{-1}$$

$$B' = 665 \text{ cm}^{-1}$$

This experimental value of B for  $[\text{Co}(\text{en})_3]^{3+}$  is  $568 \text{ cm}^{-1}$ .

The values of Racah parameter (B) for transition metal ion in the gaseous state can be noted from the table given below.

Table 14. Racah parameters for different free transition metal atoms or ions.

Metal	$M^0$	$M^{1+}$	$M^{2+}$	$M^{3+}$	$M^{4+}$
Ti	560	681	719	-	-
V	579	660	765	860	-
Cr	790	710	830	1030	1040
Mn	720	872	960	1140	-
Co	789	879	1117	-	-
Ni	1025	1038	1080	-	-
Cu	-	1218	1239	-	-
Fe	805	870	1059	-	1144

Now, on the basis of experimental and empirical results, not only the metal ions but also the ligands can be arranged in the increasing or decreasing order of  $\beta$ -values.

**1. Nephelauxetic series of ligands:** The list is shown below list commons ligands (with increasing nephelauxetic effect):



Although parts of this series may seem quite similar to the spectrochemical series of ligands, that is not true. For instance; the fluoride, ethylenediamine and cyanide seem to occupy almost similar positions; Some other ligands such as chloride, iodide and bromide, are arranged very differently. Roughly, we can say that the ordering reflects the capability of the ligands to form better covalent bonds with metals; means ligands at the end of the series i.e. with large nephelauxetic effect have better tendency to form covalent bond than the ligands present at the start of the series.

**2. Nephelauxetic series of metal ions:** The nephelauxetic effect does not only depend upon the ligand type but also upon the central metal ion. These too can be arranged in order of increasing nephelauxetic effect as follows:



It is obvious that as the oxidation number for the metal ion increases, the nephelauxetic effect also increases.

## ❖ Charge Transfer Spectra

*A charge transfer band may be defined as the peak arising from the transition in which an electron is transferred from one atom or group in the molecule to another one.*

In other words, the transition occurs between molecular orbitals that are essentially centered on different atoms or groups. These transitions are neither Laporte nor spin-forbidden in nature; and therefore, show very intense absorption. Charge transfer transitions are primarily classified in four types as:

### ➤ Ligand to Metal Charge Transfer

The ligand to metal charge transfer (LMCT) in metal complexes arises when the electrons are transferred from a molecular orbital with a ligand-like character to those with metal-like character. This type of transfer is predominant if the following conditions are fulfilled:

- i) The ligands should have lone pair of electrons with relatively high-energy such as  $O^{2-}$ ,  $Cl^-$ ,  $Br^-$ ,  $S^{2-}$  or Se.
- ii) The metal should be in a high oxidation state and must have low-lying empty orbitals.

These conditions imply that the acceptor level is available and low in energy. Moreover, the charge transfer transitions for octahedral and tetrahedral complexes are different; therefore, these two types of ligand to metal charge transfer are quite important and must be discussed in detail.

**1. LMCT in octahedral complexes:** Before we discuss the ligand to metal charge transfer in octahedral complexes, the molecular orbital diagram for  $\sigma$  and  $\pi$ -bonding in  $ML_6$  geometry should be recalled. The electrons can be excited, not only from the  $t_{2g}^*$  to  $e_g^*$  but also from the bonding molecular orbitals of  $\sigma$  and  $\pi$  nature that are predominantly associated with the ligands. The latter two types of excitation modes result in

the charge transfer spectra, labeled as the ligand to metal charge transfer. This type of transition results in a formal reduction of the metal.

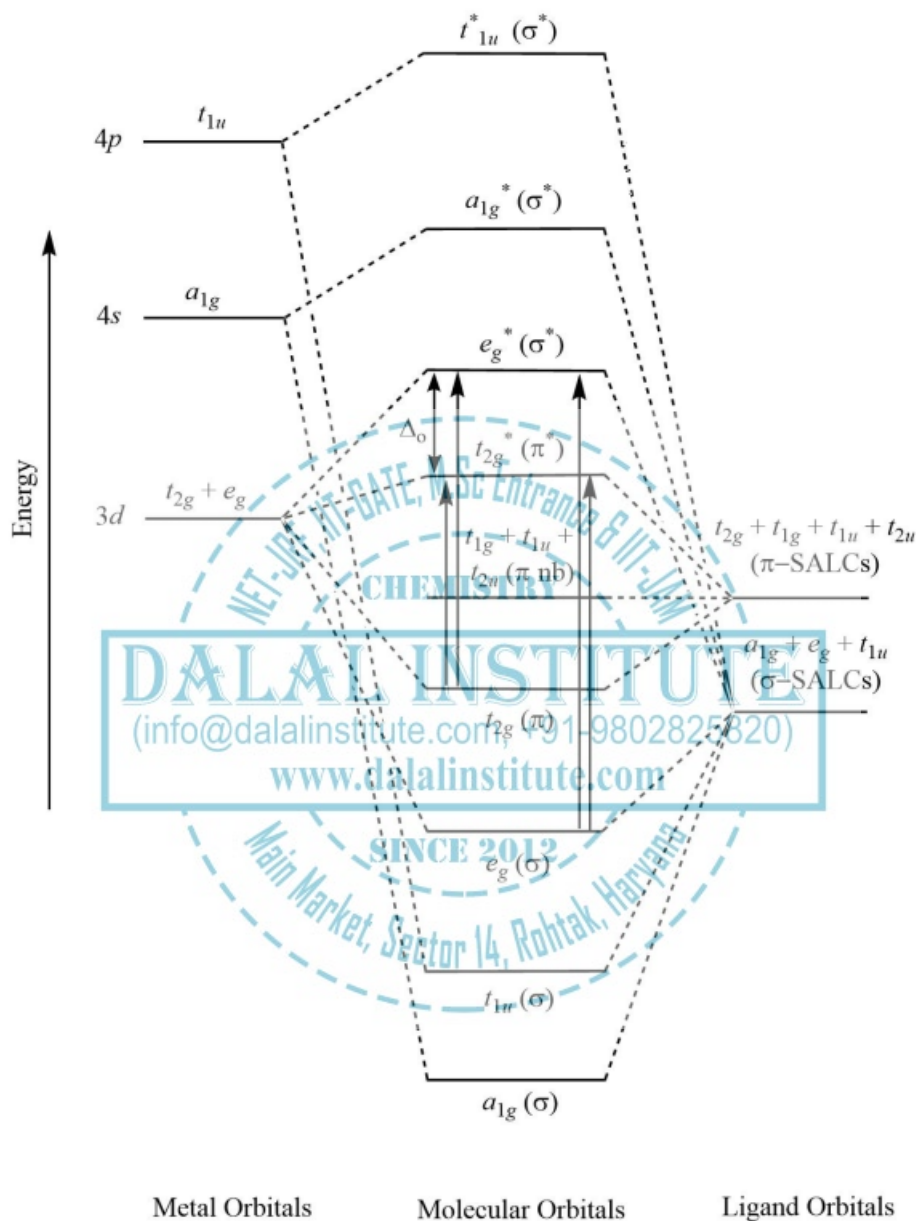


Figure 71. Ligand to metal charge transfer in octahedral ( $ML_6$ ) complexes.

Consider a  $d^6$  octahedral complex, such as  $[Co(NH_3)_5(X)]^{2+}$  ( $X = F^-$ ,  $Cl^-$ ,  $Br^-$  or  $I^-$ ), whose  $t_{2g}^*$  levels are filled. As a consequence, an intense absorption band in  $[Co(NH_3)_5F]^{2+}$  is observed above  $40000\text{ cm}^{-1}$ ; and that is corresponding to a transition from ligand  $\sigma$ -bonding molecular orbital to the empty  $e_g^*$  molecular orbital. However, in  $[Co(NH_3)_5Cl]^{2+}$  this intense band with two components is observed above  $30000\text{ cm}^{-1}$ .

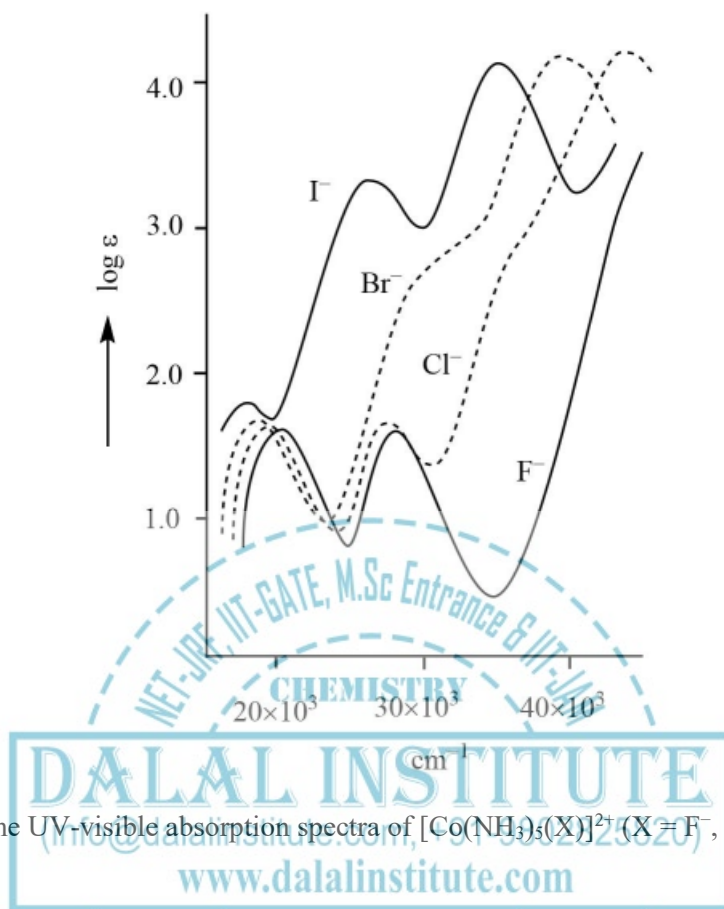


Figure 72. The UV-visible absorption spectra of  $[\text{Co}(\text{NH}_3)_5(\text{X})]^{2+}$  ( $\text{X} = \text{F}^-$ ,  $\text{Cl}^-$ ,  $\text{Br}^-$  or  $\text{I}^-$ ).

The charge-transfer bands appear at lower energy for  $[\text{Co}(\text{NH}_3)_5\text{Br}]^{2+}$  and at still lower energy for  $[\text{Co}(\text{NH}_3)_5\text{I}]^{2+}$ , overlapping with ligand-field bands and masking their higher energy peaks. It must be noted that the ligand-field peaks shift slightly according to the increasing strength of the crystal field of X, but the charge-transfer bands show very large shifts. The shifts in the energies of the LMCT transitions in  $[\text{Co}(\text{NH}_3)_5(\text{X})]^{2+}$  correspond to the changes in ease of removal of the electron (oxidation) from  $\text{X}^-$ . Though the transition corresponds to the transfer of an electron from  $\text{X}^-$  to  $\text{Co}^{3+}$ ; and therefore, no net oxidation-reduction occurs because of the very short lifetime of the excited state. Nonetheless, this process, provide a mechanism for photochemical decomposition that occurs for many complexes stored in strong light. A similar pattern has been observed in the case of  $[\text{Cr}(\text{NH}_3)_5(\text{X})]^{2+}$  ( $\text{X} = \text{F}^-$ ,  $\text{Cl}^-$ ,  $\text{Br}^-$  or  $\text{I}^-$ ).

**2. LMCT in tetrahedral complexes:** Before we discuss the ligand to metal charge transfer in tetrahedral complexes, the molecular orbital diagram for  $\sigma$  and  $\pi$ -bonding in  $\text{ML}_4$  geometry should be recalled. The electrons can be excited, not only from the  $e^*$  to  $t_2^*$ , but also from the  $\pi$ -bonding molecular orbitals of  $t_2$ -symmetry and nonbonding  $\pi$ -SALCs of  $t_1$ -symmetry; both of which are predominantly associated with the ligands. The latter two types of excitation modes result in the charge transfer spectra, labeled as the ligand to metal charge transfer. This type of transition results in a formal reduction of the metal.

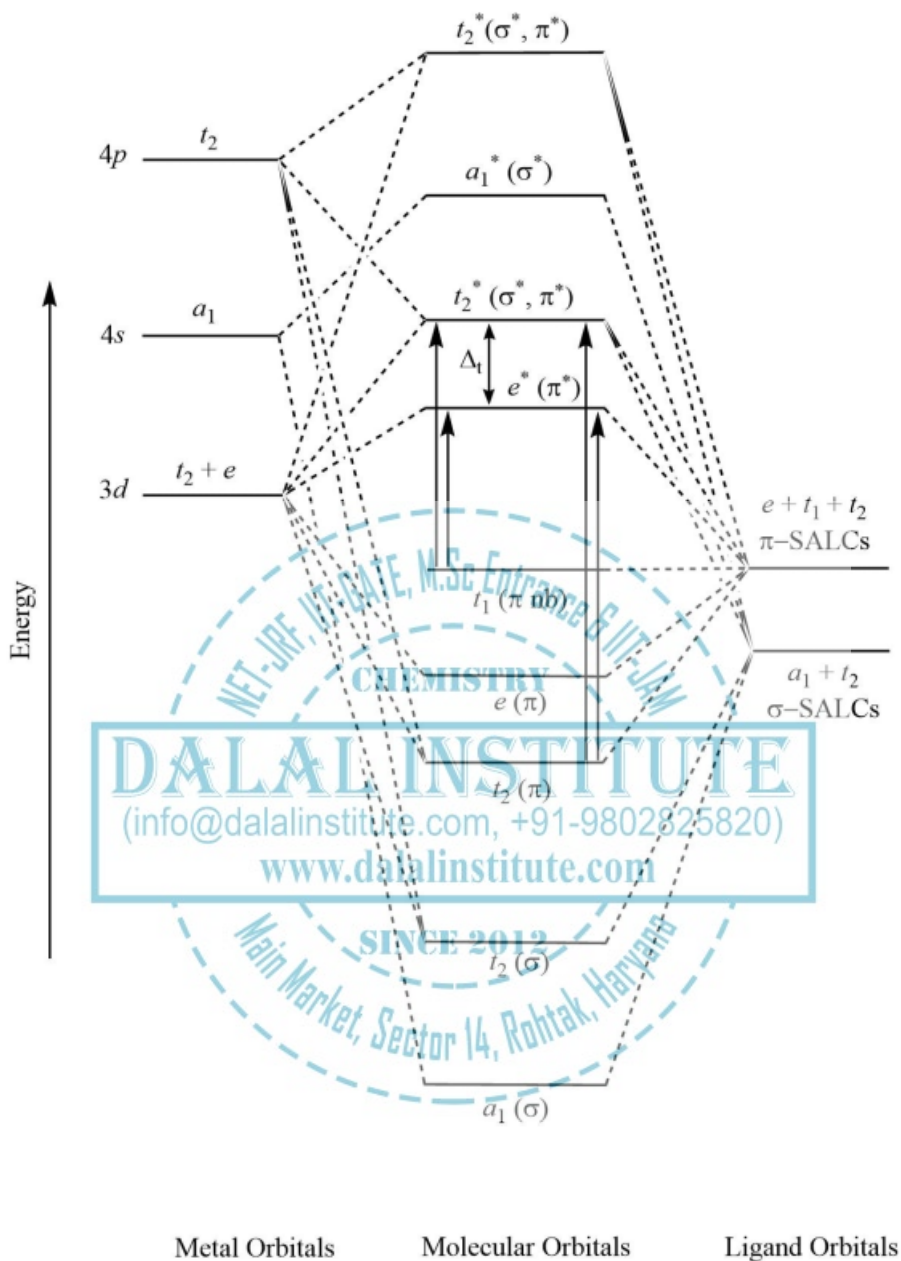


Figure 73. Ligand to metal charge transfer in tetrahedral ( $ML_4$ ) complexes.

Consider a  $d^0$  tetrahedral complex, such as  $MnO_4^-$ , whose  $e^*$  and  $t_2^*$  levels are totally empty. As a consequence, very intense absorption spectra in permanganate is obtained and all of the four ligand-to-metal-charge-transfer (LMCT) transitions are observed. However, it must be noted that three out of four peaks happen to arise in the ultra-violet region and only  $t_1 \rightarrow e^*$  transition belongs to the visible range. Moreover, this particular transition is also responsible for the deep purple color of permanganate ion.

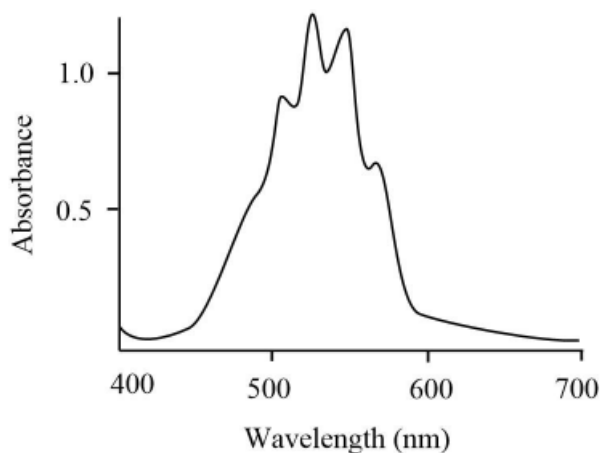


Figure 74. The UV-visible absorption spectra of  $\text{MnO}_4^-$ .

The complete profile of absorption spectra of  $\text{MnO}_4^-$  ion is given below as:

Table 15. The type of transition and their wavenumbers of the absorption peaks for  $\text{MnO}_4^-$ .

Transition type	Wavenumber ( $\text{cm}^{-1}$ )
$L(t_1) \rightarrow M(e^*)$	17700
$L(t_1) \rightarrow M(t_2^*)$	29500
$L(t_2) \rightarrow M(e^*)$	30300
$L(t_2) \rightarrow M(t_2^*)$	44400

A similar pattern has been observed in the case of  $\text{CrO}_4^{2-}$ . The energies of transitions correlate with the order of the electrochemical series. Lower energy absorption is expected for the metal ions which are reduced more easily. The abovementioned trend is in accordance to the transfer of electrons from the ligand to the metal, and hence resulting in a reduction of the metal center by the ligand attached.

Oxidation state	Complexes			
+7	$\text{MnO}_4^-$	$\text{TcO}_4^-$	$\text{ReO}_4^-$	Blue shift ↓
+6	$\text{CrO}_4^{2-}$	$\text{MoO}_4^{2-}$	$\text{WO}_4^{2-}$	
+5	$\text{VO}_4^{3-}$	$\text{NbO}_4^{3-}$	$\text{TaO}_4^{3-}$	
LMCT shows blue shift				

➤ **Metal to Ligand Charge Transfer**

The metal to ligand charge transfer (MLCT) in metal complexes arises when the electrons are transferred from a molecular orbital with a metal-like character to those with a ligand-like character. This type of transfer is predominant if the following conditions are fulfilled:

- The ligands should have high-energy empty  $\pi^*$  orbitals such as CO,  $\text{CN}^-$ ,  $\text{SCN}^-$  or NO.
- The metal should be in a low oxidation state and must have high-lying filled orbitals.

These conditions imply that the empty  $\pi^*$  orbitals on the ligands become the acceptor orbitals on the absorption of light. The available acceptor level is relatively high in energy. However, before we discuss the ligand to metal charge transfer in transition metal complexes, the molecular orbital diagram for  $\sigma$  and  $\pi$ -bonding in  $\text{ML}_6$  geometry should be recalled.

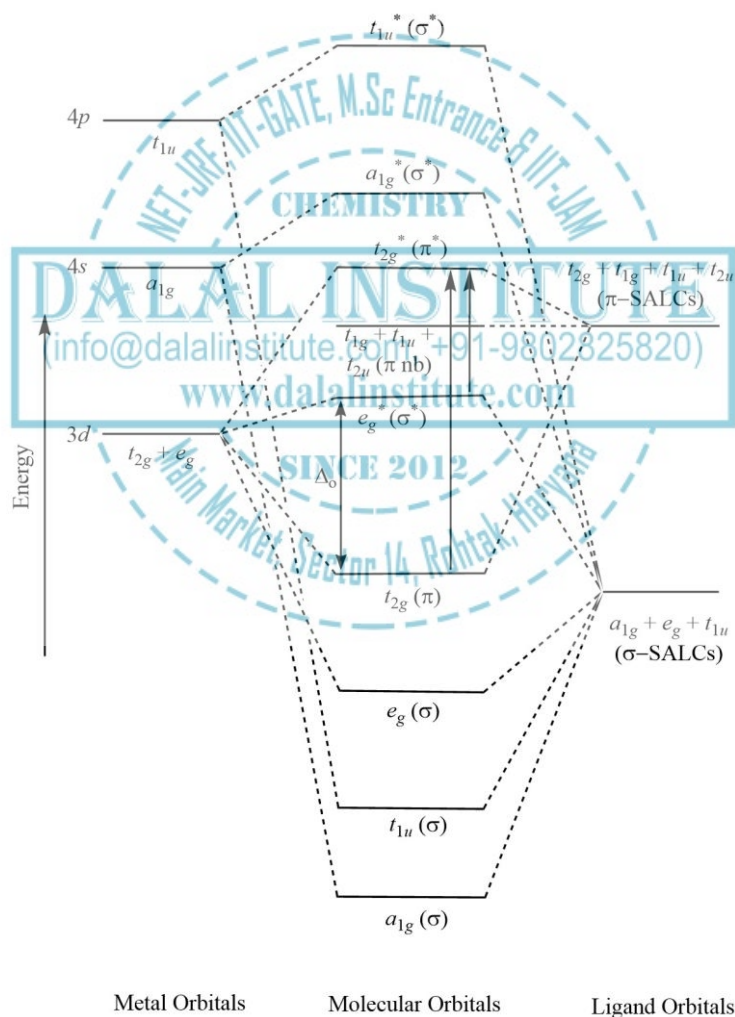


Figure 75. Metal to ligand charge transfer in octahedral ( $\text{ML}_6$ ) complexes.

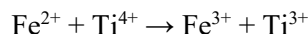
The electrons can be excited, not only from the  $t_{2g}$  to  $e_g^*$ , but also from the bonding molecular orbitals of  $\pi$  and antibonding molecular orbitals of  $\sigma$  nature (predominantly associated with the ligands) to antibonding  $\pi^*$ . The latter two types of excitation modes result in the charge transfer spectra, labeled as the metal to ligand charge transfer. This type of transition results in formal reduction of the metal. The common type of ligands taking part in MLCT include 2,2'-bipyridine (bipy), 1,10-phenanthroline (phen), CO,  $\text{CN}^-$  and  $\text{SCN}^-$ . Examples of these complexes include: Tris(2,2'-bipyridyl) ruthenium(II),  $\text{W}(\text{CO})_4(\text{phen})$ ,  $\text{K}_4[\text{Fe}(\text{CN})_6]$ ,  $\text{K}_3[\text{Fe}(\text{CN})_6]$ ,  $[\text{Fe}(\text{phen})_3]^{3+}$ ,  $[\text{Fe}(\text{acac})_3]$  and  $\text{Fe}(\text{CO})_3(\text{bipy})$ .

An orange-colored complex of bivalent ruthenium,  $[\text{Ru}(\text{bpy})_3]^{2+}$ , is being analyzed because the excited electronic state that results from this charge transfer has an average life-time around microseconds and the complex can act as an adaptable photochemical reagent. The photo-reactivity of these complexes arises from the nature of the reduced ligand and oxidized metal center. Now although the states of MLCT complexes such as  $[\text{Ru}(\text{bipy})_3]^{2+}$  and  $\text{Re}(\text{bipy})(\text{CO})_3\text{Cl}$  were intrinsically not that much reactive, there are many MLCT complexes which are characterized by reactive MLCT states. Vogler and Kunkely proposed that a MLCT complex can be considered as an isomer of the ground state, that possesses a reduced ligand and oxidized metal. Hence, many reactions like electrophilic attack, oxidative addition at the metal ion due to the reduced ligand, the radical reactions on the reduced ligand, or the outer-sphere charge-transfer reactions can be attributed to states arising from metal-to-ligand-charge-transfer transitions. The reactivity of MLCT states usually depends on the oxidation of the metal center. The succeeding processes include exciplex formation, cleavage of metal-metal bonds, associative ligand substitution.

➤ **Metal to Metal Charge Transfer**

*The metal to metal or inter-valence charge transfer may simply be defined as the excitation and subsequent transfer of an electron from a low oxidation state cation to a neighboring cation of a higher oxidation state.*

The transfer is usually excited by a certain visible portion of the light of and produces a characteristic color. The electron then drops back down, giving off the extra energy as a small amount of heat. An example is corundum with the coupled substitution. The simplified chemical equation representing various oxidation states can be given as:



This reaction absorbs red photons and gives sapphire its characteristic blue color. In hematite, the process absorbs all visible photons. Materials that exhibit this property retain their dark color regardless of how finely they are ground. Materials exhibiting metal to metal charge transfer (MMCT) are also conductors. MMCT generally shows a strong sloping spectral signature in the range 500-1000 nm. Edge-shared octahedral geometries generally exhibit MMCT in the range 700-800 nm, while face-shared octahedral complexes exhibit it in the range of 800-900 nm. In order for metal-to-metal-charge-transfer (MMCT) to occur, orbital must overlap so electrons can flight back and forth. Examples of the systems displaying metal to metal charge transfer are:

Table 16. The type of transition and their wavenumbers of the absorption peaks for  $\text{MnO}_4^-$ .

System	Absorption maxima (nm)
$\text{Fe}^{2+} \rightarrow \text{Fe}^{3+}$ (edge-shared)	700-800
$\text{Fe}^{2+} \rightarrow \text{Fe}^{3+}$ (face-shared)	800-900
$\text{Ti}^{3+} \rightarrow \text{Ti}^{4+}$	600-800
$\text{Mn}^{2+} + \text{Ti}^{4+} \rightarrow \text{Mn}^{3+} + \text{Ti}^{3+}$	380-450

The most popular example of inter-valence charge transfer is “Prussian blue”. This compound has the formula  $\text{KFe}[\text{Fe}(\text{CN})_6]$  and shows a very intense blue color owing to the transfer of an electron from  $\text{Fe}^{2+}$  to  $\text{Fe}^{3+}$ . In the crystal structure of Prussian blue, the  $\text{Fe}^{2+}$  ions are bonded with N atom while the  $\text{Fe}^{3+}$  ions are bonded with C atom of octahedrally surrounding of  $\text{CN}^-$  ligands. Therefore, the charge transfer takes place through the cyanide bridge.

➤ **Ligand to Ligand Charge Transfer**

*The ligand to ligand or inter-ligand charge transfer may be defined as the excitation and subsequent transfer of an electron from a one ligand orbitals to a neighboring ligand orbital.*

The ligand to ligand charge transfer (LLCT) or inter-ligand charge transfer transitions are quite uncommon and rarely observed. In comparison to the enormous literature on metal-to-ligand and ligand-to-metal charge transfer, very little has been published on LLCT. In most of the cases, LLCT peaks are difficult to detect in UV-visible absorption spectra; which can be attributed to the fact that these peaks may be obscured or hidden under absorption bands of different origins, or they may occur at a position very distinct from those ordinarily analyzed. The LLCT bands are of low intensity due to the poor overlap between the participating orbitals. Molecular orbitals with dominant ligand characters may have some amount of metal character also, and a transition that is labelled as ligand to ligand may in fact also involve the metal to some point. However, if the LLCT is pure, it would have transition energy that does not change considerably when the metal is changed. A more specific form of  $\text{L}_{\text{red}}-\text{M}-\text{L}_{\text{ox}}$  complexes is mixed-valence compounds (ligand-based), which possesses the same ligand in two different redox states. In this case, the interaction between ligands may yield a partial or complete electron delocalization between the oxidized and reduced form of the ligands. Therefore, the LLCT loses its charge-transfer character because now it is occurring between delocalized orbitals.

One of the recent examples of metal complexes involving ligand to ligand charge transfer is  $(\text{CuTpAsPh}_3)$ . The emission and UV-visible absorption spectra of  $(\text{CuTpAsPh}_3)$ , contain low-energy bands (with a band maximum at  $16\,500\text{ cm}^{-1}$  in emission and a weak shoulder at about  $25\,000\text{ cm}^{-1}$  in absorption) that are not present in the corresponding spectra of the phosphine or amine complexes. The peaks are assigned to the ligand to ligand charge transfer (LLCT) may have some contribution from the metal.

### ❖ Electronic Spectra of Molecular Addition Compounds

The electronic absorption spectra of molecular addition compounds can be best understood by considering the example of iodine adducts. The absorption maxima for iodine (dissolved in carbon tetrachloride) appears at about 520 nm wavelength. This band, without any doubt, can successfully be assigned to a  $\pi^* \rightarrow \sigma^*$  transition; and is also responsible for the violet color of free iodine. However, when certain ligands like macrocyclic ethers or any other donor molecules are added to the iodine solution, two obvious changes in the absorption spectrum occur. The characteristic band of free iodine shows a blue shift, and some intense peaks arise in the ultraviolet region. The hypsochromic shift is due to the complexation of free iodine, while the origin of additional peaks in the ultra-violet region can be ascribed to the charge transfer transitions. The later claim is also confirmed by the absence of any dominant peak in the absorption spectra of the ligand alone. Furthermore, the isobestic point at 490 nm suggests the presence of two absorbing species in the system; and the value of the equilibrium constant  $K$  obtained over a wide range of base concentrations also demonstrates the existence of a 1:1 molecular addition compound.

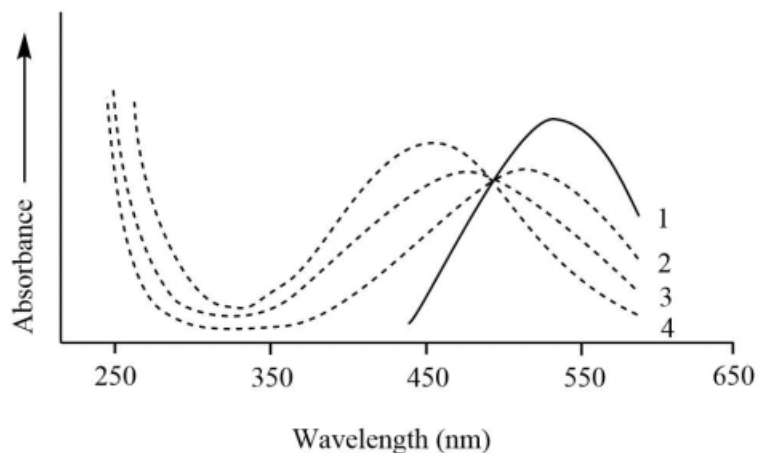


Figure 76. The UV-visible absorption spectra of iodine (1) and base-iodine solutions in  $\text{CCl}_4$  with increasing concentration of base ( $2 < 3 < 4$ ).

The observed blue shift in the free iodine band is due to the perturbation of  $\sigma^*$  molecular orbital of iodine by a repulsive interaction between the two components of the charge-transfer complex. Therefore, as the repulsive interactions increase, a larger blue shift of the iodine band would be expected. Hence, it is sensible to consider the amount of the hypsochromic shift in the free  $\text{I}_2$  band as a measure of the interaction between the iodine molecule and the ligand molecule. The limiting value of the blue shift is approximately 360 nm and which is the characteristic absorption peak for  $\text{I}_3^-$  ions. The formation of triiodide ion, implicitly, would mean that the magnitude of the polarization of the iodine molecule in base-iodine complex is so large that a clear-cut charge separation has occurred. However, the confirmation of  $\text{I}_3^-$  ions in solution must be done by checking the presence of the second characteristic peak of triiodide ion at 292 nm.

The absorption spectra of  $I_2$  in the presence of large excess of dicyclohexyl-18-crown-6 in chloroform solution at is shown in 'Figure 77'. It can clearly be seen that none of the initial reactants show any measurable absorption in 250-450 nm region, however, the addition of crown ether to the iodine solution generates in two strong absorptions bands the aforementioned wavelength range. This can be attributed to the formation of charge-transfer complexes between the dicyclohexyl-18-crown-6 and the free iodine which causes the vanishing of purple color from the solution. The spectra recorded for the electron donor-acceptor (EDA) complex between ligands and  $I_2$  are time-dependent and the intensities of the different absorptions change significantly with time. Though the general profile of the spectra remains unaffected, after some time the purple color of solution begins to disappear slowly and the intensity of the absorption bands in the 250–600 nm region declines with time.

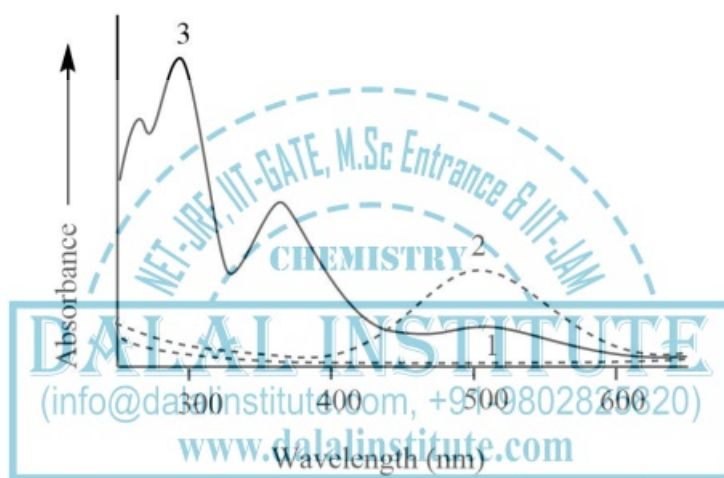


Figure 77. The UV-visible absorption spectra of  $I_2$  in the presence of excess of dicyclohexyl-18-crown-6.

If  $\psi_{cov}$  includes contributions from covalent interactions while  $\psi_{ele}$  includes contributions from purely electrostatic forces (these are described as charge-transfer interactions); then the bonding in iodine adducts can be described by the equation:

$$\psi = a\psi_{cov} + b\psi_{ele}$$

The ground state of most adducts exists with  $b > a$ ; however, as the charge-transfer transition occurs, the situation is actually reversed with  $a > b$ . This results in a band around 250 nm owing to the transition in which an electron from the ground state is promoted to an excited state. Hence, the assignment of the charge-transfer band can be approximated by a transfer of an electron from the nonbonding orbital of the base to the  $\sigma^*$  orbital iodine. The whole spectra (including normal  $\pi^* \rightarrow \sigma^*$  transition after complexation) can be explained in terms of relative energies of the molecular orbitals of iodine and the complex. The molecular orbitals ( $\sigma_{complex}$ ,  $\sigma^*_{complex}$ , and  $\pi^*_{complex}$ ) are very much like the original base and iodine orbitals because of the weak Lewis acid-base interaction.

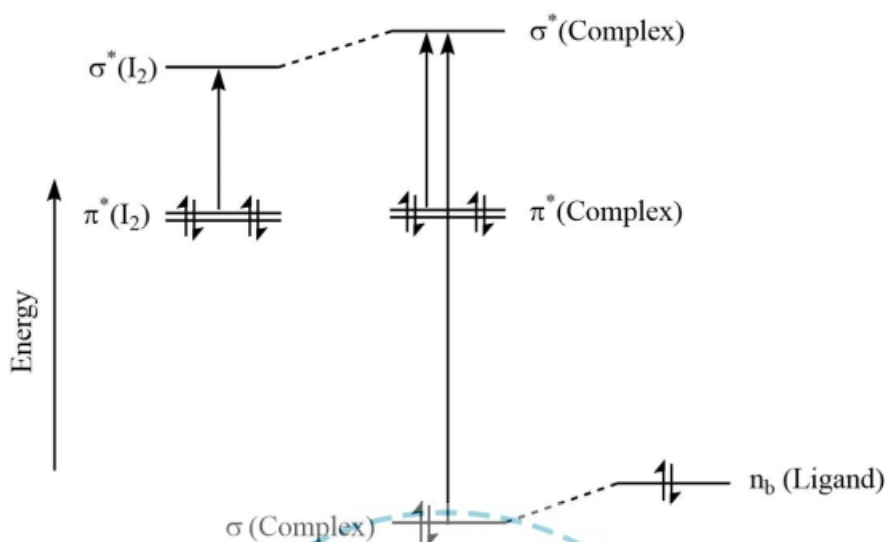


Figure 78. The partial molecular orbital diagram in base-iodine adducts.

Meanwhile,  $\sigma^*_{\text{complex}}$  is slightly higher in energy than the corresponding  $\sigma^*_{\text{iodine}}$ , the analogous transition in complexed iodine requires slightly more energy than the corresponding transition in free and a blue shift is observed. The charge-transfer transition occurs at higher energy in the ultraviolet region. The claim that the blue shift is correlated to the magnitude of the base-iodine interaction (enthalpy of formation of adduct) would be reasonable only if the energy of  $\pi^*_{\text{complex}}$  differs very little from that of  $\pi^*_{\text{iodine}}$  or its energy changes with the enthalpy in a linear fashion. When a wide range of different types of Lewis bases were studied with iodine solution, it has been found that the abovementioned correlation does exist roughly but is not of quantitative nature. The equation relating the charge transfer band, the ionization energy of the base,  $I_b$ , and the electron affinity of the acid,  $E_a$ , has also been reported:

$$\nu_{\text{charge transfer band}} = I_b - E_a - \Delta$$

where  $\Delta$  is an empirically determined constant for a related series of bases.

Both inorganic and organic researchers have always been interested in the enthalpies for the formation of these charge-transfer complexes. This is because a lot of information about donor and acceptor interactions can be obtained which is pretty much essential to an understanding of many phenomena in inorganic systems; especially in the areas of non-aqueous solvents and coordination chemistry. It should also be noted that the thermodynamic study of these adducts is easier in the solvents like hexane or carbon tetrachloride than in polar solvents, which is due to the larger magnitude of enthalpies and entropies of solvation in the later. The characteristic results from ligand-iodine solutions with minimal solvation effects for a wide range of systems can be studied and the information that can be obtained by studying enthalpies of association in weakly basic, non-polar solvents are given below:

1. A correlation of the heat of formation of iodine adducts of a series of para-substituted benzamides with the Hammett substituent constants of the benzamides.
2. The donor properties of the  $\pi$ -electron systems of alkyl-substituted benzenes
3. The donor properties of sulfites, sulfoxides, sulfones, and carbonyl compounds have been studied which shows that carbon-oxygen bonding in ketones and acetates is more effective than in sulfur-oxygen bonding.
4. The ring size effect on the donor properties of cyclic ethers and sulphides showed that for  $(\text{CH}_2)_n \text{S}$ , donor strength of sulfur follows order  $n = 5 > 6 > 4 > 3$ ; and the order for the corresponding ethers is  $4 > 5 > 6 > 3$ .
5. The donor strength of  $3^\circ$ ,  $2^\circ$ , and  $1^\circ$  amines have been assessed which varies with the acid studied.

Besides iodine, a lot of charge-transfer complexes of many other Lewis acids absorb light in the UV-visible region. The factors affecting the magnitude of the interaction and other useful information regarding the bonding in the molecular addition compounds of  $\text{SO}_2$ ,  $\text{ICI}$ ,  $\text{Br}_2$ , phenol and other acids have also been investigated.



### ❖ Problems

- Q 1. Define term symbols and also find out the ground state term for  $V^{3+}$  ion.
- Q 2. Calculate the total number of microstates for  $p^2$  and  $d^7$ -configurations.
- Q 3. Draw and discuss the pigeon-hole diagram for  $d^2$ -configuration and also comment on the energy correlation of all the free ion terms.
- Q 4. How many singlet microstates do exist for a metal ion with an electronic configuration of  $3d^1, 4f^4$ ?
- Q 5. Discuss the microstate distribution in  ${}^7F_2$  term symbol.
- Q 6. Explain the energy correlation and spin-orbit coupling in  $Cr^{3+}$  and  $Cu^{2+}$ .
- Q 7. What are Orgel diagrams? How do they differ from Tanabe-Sugano diagrams?
- Q 8. Draw and discuss the generalized Orgel diagram for  $d^2, d^3, d^7$  and  $d^8$  electronic configurations.
- Q 9. How can you find out the high-spin low spin nature of a metal complex using the Tanabe-Sugano diagram for  $d^n$ -systems? Explain in detail using a suitable example.
- Q 10. What do you understand from the trigonal distortion of octahedral complexes? How does it affect the various  $d$ -orbital energy levels in low-spin  $Co^{3+}$  complexes?
- Q 11. Write a short note on the structural evidence from the electronic spectrum of transition metal complexes.
- Q 12. Define the Jahn-Teller theorem. Discuss its effect in the coordination chemistry.
- Q 13. How does the Jahn-Teller distortion affect the electronic spectrum of transition metal complexes?
- Q 14. Distinguish between static and dynamic Jahn-Teller distortion.
- Q 15. Write a short note on the spectrochemical series.
- Q 16. What is 'the nephelauxetic' effect and what is the empirical formula to calculate the Racah parameter for different metal ions in complexation?
- Q 17. What is ligand to metal charge transfer? Draw and discuss in tetrahedral complexes using  $MnO_4^-$ .
- Q 18. What is Prussian blue? Discuss the cause of its characteristic blue color.
- Q 19. What are the molecular addition compounds? Discuss the spectra of iodine in carbon tetrachloride.
- Q 20. Give any five applications of the enthalpy of adduct formation.

---

### ❖ Bibliography

- [1] N. N. Greenwood, A. Earnshaw, *Chemistry of the Elements*, Butterworth-Heinemann, Oxford, Britain, 1998.
- [2] B. W. Pfennig, *Principles of Inorganic Chemistry*, John Wiley & Sons, New Jersey, USA, 2015.
- [3] J. E. Huheey, E. A. Keiter, R. L. Keiter, *Inorganic Chemistry: Principals of Structure and Reactivity*, HarperCollins College Publishers, New York, USA, 1993.
- [4] B. R. Puri, L. R. Sharma, K. C. Kalia, *Principals of Inorganic Chemistry*, Milestone Publishers, Delhi, India, 2012.
- [5] S. F. A. Kettle, *Physical Inorganic Chemistry: A Coordination Chemistry Approach*, Springer-Verlag, Berlin, Germany, 1996.
- [6] B. N. Figgis, M. A. Hitchman, *Ligand Field Theory and its Applications*, Wiley-VCH, New York, USA, 2000.
- [7] J. E. House, *Inorganic Chemistry*, Academic Press, California, USA, 2008.
- [8] Y. Tanabe, S. Sugano, *On the Absorption Spectra of Complex Ions. I*, Journal of the Physical Society of Japan, 9, 1954, 753.
- [9] Y. Tanabe, S. Sugano, *On the Absorption Spectra of Complex Ions. II*, Journal of the Physical Society of Japan, 9, 1954, 766.
- [10] A. L. Tchougréeff, R. Dronskowski, *Nephelauxetic Effect Revisited*, International Journal of Quantum Chemistry, 109, 2009, 2606.
- [11] C. K. Jørgensen, C. H. D. Verdier, J. Glomset, N.A. Sørensen, *Studies of Absorption Spectra IV: Some New Transition Group Bands of Low Intensity*, Acta Chem. Scand., 8, 1954, 1502.
- [12] R. S. Drago, *Physical Methods for Chemists*, Surfside Scientific Publishers, Florida, USA, 1992.

## LEGAL NOTICE

This document is an excerpt from the book entitled “A Textbook of Inorganic Chemistry – Volume 1 by Mandeep Dalal”, and is the intellectual property of the Author/Publisher. The content of this document is protected by international copyright law and is valid only for the personal preview of the user who has originally downloaded it from the publisher’s website ([www.dalalinstitute.com](http://www.dalalinstitute.com)). Any act of copying (including plagiarizing its language) or sharing this document will result in severe civil and criminal prosecution to the maximum extent possible under law.



*This is a low resolution version only for preview purpose. If you want to read the full book, please consider buying.*

**Buy the complete book with TOC navigation, high resolution images and no watermark.**

## Home

### CLASSES

#### NET-JRF, IIT-GATE, M.Sc Entrance & IIT-JAM

Want to study chemistry for CSIR UGC - NET JRF, IIT-GATE, M.Sc Entrance, IIT-JAM, UPSC, ISRO, IISc, TIFR, DRDO, BARC, JEST, GRE, Ph.D Entrance or any other competitive examination where chemistry is a paper ?

[READ MORE](#)

### BOOKS

#### Publications

Are you interested in books (Print and Ebook) published by Dalal Institute ?

[READ MORE](#)

### VIDEOS

#### Video Lectures

Want video lectures in chemistry for CSIR UGC - NET JRF, IIT-GATE, M.Sc Entrance, IIT-JAM, UPSC, ISRO, IISc, TIFR, DRDO, BARC, JEST, GRE, Ph.D Entrance or any other competitive examination where chemistry is a paper ?

[READ MORE](#)

**Home:** <https://www.dalalinstitute.com/>

**Classes:** <https://www.dalalinstitute.com/classes/>

**Books:** <https://www.dalalinstitute.com/books/>

**Videos:** <https://www.dalalinstitute.com/videos/>

**Location:** <https://www.dalalinstitute.com/location/>

**Contact Us:** <https://www.dalalinstitute.com/contact-us/>

**About Us:** <https://www.dalalinstitute.com/about-us/>

#### Postgraduate Level Classes (NET-JRF & IIT-GATE)

##### Admission

[Regular Program](#)

[Test Series](#)

[Distance Learning](#)

[Result](#)

#### Undergraduate Level Classes (M.Sc Entrance & IIT-JAM)

##### Admission

[Regular Program](#)

[Test Series](#)

[Distance Learning](#)

[Result](#)

#### A Textbook of Inorganic Chemistry – Volume 1

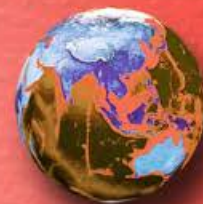
“A Textbook of Inorganic Chemistry – Volume 1 by Mandeep Dalal” is now available globally; including India, America and most of the European continent. Please ask at your local bookshop or get it online here.

[READ MORE](#)

*Join the revolution by becoming a part of our community and get all of the member benefits like downloading any PDF document for your personal preview.*

[Sign Up](#)

International  
Edition



# A TEXTBOOK OF INORGANIC CHEMISTRY

**Volume I**

**MANDEEP DALAL**



*First Edition*

**DALAL INSTITUTE**

# Table of Contents

<b>CHAPTER 1 .....</b>	<b>11</b>
<b>Stereochemistry and Bonding in Main Group Compounds:.....</b>	<b>11</b>
❖ VSEPR Theory .....	11
❖ $d\pi-p\pi$ Bonds .....	23
❖ Bent Rule and Energetic of Hybridization.....	28
❖ Problems .....	42
❖ Bibliography .....	43
<b>CHAPTER 2 .....</b>	<b>44</b>
<b>Metal-Ligand Equilibria in Solution:.....</b>	<b>44</b>
❖ Stepwise and Overall Formation Constants and Their Interactions .....	44
❖ Trends in Stepwise Constants.....	46
❖ Factors Affecting Stability of Metal Complexes with Reference to the Nature of Metal Ion and Ligand.....	49
❖ Chelate Effect and Its Thermodynamic Origin.....	56
❖ Determination of Binary Formation Constants by pH-metry and Spectrophotometry.....	63
❖ Problems .....	68
❖ Bibliography .....	69
<b>CHAPTER 3 .....</b>	<b>70</b>
<b>Reaction Mechanism of Transition Metal Complexes – I:.....</b>	<b>70</b>
❖ Inert and Labile Complexes.....	70
❖ Mechanisms for Ligand Replacement Reactions .....	77
❖ Formation of Complexes from Aquo Ions.....	82
❖ Ligand Displacement Reactions in Octahedral Complexes- Acid Hydrolysis, Base Hydrolysis....	86
❖ Racemization of Tris Chelate Complexes .....	89
❖ Electrophilic Attack on Ligands .....	92
❖ Problems .....	94
❖ Bibliography .....	95

<b>CHAPTER 4</b> .....	<b>96</b>
<b>Reaction Mechanism of Transition Metal Complexes – II:</b> .....	96
❖ Mechanism of Ligand Displacement Reactions in Square Planar Complexes.....	96
❖ The Trans Effect.....	98
❖ Theories of Trans Effect.....	103
❖ Mechanism of Electron Transfer Reactions – Types; Outer Sphere Electron Transfer Mechanism and Inner Sphere Electron Transfer Mechanism.....	106
❖ Electron Exchange.....	117
❖ Problems.....	121
❖ Bibliography.....	122
<b>CHAPTER 5</b> .....	<b>123</b>
<b>Isopoly and Heteropoly Acids and Salts:</b> .....	123
❖ Isopoly and Heteropoly Acids and Salts of Mo and W: Structures of Isopoly and Heteropoly Anions .....	123
❖ Problems.....	152
❖ Bibliography.....	153
<b>CHAPTER 6</b> .....	<b>154</b>
<b>Crystal Structures:</b> .....	154
❖ Structures of Some Binary and Ternary Compounds Such as Fluorite, Antifluorite, Rutile, Antirutile, Cristobalite, Layer Lattices - CdI <sub>2</sub> , BiI <sub>3</sub> ; ReO <sub>3</sub> , Mn <sub>2</sub> O <sub>3</sub> , Corundum, Pervoskite, Ilmenite and Calcite.....	154
❖ Problems.....	178
❖ Bibliography.....	179
<b>CHAPTER 7</b> .....	<b>180</b>
<b>Metal-Ligand Bonding:</b> .....	180
❖ Limitation of Crystal Field Theory.....	180
❖ Molecular Orbital Theory – Octahedral, Tetrahedral or Square Planar Complexes.....	184
❖ $\pi$ -Bonding and Molecular Orbital Theory .....	198
❖ Problems.....	212
❖ Bibliography.....	213

<b>CHAPTER 8 .....</b>	<b>214</b>
<b>Electronic Spectra of Transition Metal Complexes: .....</b>	<b>214</b>
❖ Spectroscopic Ground States .....	214
❖ Correlation and Spin-Orbit Coupling in Free Ions for 1st Series of Transition Metals.....	243
❖ Orgel and Tanabe-Sugano Diagrams for Transition Metal Complexes ( $d^1 - d^9$ States).....	248
❖ Calculation of $Dq$ , $B$ and $\beta$ Parameters .....	280
❖ Effect of Distortion on the $d$ -Orbital Energy Levels .....	300
❖ Structural Evidence from Electronic Spectrum .....	307
❖ Jahn-Teller Effect .....	312
❖ Spectrochemical and Nephelauxetic Series .....	324
❖ Charge Transfer Spectra .....	328
❖ Electronic Spectra of Molecular Addition Compounds.....	336
❖ Problems .....	340
❖ Bibliography .....	341
<b>CHAPTER 9 .....</b>	<b>342</b>
<b>Magnetic Properties of Transition Metal Complexes: .....</b>	<b>342</b>
❖ Elementary Theory of Magneto-Chemistry .....	342
❖ Guoy's Method for Determination of Magnetic Susceptibility .....	351
❖ Calculation of Magnetic Moments .....	354
❖ Magnetic Properties of Free Ions.....	359
❖ Orbital Contribution: Effect of Ligand-Field .....	362
❖ Application of Magneto-Chemistry in Structure Determination .....	370
❖ Magnetic Exchange Coupling and Spin State Cross Over .....	375
❖ Problems .....	384
❖ Bibliography .....	385
<b>CHAPTER 10 .....</b>	<b>386</b>
<b>Metal Clusters: .....</b>	<b>386</b>
❖ Structure and Bonding in Higher Boranes.....	386
❖ Wade's Rules.....	401

❖ Carboranes.....	407
❖ Metal Carbonyl Clusters- Low Nuclearity Carbonyl Clusters.....	412
❖ Total Electron Count (TEC).....	417
❖ Problems.....	424
❖ Bibliography.....	425
<b>CHAPTER 11.....</b>	<b>426</b>
<b>Metal-II Complexes: .....</b>	<b>426</b>
❖ Metal Carbonyls: Structure and Bonding.....	426
❖ Vibrational Spectra of Metal Carbonyls for Bonding and Structure Elucidation.....	439
❖ Important Reactions of Metal Carbonyls.....	446
❖ Preparation, Bonding, Structure and Important Reactions of Transition Metal Nitrosyl, Dinitrogen and Dioxygen Complexes.....	450
❖ Tertiary Phosphine as Ligand.....	463
❖ Problems.....	469
❖ Bibliography.....	470
<b>INDEX.....</b>	<b>471</b>



*Mandeep Dalal*

*(M.Sc, Ph.D, CSIR UGC - NET JRF, IIT - GATE)*

*Founder & Director, Dalal Institute*

*Contact No: +91-9802825820*

*Homepage: [www.mandeepdalal.com](http://www.mandeepdalal.com)*

*E-Mail: [dr.mandeep.dalal@gmail.com](mailto:dr.mandeep.dalal@gmail.com)*

Mandeep Dalal is an Indian research scholar who is primarily working in the field of Science and Philosophy. He received his Ph.D in Chemistry from Maharshi Dayanand University, Rohtak, in 2018. He is also the Founder and Director of "Dalal Institute", an India-based educational organization which is trying to revolutionize the mode of higher education in Chemistry across the globe. He has published more than 40 research papers in various international scientific journals, including mostly from Elsevier (USA), IOP (UK) and Springer (Netherlands) .

*Other Books by the Author*

**A TEXTBOOK OF INORGANIC CHEMISTRY - VOLUME I, II, III, IV**

**A TEXTBOOK OF PHYSICAL CHEMISTRY - VOLUME I, II, III, IV**

**A TEXTBOOK OF ORGANIC CHEMISTRY - VOLUME I, II, III, IV**

ISBN: 978-81-938720-0-0



9 788193 872000 >

MRP: Rs 800.00

**D** DALAL  
INSTITUTE

Main Market, Sector 14, Rohtak, Haryana 124001, India

(+91-9802825820, [info@dalalinstitute.com](mailto:info@dalalinstitute.com))

[www.dalalinstitute.com](http://www.dalalinstitute.com)